The University of Edinburgh

School of Engineering

Academic Year 2020-2021

Numerical Modelling of The Fire Performance of CLT Compression Members

Ahmed Ahmed Ali Awadallah

Supervisor: Luke Bisby

Master thesis submitted in the Erasmus+ Study Programme

International Master of Science in Fire Safety Engineering

DISCLAIMER

This thesis is submitted in partial fulfillment of the requirements for the degree of The International Master of Science in Fire Safety Engineering (IMFSE). This thesis has never been submitted for any degree or examination to any other University/programme. The author(s) declare(s) that this thesis is original work except where stated. This declaration constitutes an assertion that full and accurate references and citations have been included for all material, directly included and indirectly contributing to the thesis. The author(s) gives (give) permission to make this master thesis available for consultation and to copy parts of this master thesis for personal use. In the case of any other use, the limitations of the copyright have to be respected, in particular with regard to the obligation to state expressly the source when quoting results from this master thesis. The thesis supervisor must be informed when data or results are used.

Word count: 18680

Read and approved,

11th May 2021

ABSTRACT

The global movement to reduce the carbon footprint in the construction industry has refueled interests in sustainable construction materials. Engineered wood products like Cross Laminated Timber (CLT) have facilitated this transition owing to numerous advantages compared to steel or concrete. CLT like other timber products degrades and combusts under fire, losing structural capacity in the process. This study aims to numerically evaluate the structural fire performance of CLT walls according to EN 1995-1-2 under different fire curves and perform a parametric study to investigate the optimal CLT buildup for best performance in fire.

A one-dimensional transient heat transfer model was employed to predict the temperature distribution in-depth of a CLT cross-section while accounting for temperature dependent thermal properties modeled according to the advanced method outlined in Annex B of EN 1995-1-2. A decoupled structural model accounting for the reduction in strength and stiffness based on the thermomechanical properties outlined in Annex B of EN 1995-1-2 is used to predict the crushing and buckling load capacity of the CLT. The reduced cross-section method (RCSM) and recoverability of strength during cooling was also incorporated.

The intensity and duration of a fire influenced the extent of loss in capacity and further strength reduction was observed during the cooling phase. The RCSM overpredicted the crushing capacity in all cases while conservative results were obtained for buckling when the effective char depth penetrates the second and third plies for 3-ply, and 5 and 7-ply CLTs, respectively. Changes in end restraints or wall height mainly affected ambient capacity with minimal effect on fire performance. CLTs with thicker longitudinal plies have been found to outperform other ply arrangements. Under a short fire, 3-ply CLTs with thicker longitudinal plies outperformed other CLTs. Under more severe fires, 7-ply CLTs with thicker longitudinal plies were better performing.

ACKNOWLEDGMENT

I would like to extend my immense gratitude to the Erasmus+, sponsoring companies and the IMFSE management board for granting me the opportunity to be part of this program. I also want to thank all the professors from the different universities who impacted their knowledge onto me.

My utmost thanks go to my promoter and supervisor Prof. Luke Bisby for his support, encouragement, and guidance throughout this thesis.

I would also like to thank all my IMFSE classmates with whom I have shared the last two years of my life with.

To my parents and siblings, thank you for being my backbone throughout this journey.

“Above all, don't fear difficult moments. The best comes from them.” – Rita Levi-Montalcini

Table of Contents

LIST OF TABLES

LIST OF FIGURES

NOTATIONS

A	area of the exposed residual cross-section, m^2
A_i	area of slice i, mm^2
A_j	area of vertical opening j, m^2
A_t	total area of the compartment, m^2
A_v	total area of vertical openings, m^2
b	absorptivity for the total enclosure, $J \cdot m^{-2} s^{-0.5} K^{-1}$
c	specific heat, $J \cdot kg^{-1} \cdot K^{-1}$
d	depth of the cross-section, mm
d_{char}	char depth, mm
d_{char_eff}	effective char depth, mm
d_o	zero-strength layer, mm
$d_{residual}$	residual depth of cross-section, mm
E	modulus of elasticity, MPa
H	height of the member, m
h	convective heat transfer coefficient, $W \cdot m^{-2} \cdot K^{-1}$
h_{eq}	weighted average of heights of all vertical openings, m
h_i	height of vertical opening i, m
I	second moment of inertia of the cross-section in mm^4
k	thermal conductivity, $W \cdot m^{-1} \cdot K^{-1}$
O	opening factor, $m^{1/2}$
P	perimeter of the exposed residual cross-section, m
q_{cond}	heat contributed by conduction, kW
q_{conv}	heat contributed by convection, kW
q_{rad}	heat contributed by radiation, kW

$q_{t,d}$	design fire load density related to the total area of floors, walls and ceilings which enclose the fire compartment, $MJ \cdot m^{-2}$
T	temperature, K/°C
t	time, s/min
w	width of the cross-section, mm

Greek Letters

α	thermal diffusivity, $m^2 \cdot s^{-1}$
ε	emissivity
β_o	one-dimensional charring rate, mm/min
β_n	notional charring rate, mm/min
β_{par}	parametric charring rate, mm/min
ρ	Density, $kg \cdot m^{-3}$
σ	Stefan-Boltzmann constant, $W \cdot m^{-2} \cdot K^{-4}$
Γ	heating rate

Abbreviations

CLT	Cross Laminated Timber
LVL	Laminated Veneer Lumber
PUR	Polyurethane
MUF	Melamine-Urea-Formaldehyde
MF	Melamine-Formaldehyde
RCSM	Reduced Cross-Section Method
RPM	Reduced Properties Method

1 INTRODUCTION

Timber construction has recently seen a surge in its demand across the world owing to the move towards a more sustainable approach to construction [1]. However, a lot of hesitations exist about the use of structural timber in tall buildings due to the perceived fire safety apprehensions. Such prejudice stems from past experiences where cities made of wood burned down (for example Great fire of London [2], Meireki Fire in Japan [3]) leading to the adoption of noncombustible materials in the construction industry. With the advent of new technology and engineered timber (such as glulam and more recently cross laminated timber), breaching this gap seems underway. Nevertheless, it is imperative to conduct extensive research into the fire performance of said inventions.

1.1 Background

Timber refers to products processed and obtained from the wood of trees for the purposes of construction [4]. Chemically, it is made up of three main constituents namely cellulose (50% by weight), hemi-cellulose (25%) and lignin (25%) [5]. The main function of the lignin is to bond the other constituents together [6],[7] and the amount of lignin present dictates the compressive strength of the timber, hence wood with higher concentration of lignin is relatively stronger in compression [8]. Unlike other construction materials, timber is anisotropic, which means it exhibits different properties depending on the direction of loading. Two directions are recognized structurally: parallel to and perpendicular to the grain [9].

Timber boasts of several advantages over the more conventional construction materials for example masonry, steel, and concrete. It has a high strength to weight ratio translating into easier workability during the construction let alone being cost effective in the process [1],[10],[11], [12]. Furthermore, it makes it desirable for use in areas with soils having weak bearing capacities [1] as well as for the erection of tall buildings since the self-weight will induce far less deadloads as compared to concrete or steel [7]. The ability to fabricate and preassemble structural timber members off site leads to fast construction times [12],[13],[14],[15] which translates into cost effectiveness. However, protecting timber members against fire may be more costly as opposed to other construction materials [16].

The use of timber in construction also promises huge gains in the fight against climate change. According to the World Green Building Council [17], 11% of the total carbon emissions stems from activities associated with the manufacturing of construction materials such as steel and concrete. Less energy (~10%) is required for, and less pollution is produced by the harvest of timber as compared to the extraction of raw materials for the manufacturing of steel and concrete [4],[18]. Used up and by products of timber (for example sawdust) can also be recycled into other useful products such as plywood. Ergo, the transition to timber construction is not only eco-friendly but also sustainable.

Howbeit, other than its tendency to combust, there are certain disadvantages with using timber due to its inherent organic nature. Unlike steel or concrete which can be designed to achieve a desired strength, timber on the other hand is naturally occurring with variable strength [6],[19] influenced by many factors including genetics, species, and environmental conditions [4]. Timber is also prone to defects and knots, as well as insect attack which greatly reduce its strength [8],[20],[21].

The advent of engineered timber in recent years aims to address these issues. Wood is processed into boards, veneers, strands or panels [7] which are then mechanically or visually graded into strength classes [4] and bonded together with an adhesive to achieve a usable product. This attempts to tackle variability in strength and minimizes the defects present while achieving high dimensional stability (effects of humidity or temperature do not greatly cause swelling and shrinkage)[1], [22]. Several engineered timber products are available in the market such as glue laminated timber (glulam), laminated veneer lumber (LVL) and cross laminated timber (CLT). This thesis will mainly focus on CLT with some reference and comparisons made to solid timber and glulam.

Cross laminated timber (CLT or XLAM or Brettsperrholz in German) refers to an engineered timber product made up of odd number of laminations (three, five, seven and less commonly nine) arranged in a crosswise manner and bonded together by adhesives under pressure. Figure 1-1 shows an illustrative three-ply CLT. Its development began a few decades ago particularly in Central Europe (Germany, Switzerland and Austria) and has recently seen a growing interest in the product evident by the numerous research currently being

undertaken. In Europe, most CLTs are made from softwood species of spruce [1],[23] and in some cases Doulas fir [23]. Unlike solid timber and glulam, CLT is capable of withstanding in-plane and out-of-plane loadings making it apt for usage as wall and floor structural elements [1]. Typical dimensions of CLT are lengths from 18-30 m, breadths ranging from 3-4.8 m and thicknesses of up to 400 mm [1]. Ply thicknesses commonly range between 12-45 mm and thicknesses of 20, 30 and 40 mm are generally adopted in Central Europe[1].

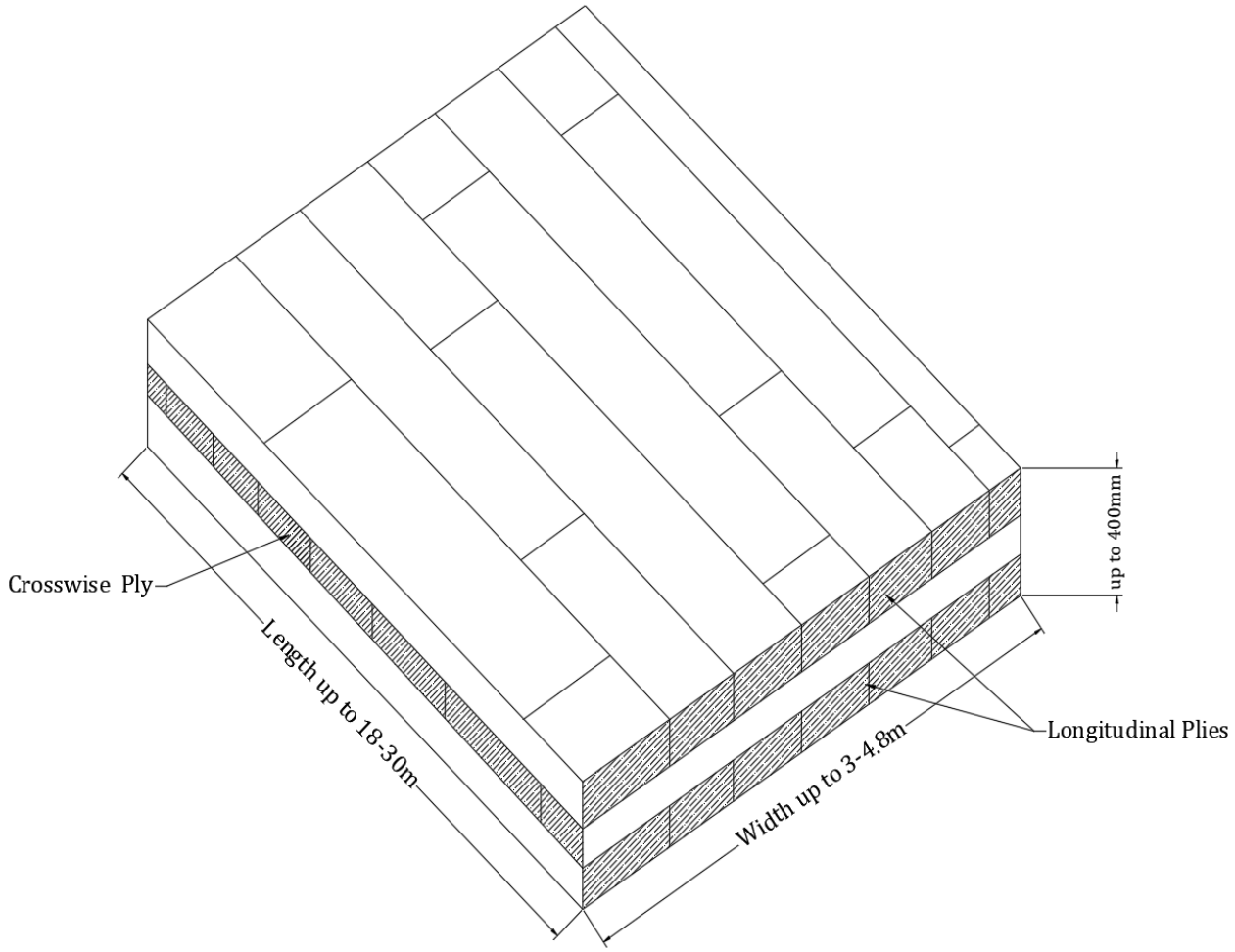

Figure 1-1 Illustrative diagram of a three-ply cross laminated timber panel (wall or ceiling)

CLT being a new product, designers and manufacturers are still experimenting with different ply layup arrangements and thicknesses to achieve optimum strength. For example, having thicker first and last plies translates into more load carrying capacity relative to equally thick plies. Under ambient conditions, determining the performance of these arrangements and thicknesses can easily be achieved through simple calculations or by carrying out loading

tests. In fire however, the performance of these new inventions requires a more in-depth analysis. The order and thickness of layups will be investigated here to give designers and manufacturers a basic idea about what combination of layups and thicknesses will give the best performance in fire.

1.2 Combustibility of Timber

Unlike other building materials for example concrete and steel, when exposed to high temperatures, wood has the propensity to pyrolyze giving off volatile gases and developing a char layer, losing mass and cross-section in the process [24]. Volatile gases escape to the surface providing fuel for sustained flaming. Heat is transferred to the timber surface mainly by radiation and convection, which is then conducted through its depth (see Figure 1-2). The outward movement of volatile gases leads convective losses. Different temperature regimes signify changes in mechanical and thermo-physical properties of timber and owing to its thermally thick nature there exists a temperature gradient as shown in Figure 1-2. Heated timber begins to lose its strength at temperatures as low as 65 °C [4]. Moisture begins to evaporate around 100 °C, leading to a plateau in the temperature distribution (latent heat of vaporization) [25], [26], [27]. The onset of pyrolysis and mass loss occurs at temperatures ranging from 200-225 °C [25], [26]. Continued heat exposure results in gradual increase of the depth of the charred layer leading to further mass loss and reduction in cross-section. Char is beneficial and serves as an insulator, protecting the wood beneath from direct heating and inhibits the escape of volatile gases thusly reducing the thermal penetration depth and rate of pyrolysis [24],[25],[27],[28]. This protection may be hindered by surface regression (shrinkage) of the char layer which occurs at temperatures greater than 550 C due to the oxidation of char resulting in reduced char depth and consequently the protection of the wood underneath [4],[30]. The development of fissures or cracks in the char layer hampers the protection provided and results in higher heat transfer into the timber.

1.3 Compartment Fire Dynamics

Since timber is a combustible material and can serve as additional fuel when used as a structural element(s), its contribution to the fire dynamics of the compartment must be accounted for. It has been found out that compartment temperatures do not vary greatly between experiments with exposed timber members as opposed to protected timber

members (owing to insufficient oxygen), however, time to flashover is shorter [31] and the heat produced in the exposed cases was much higher with most of it being released externally [32],[33].

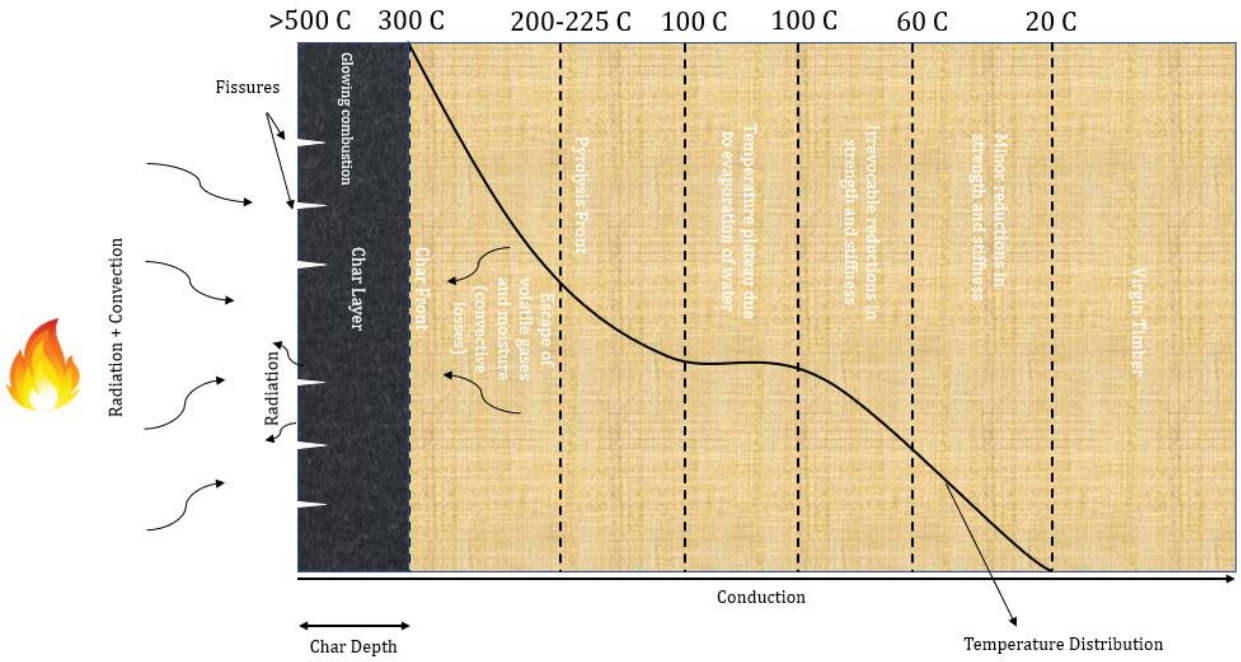

Figure 1-2 Fire exposed timber cross-section showing the heat transfer process and in-depth thermal degradation.

Undoubtedly, factors such as ventilation conditions and fuel load will play a role in the behavior of construction material in fire [32]. To maintain structural integrity and or to achieve a desired fire strategy (for example defend in place), it is imperative to ensure burnout and auto-extinguishment of exposed timber element(s). This is important since the timber itself serves as additional fuel and its continued burning will eventually lead to loss of structural load carrying capacity leading to collapse. This is of particular importance for compartments made of CLT due to the potential for char fall off. Experimental investigations on CLT compartment fires revealed that burnout and auto-extinguishment can be achieved given that the necessary conditions are present [34]–[38]. It is however highly dependent on whether char fall off occurs or not. The conditions include the potential for char fall off, the amount of fuel load present [36], ventilation, amount of wood exposed and the type of glue used (hence its performance when heated) [32],[33].

1.4 Charring Rate

From a structural perspective, charring of timber is of utmost importance since a charred layer is assumed to have zero strength and stiffness. It is therefore crucial to quantify the gradual evolution of char depth of a heat-exposed timber member (defined as charring rate) to have an estimate of its residual structural capacity. At the start of ignition, an initial maximum charring rate is achieved after which it reduces to a quasi-constant rate [25], [39], [40] as illustrated in Figure 1-3. Several temperatures for the start of charring have been reported in literature: temperatures as low as 253 [41], 260 [42], 265 [43], and 360 °C [29]. However, a temperature of 300 °C (represented by the 300 °C isotherm) is generally a good indication of char onset, and the location of the char front [18], [44]–[47].

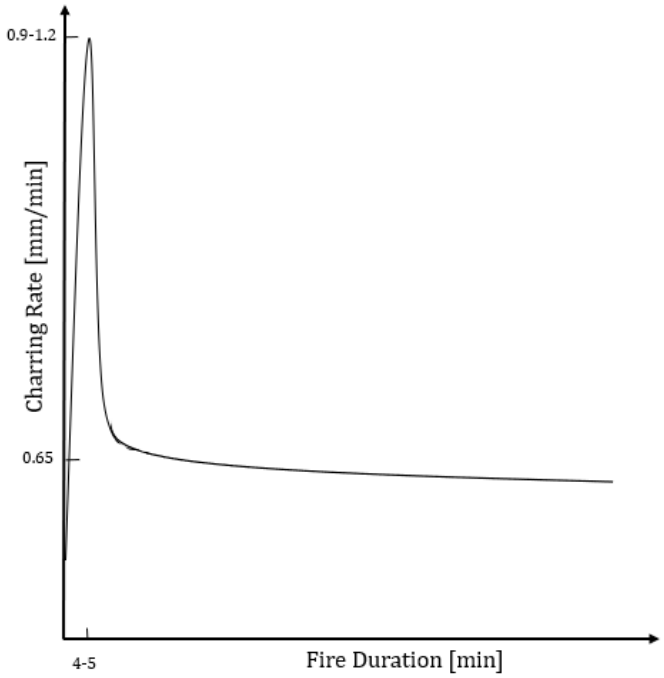

Figure 1-3 Charring rate for an exposed initially unprotected timber member.

Charring rates have been widely investigated by several researchers, with values ranging from 0.6 mm/min to 0.8 mm/min [4], [25], [48] obtained from tests done on glulam members exposed to the standard fire curve. EN 1995-1-2 [49] specifies two types of charring rates for softwood: β_o equal to 0.65 mm/min (glulam and solid wood) which accounts for one dimensional charring and β_n equal to 0.7 mm/min and 0.8 mm/min for

glulam and solid wood members respectively, referred to as the notional charring rate that accounts for the effects of corner roundings and fissures. These charring rates have been developed for timber elements subjected to the standard fire curve. For parametric fire curves, Annex A of EN 1995-1-2 [49] outlines a relation for the determining the charring rate during the heating phase given by:

$$\beta_{par} = 1.5\beta_n \frac{0.2\sqrt{\Gamma} - 0.04}{0.16\sqrt{\Gamma} + 0.08} \quad \text{Eq. 1}$$

Where β_n is the notional charring rate and Γ is given by:

$$\Gamma = \frac{\left(\frac{O}{b}\right)^2}{\left(\frac{0.04}{1160}\right)^2} \quad \text{Eq. 2}$$

$$O = \frac{A_v}{A_t}\sqrt{h_{eq}} \quad \text{Eq. 3}$$

$$b = \sqrt{\rho c k} \quad \text{Eq. 4}$$

$$h_{eq} = \sum \frac{A_i h_i}{A} \quad \text{Eq. 5}$$

Where Γ is the heating rate, O is the opening factor in $m^{1/2}$, A_v is the total area of vertical openings in m^2, A_t is the total area of the compartment in m^2, A_i is the area of vertical opening i in m^2, h_{eq} is the weighted average of heights of all vertical openings in m, h_i is the height of vertical opening i in m, b is the absorptivity for the total enclosure in

$J \cdot m^{-2} s^{-0.5} K^{-1}$, ρ is the density in $kg \cdot m^{-3}$, c is the specific heat in $J \cdot kg^{-1} \cdot K^{-1}$ and k is the thermal conductivity in $W \cdot m^{-1} \cdot K^{-1}$ of the boundary compartment respectively.

For the cooling phase, a linear decline of β_{par} as shown in Figure 1-4 is proposed. It is however only applicable to situations where $t_0 \leq 40\,\text{min}$, opening factor between 0.02-0.3 $m^{1/2}$, $d_{char} \leq \frac{w}{4}$ and $d_{char} \leq \frac{d}{4}$ with w, d_{char} and d being the width, char depth and depth of the cross-section in mm, respectively. This is therefore inapplicable to parametric fires with

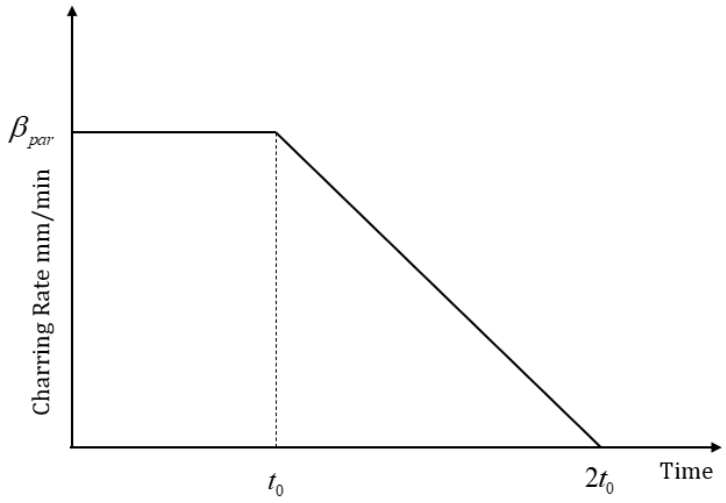

Figure 1-4 Parametric charring rate according to Annex A of EN 1995-1-2 [49]

Where

$$t_0 = 0.009 \frac{q_{t,d}}{O} \qquad \text{Eq. 6}$$

And $q_{t,d}$ is the design fire load density related to the total area of floors, walls and ceilings which enclose the fire compartment in $MJ \cdot m^{-2}$.

Using these charring rates, the charred depth d_{char} in mm and residual cross-section can be determined by:

$$d_{char} = \beta \cdot t \qquad \text{Eq. 7}$$

1.5 Delamination and Debonding

With CLT in fire, charring rates maybe be higher due to the risk of delamination – the detachment of charred lamella from the CLT at the glue line when the char front reaches it, thereby exposing fresh unburnt timber to fire resulting in increased charring rates as compared to glulam members [4], [25]. The charring rate of the freshly exposed ply is expected to be amplified and a double charring rate can be assumed for the first 25 mm [24] since the surrounding temperatures are already high. This is analogous to an initially protected timber member losing its protection This was confirmed by Li et al. [32] who arrived at charring rates of 1.22 mm/min from experiments they carried out on exposed CLT members. Charring rates of up to 1.5 mm/min were also observed by Johansson and Svenningsson [50] from their fire tests on CLT. Contrary to the above assumption, charring rates from furnace experiments on loaded CLT panels by Goina [51] were rather low (between 0.37-0.79 mm/min). CLT panels that do not experience char fall off behave similarly to solid timber members in fire [24], [52].

The potential for delamination however depends on several factors including thickness of individual lamella, orientation of the member, and type of adhesive used. Thicker lamellae will char more slowly as compared to thinner lamellae, hence it will take longer for the char layer to reach the first adhesive bond [44]. This was corroborated by tests done by Osborne et al. [53] on CLT walls and floors with varying number of plies (3,5 and 7) and thicknesses. CLT panels used in the horizontal configuration (for example CLT slabs) are more susceptible to char fall off as compared to CLT panels used in walls (vertical configuration) [53], [54] albeit delamination was yet observed on test done on CTL walls [55], [56]. The type of adhesive used for bonding CLT plies also influences its vulnerability to delamination. Several adhesives are used in the manufacturing process of CLT with the most widely used being Polyurethane (PUR), Melamine-Urea-Formaldehyde (MUF) and Melamine-Formaldehyde (MF) [4]. The use of PUR has been reported in several papers as a positively contributing factor to char fall off in contrast to other adhesive types where delamination was either

limited or not observed [50], [57]. Moreover, the newly exposed timber surfaces will serve as additional fuel and potentially hinder self-extinction [38].

Debonding occurs when the adhesive holding plies together losses its bonding property (that is, ceases to stick), resulting in the separation of two plies and consequently loss in composite action, though, the separated plies still maintain their individual strength and stiffness [4]. This loss of adhesive bonding property is induced when the glue line is heated beyond a certain temperature. Temperatures as low as 80 °C have been reported to result in bond line failure from single lap shear tests done by Nicolaidis et al. [58] on timber with PUR adhesive. Emberley and Torero [59] also noted that the loss in strength of the bond lines will induce ply slip, resulting in a reduction in the CLT's composite action, accelerating deflections and hence failure.

1.6 Fire Protection Methods

A timber member can either be chemically treated or covered on its surface with a non-combustible insulation material. The latter method is sometimes referred to as encapsulation. Fire protecting a timber surface may appear to improve its fire performance, however it should be noted that the inherent tendency of the timber to combust is not eliminated but delayed [28], [60], [61]. From the sustainability point of view, chemically treating timber will render it unusable for energy purposes at the end of its work life due to the harmful chemical toxins that may be released [7].

Experiments carried out by Su et al. [36] on CLT compartment fires achieved complete burn out of the movable fuel while limiting or preventing the participation of the structural timber members in fire when they applied three layers of plasterboard as protection. These findings are however subjected to the constraints of the experiment and do not necessarily mean all CLT members ought to be protected by three layers of plasterboard. Similarly, results from Hasburgh et al. [62] revealed that having more layers of protection delayed the start of charring but lead to higher charring rates following the failure of the protection. This is logical since temperatures will be much higher, hence the increased charring rate.

No concrete conclusions can be made about the performance of air-tight encapsulation versus encapsulations with an air gap. From experiments by Li et al. [32] it was reported that

closely fitted encapsulations (with no air gaps) on CLT performed better than those tested on timber frames having air gaps between the studs. However, Hasburgh et al. [62] found that air gaps improved performance by delaying the start of charring.

Encapsulation of timber members is desired among product manufacturers since the contribution from the protective layer(s) can be used to achieve a desired fire resistance rating. However, encapsulation can drive the cost of a project high, increase the overall weight and hide the aesthetic nature of the timber, a property most desired by clients and architects.

The Eurocode [49] stipulates higher charring rates following the failure of a protective layer until the first 25 mm. This makes sense since at the time of its failure, compartment temperatures are high enough to cause accelerated charring rates. Three cases are considered by the Eurocode: 1. following the failure of protection, an increased charring rate until the char depth equals 25 mm after then charring returns to the charring rate of an initially unprotected timber. 2. An increased charring rate after failure until a certain time after which charring rate returns to the charring rate of an initially unprotected timber. 3. Charring of the wood starts before the protective layer fails, but at a reduced rate. After the protection has failed, an increased charring rate until the char depth equals 25 mm after then charring returns to the charring rate of an initially unprotected timber.

1.7 Structural Design of Timber in Fire

EN 1995 1-2 [49] outlines three methods for the structural fire design of timber members. The most widely used method, the reduced cross-section method (RCSM), and the less known reduced properties method (RPM) as well as an advanced method given in its Annex B. Although these methods were developed for other types of timber constructions, designers and engineers use it for CLT design regardless as there are no alternative codes for CLT [4], [63]. The RPM provides pre-multiplying factors $k_{\mathrm{mod},\,fi}$, as shown in Eq. 8, for the reduction of strength and stiffness of the section.

$$k_{\mathrm{mod},\,fi} = 1 - \frac{1}{S}\frac{P}{A} \qquad \text{Eq. 8}$$

Where P is the perimeter in m and A is the area in m^2 of the exposed residual cross-section, respectively and S is a factor equal to 200 for bending strength, 125 for compressive strength and 330 for tensile strength and elastic modulus.

$k_{\mathrm{mod},\,fi}$ depends on the perimeter and area of the effective cross-section, that is, the section factor. However, using the section factor to define $k_{\mathrm{mod},\,fi}$ is not a proper representation of reality [64]. This method is only applicable for wood members with three or four side exposure and hence cannot be used for slabs or walls heated on one side. A study carried out by Konig and Kallsner [64] on four timber cross-sections concluded that the level of complexity of the RPM does correspond to improved accuracy relative to the RCSM. Other issues with the RPM are that shear strength reductions are not accounted for [64]. Due to its limited applicability, it is set to be removed from the upcoming revision of part two of EC 5 [45][63].

In the RCSM, the design begins by subtracting the original cross-section of the timber member by the effective charred depth (determined as per EC 5 [49]) plus a zero-strength layer. The rationale behind using a zero-strength layer stems from the assumption that beyond the charred layer, there exists a heat affected zone with no strength or stiffness. The basis for this assumption was derived from the work of Schaffer [65] on glulam beams who used a zero-strength layer of 7.62 mm (0.3in). The capacity of the residual cross-section is determined as one would for timber at ambient conditions. Figure 1-5 shows a schematic diagram of a residual cross-section.

The use of a constant zero-strength layer has been the subject of major debate in the structural fire timber community. Using a constant value of 7 mm has been found to give unconservative results for timber members exposed to fires other than the standard fire curves [66]–[70]. This is of more concern for CLT members especially as the zero-strength layer has been found to be insufficient to predict residual capacity of CLT members subjected to standard [69], [71] and other fire exposures [66], [70]. Schimd et al. [69] proposed a procedure for the calculation of the zero-strength layer of members subjected to bending, tension and or compression. Due to the layered arrangement of CLT plies, the load carrying

capacity can exhibit sudden changes and hence the structure of the CLT has to be taken into account when determining a zero-strength layer [68].

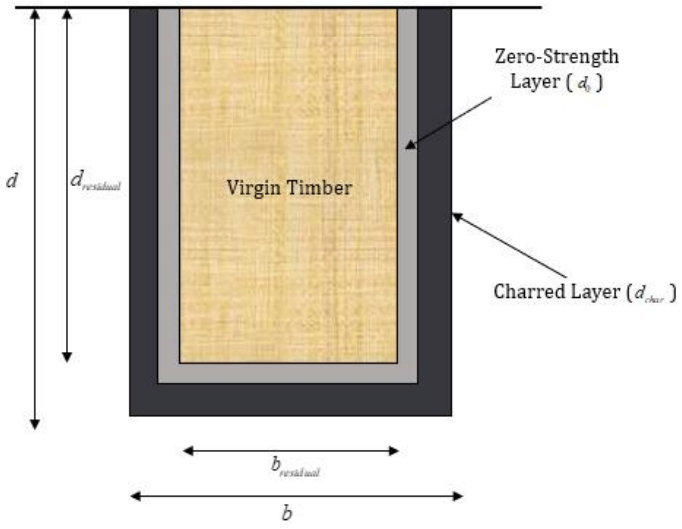

Figure 1-5 Illustrative diagram of a residual timber cross-section.

1.8 Advanced Calculation Methods

Annex B of EN 1995-1-2 [49] outlines advanced calculation methods that can be used in computer models to assess the fire performance of wood members. These methods can be applied to determine the evolution and distribution of temperature in-depth of a wood member using heat transfer equations (with the use of effective thermal properties), and for the structural analysis of the structure or part thereof accounting for the temperature-dependent mechanical properties [45].

1.8.1 Thermal Properties

Several models for thermal properties exist in literature as shown in Figure 1-6, Figure 1-7 and Figure 1-8 for thermal conductivity, specific heat and density, respectively. Some of these thermal properties represent the true physically measured values (for example Fredlund [72]) while others are calibrated against test data to account for processes such as mass transport and the formation of fissures. Thomas [73] included the effects of vaporization of water and its recondensation as the vapor is transported into the much cooler parts of the timber section giving rise to higher conductivity values at around 100 °C (boiling point of water) and lower conductivity values after 100C and until 350 °C.

This depicts reality as temperature rise will slow down, since much of the heat is used up to vaporize the moisture. Between 200 °C and 300 °C, Frangi [74] and Mehaffey et al [75] included the effects of the heat of combustion by introducing a heat sink to simulate an endothermic reaction in that temperature range. Mehaffey et al [75] empirically included the effects of water vapor and radiative heat transfer in their conductivity values.

The thermal conductivity model in EN 1995-1-2 [49] is obtained from calibrated test results carried out by Konig and Walleij [46] under standard fire curves. Density (Figure 1-8) and specific heat values provided in annex B of EC 5 [49] originate from the work of Janssens [76], however, modified by Konig and Walleij [46] to account for char shrinkage.

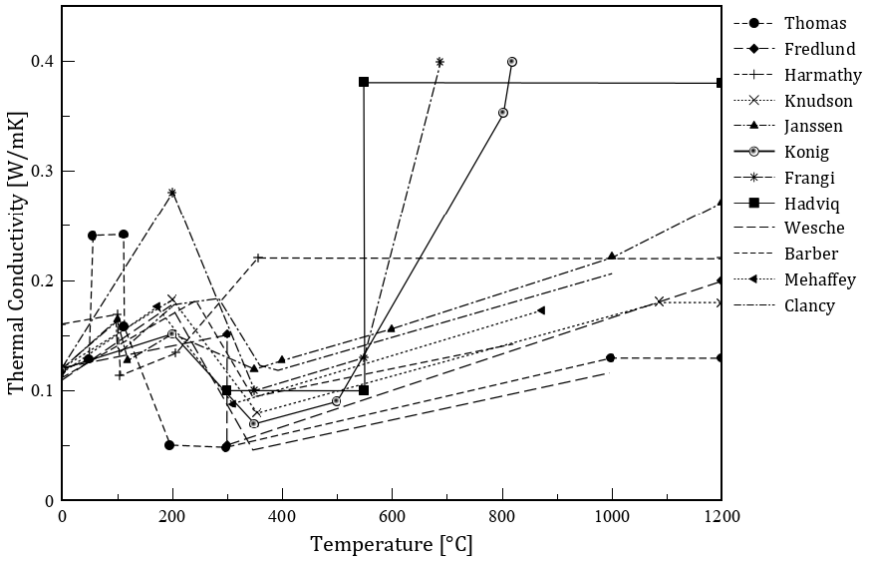

Figure 1-6 Temperature-dependent thermal conductivity values for wood ([46], [72]–[74], [76]–[78] as referenced by [30] and [75], [79] as referenced by [80], and [81], [82] as referenced by [74].)

The formation of cracks in the char layer was first roughly modeled by Hadvig [78] who assumed the formation of cracks 6 mm away from the char layer depicted by a sharp change in conductivity after 550 °C, which then remains constant for higher temperatures. These cracks will result in enhanced heat transfer by convection and radiation. These effects and shrinkage of the char layer were later also represented by Konig and Walleij [46] resulting

in a sharp linear increase in conductivity values after 500 °C and a much steeper increase after 800 °C.

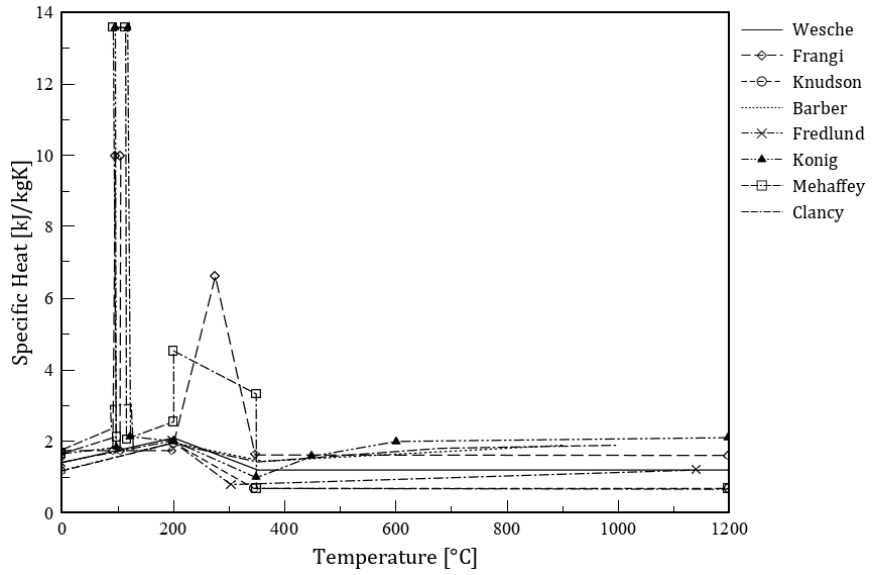

Figure 1-7 Temperature-dependent specific heat values for wood ([44], [64], [66], [74], [73], [74] as referenced by [74] and [75] and [79] as referenced by [80])

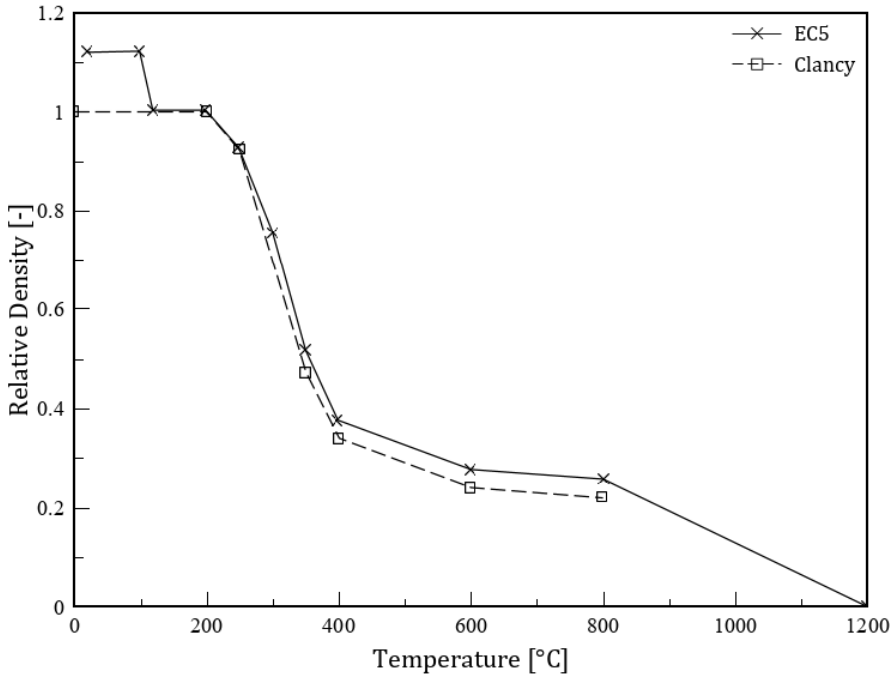

Figure 1-8 Temperature-dependent density values for wood ([49] [79] as referenced by [80])

However, one major drawback of the thermal properties defined in EC 5 [49] is their inapplicability to fires other than standard fire exposures [30], [45], [83]. This puts a huge limitation with regards to designing timber elements under natural fire scenarios. Konig and Wallei [46] proposed that for natural fires, the effective conductivity values should be modified depending on the stage of the fire scenario. This was corroborated by the work of Konig [30], who demonstrated that the effective thermal conductivity for the standard fire exposure can be modified to better predict the temperature distribution in a timber member with great accuracy during the heating phase. Through a process of trial and error, he concluded that for natural fires with a more severe heating phase as compared to the ISO curve, reducing the thermal conductivity values from temperatures above 350 °C resulted in better agreement with test results and vice versa for natural fires with a less severe heating phase. However, during the decay phase, Konig [30] found that just modifying the conductivity values did not give good results. As pyrolysis slows down, the escape of volatile gases, which hindered interaction of oxygen and the char, slows down. Hence, glowing combustion of the char layer is now more dominant leading to higher surface temperatures as compared to gas temperature, resulting in a higher temperature effect inside the timber section (as compared to what one would expect just based on the gas temperature). By applying an increased effective gas temperature and modifying the conductivity values, good agreement with experimental results was achieved for the decay phase [30].

Analytical investigations by Hopkin el al [83] also corroborate the issues of applicability of the thermal properties in part two of EC 5 [49] to natural fires. Hopkin et al [83] carried out an analytical analysis to arrive at an expression k_{mod}, given by Eq. 10, for the modification of thermal conductivity values beyond 350 °C.

$$k_{\lambda,\text{mod}} = k_{\Gamma,\text{mod}} k_{qtd,\text{mod}} \qquad \text{Eq. 9}$$

Where

$$k_{\Gamma,\text{mod}} = 1.5\Gamma^{-0.48} \qquad \text{Eq. 10}$$

$$k_{qtd,\mathrm{mod}} = \sqrt{\frac{q_{td}}{210}}$$ Eq. 11

They carried out a regression analysis by comparing the charring rates for parametric fires given in Annex A of part two of EC 5 [49] with the results obtained from a finite element analysis. This modification factor considers the heating rate and fuel load of a parametric fire and can only be applied to the heating stage of a parametric fire curve.

1.8.2 Thermo-Mechanical Properties

Annex B of part two of EC 5 [49] gives the relative thermo-mechanical properties to be used in an advanced calculation as shown in Figure 1-9 and Figure 1-10 for compression, and elastic modulus, respectively, as derived by Konig and Walleij [46] from the works of Konig [84] and Konig et al [85], with the exception of the relationship for shear strength which originates from the work of Gerhards [86]. Attention will be paid to compressive strength and modulus of elasticity since these are the most important properties for structural elements under compression. These properties are defined by bi-linear relationships with full strength at 20 °C (the assumed ambient temperature in EC 5 [49]). The slopes of these lines change at 100 °C and reduce to zero at 300 °C (indicating the char layer with zero strength and stiffness). As with the thermal properties, there exists other relationships for these mechanical properties as shown in Figure 1-9 and Figure 1-10, however there is a scatter in the measured reduction values for both compressive strength and elastic modulus reported by different researchers. Such scatter is expected and can be attributed to the different experimental conditions under which such measurements were done for example oven heating of samples [87] versus steel plate heating [21]. In a similar manner, the tested wood species also play a role in the variability of results. Knudson and Schniewind [77] carried out their tests on Douglas fir whereas Zeeland [87] and Young and Clancy [21] carried out their tests on Pinus Contarta and Pinus Radiata, respectively. While some researchers are of the view that species do not play a major role in determining the mechanical properties of timber reasoning that the constituents of wood responsible for mechanical strength are of similar proportion and hence will lose strength in a similar way

[21][88]. Such assumption is opposed to experimental results by Figueroa [89] whose tests on three different species yielded different results.

Moisture content is another contributing factor to the variability in the reduction factors and leads to the deterioration and softening of wood [90]. Drier samples will therefore have a higher ultimate strength and would lose their strength much slower than more moist samples [21]. For example, samples by Young and Clancy are pre-dried before loading leading to higher strength values around 100 °C. The reduction factors by Konig and Wallej [46] implicitly consider the effects of creep and moisture content.

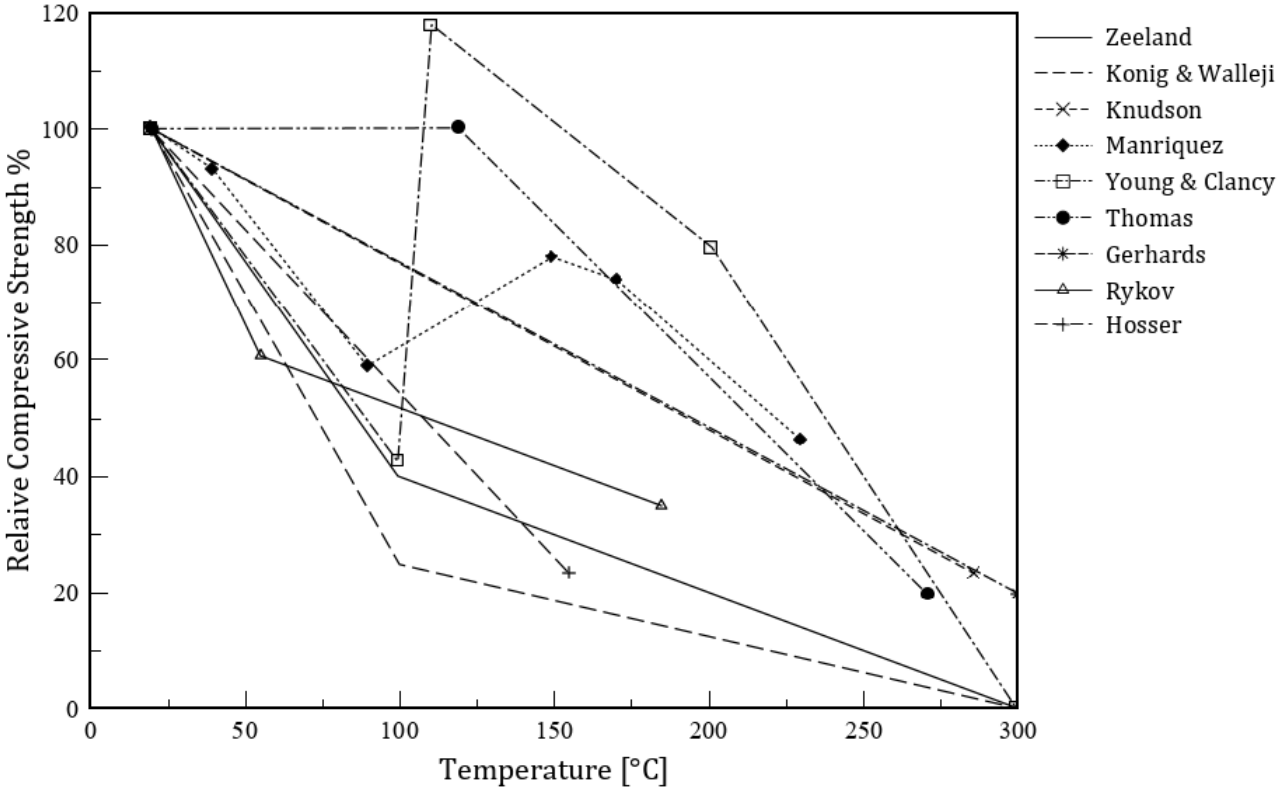

Figure 1-9 Reduction in compressive strength of wood with temperature ([21], [46], [77], [87], [89] as referenced by [4] and [91], [92] as referenced by [87], and [93] and [94] as referenced by [21])

1.9 Heat Transfer Models

Heat transfer models are tools that allow in-depth temperature predictions in timber members subjected to high temperatures. Depending on the sophistication and complexity of the models, they can be used to simulate the behavior and deterioration of timber elements subjected to fire. Several models available in literature will be briefly presented in

this section. The models presented here are not exhaustive nor presented in a chronological order.

These models can be broadly grouped into simple thermal models and comprehensive models [95]. Simple thermal models do not constitute the chemical processes that ensue due to heating and decomposition of the material, but rather, pyrolysis (and hence charring) is assumed to occur once the temperature reaches a predefined pyrolysis temperature (300 °C for wood) by conducting simple thermal energy balance(s). Although a simplification of reality, this critical temperature coincides with the onset of thermal decomposition and hence can be representative of charring of wood [95].

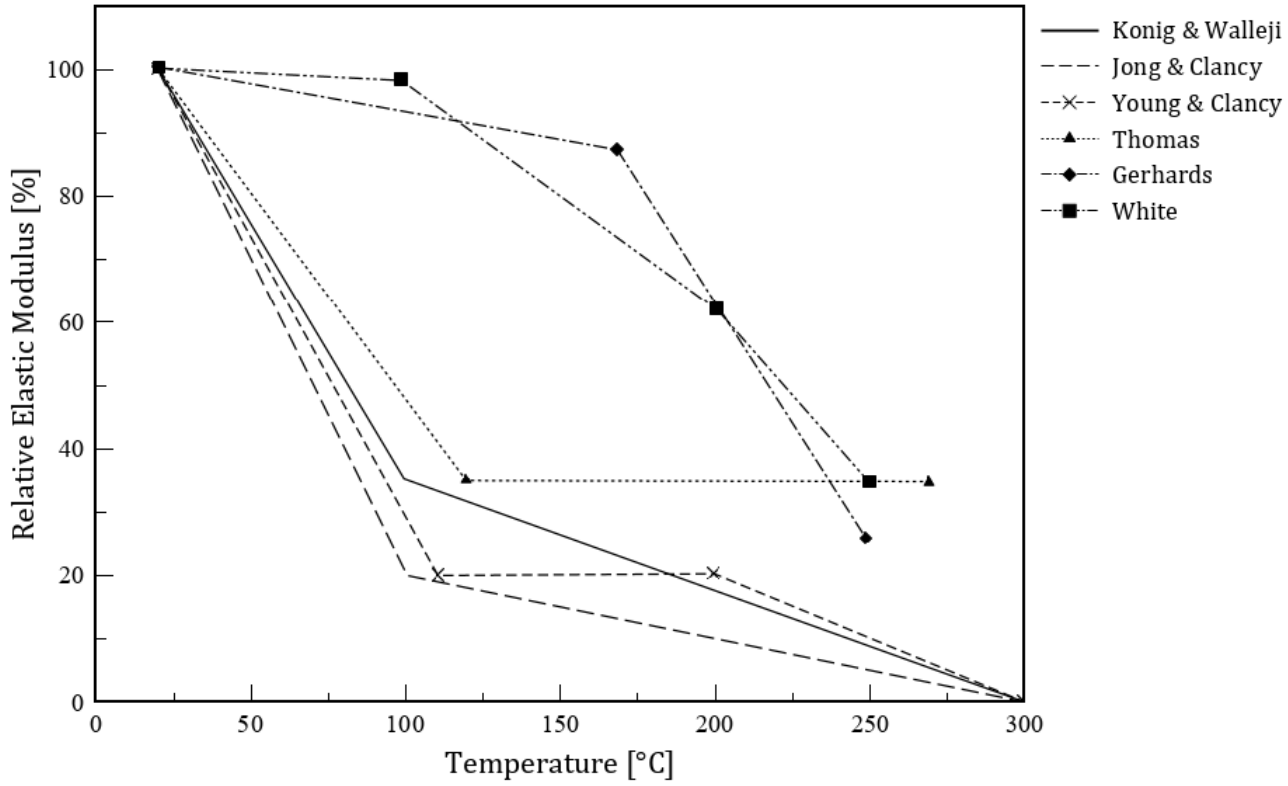

Figure 1-10 Reduction of elastic modulus of wood with temperature ([21], [46], [96] as referenced by [4] and [93], [97], [94] as referenced by [21])

Comprehensive models on the other hand attempt to capture the complex chemical processes that result from the heating up of the material and hence calculate the pyrolysis

rate by implementing kinetic schemes of the chemical decomposition and solving mass and energy balance. First order kinetic schemes are mostly employed and could vary in complexity from one-step global schemes to multi-step semi-global schemes [95].

The earliest model proposed by Bamford et al. [98] for charring of an infinitely thick wooden slab heated equally on each side, given by the differential energy equation below:

$$\rho c \frac{\partial T}{\partial t} = K \frac{\partial^2 T}{\partial x^2} - q \frac{\partial w}{\partial t} \qquad \text{Eq. 12}$$

Where K is the thermal conductivity, T is the temperature, x is the distance, w is the weight of volatile products per c.c of wood, t is time, q is the heat given out at a steady pressure per gram of volatile product produced, c and ρ are the specific heat and density respectively.

The model considers the heat conduction into and away from a location as well as the energy given off by thermal decomposition for constant wood and char thickness. Thermal properties of timber and char were assumed to be constant and hence independent of temperature. Bamford el at. [98] modelled the rate of decomposition using a unimolecular Arrhenius equation.

Later modifications to the above model were made including a convective term representing the heat transferred by convection of the volatile gases moving into or out of the material, caused by a temperature gradient to give [99]:

$$\rho c \frac{\partial T}{\partial t} = K \frac{\partial^2 T}{\partial x^2} + M c_g \frac{\partial T}{\partial x} - q \frac{\partial w}{\partial t} \qquad \text{Eq. 13}$$

Where M and c_g are the local mass flow and the specific heat of the volatile gases, respectively. This model is applicable to an infinitely wide and thick wooden slab and assumes constant properties (both thermal and physical) of the wood and char.

To account for temperature dependent properties, Kung [100] modified the above model to include temperature-varying density, specific heat, and thermal conductivity as well as internal heat convection by the outward movement of volatile gases. The model was

developed for a non-porous wooden slab heated from one side and insulated from the other. Several modifications to Kung's model have so far been carried out to include the effects of shrinkage, swelling porous materials as well as moisture content [95].

Ritcher and Rein [101] developed a multiscale model of wood pyrolysis that takes into account the complex chemical processes involved in the decomposition of cellulose, hemicellulose and lignin (main components of wood) and oxidation of the resulting products to predict charring rates. The model solves the solid phase's density, momentum, and energy conservation equations, and the gas phase's mass conservation equations.

Lautenberger and Pello [102] applied a generalized pyrolysis model (Gpyro [103]) to mimic the oxidative combustion of wood under heat fluxes below 40 kW/m2. Mass, energy and momentum conservation equations of the degrading wood are computed to obtain temperature, mass fraction and pressure profiles. The model contains four solid species, seven gaseous species and six reactions (four solid and two gas).

The heat transfer model proposed by Reszka and Torero [104] assumes a non-reacting, semi-infinite solid with thermal properties of virgin wood. This model performed well during the early stages of heating while overestimating the temperature as heating progressed. This could be attributed to the inability of the model to account for the heat sink caused by moisture evaporation or the reduced heat transfer due to the insulation property of the char layer. Although this model does not account for complex phenomenon such as surface oxidation, kinetics of the pyrolysis reactions, moisture movement/evaporation and pressure gradients, it can be used to study the stages of heating where such sub-models can be applied to get a better approximation of reality.

With practitioners and engineers in mind, comprehensive models such as those discussed above are of limited use as they require a lot of input data and are overly sophisticated for everyday use in the field. As such, the use conventional heat transfer models with the inclusion of effective thermal properties of timber to implicitly account for inherent phenomena caused by thermal degradation such as the movement of moisture and volatile gases, provides a more practical approach [30][83].

1.10 Burnout Resistance

Burnout resistance can simply be described as the ability of a structural member to survive the throughout or beyond the cooling stage of a fire [105]. After the heating phase, a thermal wave persists and this penetrates further into the cross-section, heating up parts of the cross-section that were previously unheated. The maximum depth reached by this wave is referred to as the thermal penetration depth [106]. This generates further losses in strength due to the mechanical degradation resulting from the additional heating and would lead to more adverse reduction in structural capacity as opposed to one would have designed for under for example, a standard fire consisting of only a heating phase. Burnout resistance is a major concern for the different types of construction materials however more prominent for timber construction since mechanical degradation occurs at considerably lower temperatures (as opposed to steel or concrete).

Current regulations specify fire resistance ratings based on the ability of a structural member to withstand a standard fire curve in a furnace test without losing its load bearing capability as well as its fulfilment of other criteria. Once a structural member survives a certain period of time under such test, it is deemed safe for use and given a rating, for example R60 - meaning the member was able to survive 60 minutes of standard fire exposure. This method is lacking as it does not account for further reduction in the load carrying capacity of the member beyond the heating phase as explained above.

The importance of burnout resistance has been investigated and illustrated to be very crucial both experimentally and numerically. From full-scale CLT compartment fire experiments carried out by Wiesner et al. [106], it was reported that thermal penetration continued for at least an hour after the fuel load was consumed and auto-extinguishment achieved. Up to 25 mm of additional depth was heated beyond 60 °C which led to considerable reduction in load bearing capacity.

This phenomenon was also numerically investigated for steel and concrete [105] as well as timber [107] leading to the coining of the term ‘duration of heating phase’ used to describe the minimum fire duration to which if a member is exposed to, would fail during the decay phase. A comprehensive FEA modeling of loaded timber columns tested under standard fire exposures was undertaken with the inclusion of a linear cooling phase at a rate of 10.4 C/min

revealed that the minimum DHP of the modeled columns lay between 20 to 50% of their respective fire resistance rating [107]. This translates to failure of columns during the cooling phase after being subjected to only a fraction of their standard fire curve rating.

1.11 Problem Statement

Cross laminated timber is a fairly new engineered timber product that is famously utilized for the construction of load bearing panels such as walls and slabs. While its behavior under ambient conditions can be easily predicted, this is not the case under fire conditions. The codified methods and assumptions for design of timber members in fire have been originally developed for solid and glulam timber members, however, their applicability for the fire design of CLT members requires further analysis. Additionally, designers and manufacturers are still experimenting with different ply numbers, arrangements, thicknesses, wall heights and end restraints and how these parameters will influence the performance of a CLT member in fire. A parametric study taking into accounting how these variables affect fire performance of CLT load bearing walls is deemed necessary.

1.12 Project Aims and Objectives

This thesis aims to numerically investigate the performance of CLT structural elements, particularly CLT load bearing walls in fire. The outcome of this thesis aims to serve as a guide to engineers and designers when designing CLT walls providing them with insight as to best approaches for optimal performance. The following objectives have been defined in this thesis:

- Numerical modeling of the heat transfer through a CLT cross-section as well as modelling of the thermomechanical degradation of the wall according to the advanced method outlined in Annex B of EN 1995-1-2 [49].
- An analysis of the existing codified methods for design of CLT load bearing walls under standard and parametric fire conditions.
- Carry out a parametric study to investigate the influence of several parameters such as wall height, end support conditions, number, arrangement, and thickness of plies on the performance of load bearing CLT walls in fire.

- Develop a tool to that can be utilized by engineers and designers alike serving as a guide in their design process for CLT walls.

2 METHODOLOGY

In this section, the basis of the model developed including equations and procedures will be outlined. All steps and procedures are coded in the MATLAB programming language developed by MathWorks [108]. MATLAB is a programming language that enables matrix manipulation, feature plotting and data, algorithm execution, user experience design and interface with programs written in other languages.

To model the behavior of structural timber elements in fire it is essential to accurately model the heat transfer to obtain precise temperature profiles in-depth. The temperature data from the heat transfer analysis is then used as input data for the structural analysis to compute the loading bearing capacity of the member in question. It can be therefore inferred that a decoupled thermal and structural approach is employed in this model. Focus here will be on pure crushing and pure buckling load carrying capacities. It is assumed that the glue lines remain intact and hence no delamination and or debonding occur.

Although there exists numerous research on charring rates, thermal properties, strength reduction factors and other methods, the focus here will be on the information and methods contained in part two of EC 5 [49] as this is the current standard available to designers and to which the authorities having jurisdiction will assess compliance against.

2.1 Thermal Analysis

2.1.1 Heat Transfer Modelling

To accurately predict the temperature profiles in a timber cross-section, the heat transfer throughout its depth must be modeled. Taking a timber member located in a compartment with fire, the heat transfer mechanisms can be simplified as shown in Figure 2-1. Heat is transferred onto the surface of the member by convection and radiation. This heat is then conducted throughout the member as illustrated in Figure 2-1. Heat transfer inside the timber section is modeled by solving an explicit, one-dimensional, transient heat transfer (conduction) equation without heat generation using the finite difference method. This solving scheme was selected because it enables the time derivative to be measured using forward differences. Small steps in the space and time domains will lead to convergence to

the exact solution. This solution scheme can be reversed with an expansion of the Taylor series by reversing its discretization mechanism to retrieve the governing partial differential equation for specific time and space steps. Any random errors resulting in the solution for example, round-off error, will eventually decay or be limited.

The transient heat conduction equation is given by:

$$\rho c_p \frac{\partial T}{\partial t} = \frac{\partial}{\partial x}\left(k \frac{\partial T}{\partial x} \right) \qquad \text{Eq. 14}$$

where ρ is the density in $kg \cdot m^{-3}$, c_p is the specific heat in $J \cdot kg^{-1} \cdot K^{-1}$, T is the temperature in K, t is the time in s, x is the distance in m and k is the thermal conductivity in $W \cdot m^{-1} \cdot K^{-1}$

The right-hand side term represents the energy conducted and the left-hand side term represents the energy required to increase the temperature.

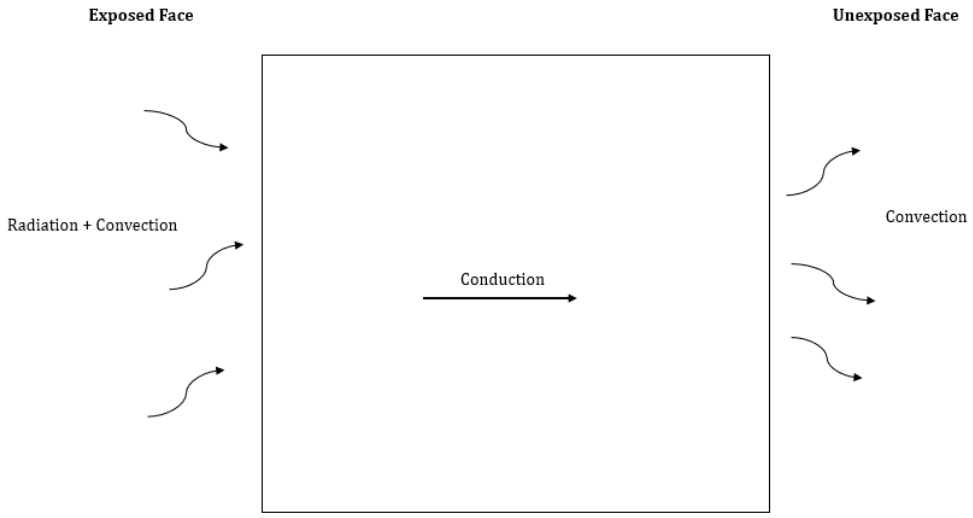

Figure 2-1 Simplified heat transfer modes for a timber member in a compartment fire. Note: conduction is moving away from the exposed surface

The ratio of the thermal conductivity to the product of the density and specific heat can be given by:

$$\alpha = \frac{k}{\rho c_p} \qquad \text{Eq. 15}$$

where α is the thermal diffusivity in $m^2 \cdot s^{-1}$.

Simplifying,

$$\frac{\partial T}{\partial t} = \alpha \frac{\partial^2 T}{\partial x^2} \qquad \text{Eq. 16}$$

Applying finite difference method:

$$\frac{\partial T}{\partial t} = \frac{T_i^{j+1} - T_i^j}{t^{j+1} - t^j} = \frac{T_i^{j+1} - T_i^j}{\Delta t} \qquad \text{Eq. 17}$$

$$\frac{\partial^2 T}{\partial x^2} = \frac{\frac{T_{i+1}^j - T_i^j}{\Delta x} - \frac{T_i^j - T_{i-1}^j}{\Delta x}}{\Delta x} = \frac{T_{i+1}^j - 2T_i^j + T_{i-1}^j}{(\Delta x)^2} \qquad \text{Eq. 18}$$

Combining Eq. 17 and Eq. 18 above:

$$\frac{T_i^{j+1} - T_i^j}{\Delta t} = \alpha \left(\frac{T_{i+1}^j - 2T_i^j + T_{i-1}^j}{(\Delta x)^2} \right) \qquad \text{Eq. 19}$$

Including temperature dependent properties gives:

$$T_i^{j+1} = T_i^j + \frac{k(T)}{\rho(T) c_p(T)} \Delta t \left(\frac{T_{i+1}^j - 2T_i^j + T_{i-1}^j}{(\Delta x)^2} \right) \qquad \text{Eq. 20}$$

where i and j represent a step in the space and time domain respectively, as shown in Figure 2-2. The cross-section is divided into slices of 1 mm thickness and a time step of 0.01 s is used.

2.1.2 Initial and Boundary Conditions

To solve equation Eq. 20 above, a set of initial and boundary conditions are necessary. It is assumed that at t = 0, the temperature inside the timber is at ambient (20 °C), therefore:

$$T(x, t = 0) = 20^{\circ}C$$

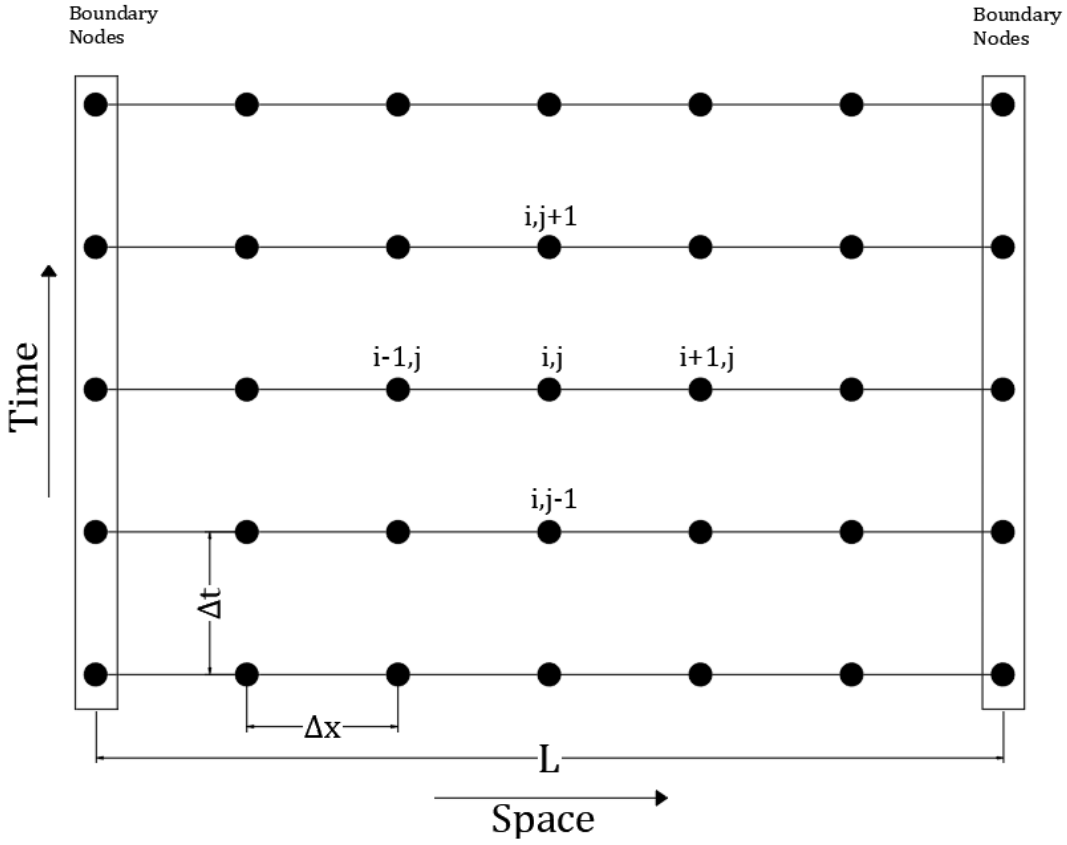

Figure 2-2 Finite difference discretization of a one-dimensional heat conduction equation

2.1.3 Surface temperature

By solving the heat transfer equations on the timber front, the surface temperature is obtained. As shown in Figure 2-1, the main modes of energy transfer to the surface are by radiation and convection. The heat transfer equation is therefore given by:

$$\frac{\rho c_p \delta T}{\delta t} = q_{rad} + q_{conv} - q_{cond} \qquad \text{Eq. 21}$$

and

$$q_{rad} = \varepsilon\sigma({T_g}^{j\,4} - {T_i}^{j\,4})$$
$$q_{conv} = h({T}^{j}{}_{g} - {T_i}^{j})$$
$$q_{cond} = k\frac{\partial T}{\partial x} \qquad \text{Eq. 22}$$

Where q_{rad}, q_{conv}, and q_{cond} are heat contributed by radiation, convection and conduction respectively, ε is the emissivity taken as 0.8 as per EN 1995-1-2 [49], σ is the Stefan-Boltzmann constant taken as 5.67 x 10^{-8} $W \cdot m^{-2} \cdot K^{-4}$, T_g is the gas temperature in K, T_i is the temperature of the timber slice in K, h is the convective heat transfer coefficient taken as 25 $W \cdot m^{-2} \cdot K^{-1}$ or 35 $W \cdot m^{-2} \cdot K^{-1}$ for standard fire exposure or parametric fire exposures respectively as per EN 1995-1-2 [49].

Simplifying Eq. 21 above, the temperature at the surface is given by:

$$T_1^{j+1} = T_1^{j} + \frac{\Delta t}{\Delta x \rho(T) c_p(T)}\left(\varepsilon\sigma({T_g}^{j\,4} - {T_1}^{j\,4}) + h({T}^{j}{}_{g} - {T_1}^{j}) - \frac{k(T)}{\Delta x}(T_2^{j} - T_1^{j})\right) \qquad \text{Eq. 23}$$

At the unexposed side of the timber member, heat will be lost to the surroundings by convection. Temperatures are not expected to be high enough for radiative losses to be considered. Therefore, at x = L the heat transfer equation is given by:

$$\frac{\rho c_p \delta T}{\delta t} = q_{cond} - q_{conv} \qquad \text{Eq. 24}$$

Simplifying, the temperature at x = L is given by:

$$T_n^{j+1} = T_n^{j} + \frac{\Delta t}{\Delta x \rho(T) c_p(T)}\left(-\frac{k(T)}{\Delta x}(T_n^{j} - T_{n-1}^{j}) - h({T}^{j}{}_{g} - T_1^{j})\right) \qquad \text{Eq. 25}$$

2.1.4 Thermal Properties

The temperature dependent thermal properties are modeled using the properties outlined in the advanced method of EN 1995-1-2 given in its Annex B [49] as shown in Figure 2-3. A slight modification to the density is made to avoid division by zero error when computing the thermal diffusivity. The value for the relative density at 1200 °C and beyond was set to a small number 0.1 (instead of zero). The model is capable of accounting for the recovery and irreversibility of these thermal properties during the decay phase of a fire when temperatures revert to ambient conditions.

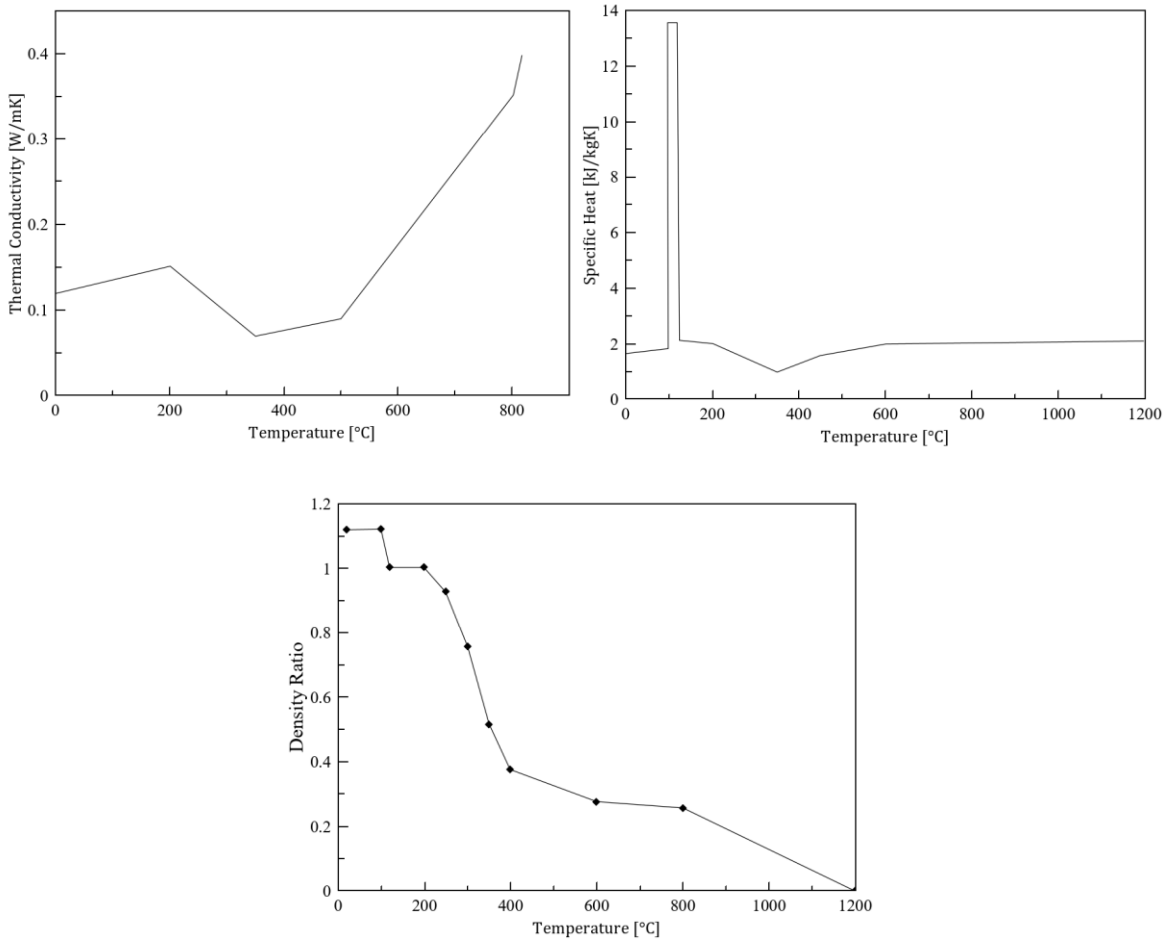

Figure 2-3 Thermal properties of wood used in this model as per EN 1995-1-2 [49]

2.1.5 Temperature Input

The model is created in a versatile way and can accept different time-temperature curves as input to simulate compartment temperatures. The user can specify standard fire curves,

parametric fire curves (with heating and cooling phases) as well as any other curves. The input data is fed to the model with a csv file format containing the time in seconds (starting at t=0s) and temperature in Celsius (starting at ambient temperature).

2.2 Structural Analysis

Using the in-depth temperature distributions obtained from the thermal analysis, the residual load bearing capacity of the member is evaluated. The codified compressive strength and elastic modulus reduction factors (Figure 2-4) defined in the advance method in Annex B of EN 1995-1-2 [49] are used to compute the buckling and compressive load capacities throughout the fire duration.

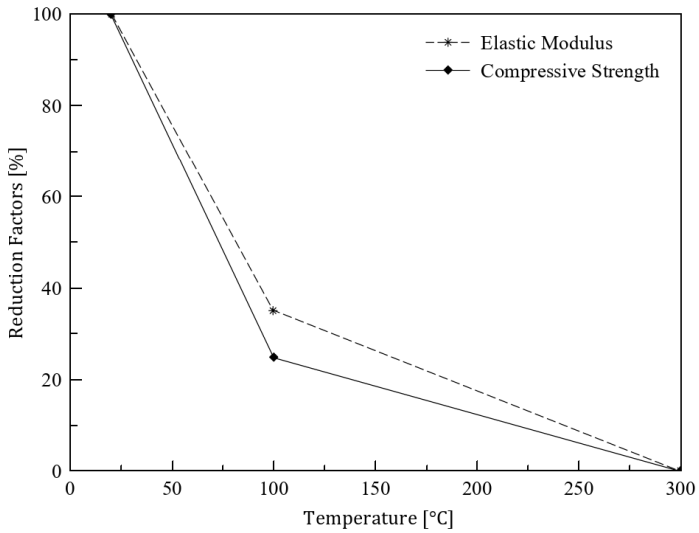

Figure 2-4 Strength and stiffness reduction factors used in this model [49]

An extra model accounting for the recovery of strength and stiffness of the member as it cools down is incorporated in the model. This aims to quantify the extent to which the member regains a portion of its mechanical properties during the cooling phase. This model does not depict reality but is employed here for comparison and research purposes. It is worth noting that recoverable thermal properties of the member are used in this case.

2.2.1 Crushing Load Capacity

Estimating the crushing load capacity of compression members is the most basic requirement to check structural resistance against axial loads. Due to the nature of ply layup in CLT elements, almost all the load carrying capacity stems from the longitudinal plies. The

crosswise plies are sometimes assumed to have negligible strength [22]. In this thesis just as with the elastic modulus, it is assumed that the compressive strength of the crosswise layer is one thirtieth (1/30) of that of the longitudinal layer [4]. The procedure for calculating the crushing load capacity is as follows:

At each time step:

- The residual compressive strength of each slice is computed from the temperature-dependent reduction factors in Figure 2-4 using the corresponding temperature at that slice obtained from the thermal analysis.
- The crushing load capacity of each slice is then computed by multiplying the area with the temperature reduced compressive strength as follows:

$$Cs_i = A_i \, fc_i(T) \qquad \text{Eq. 26}$$

  Where Cs_i is the crushing load capacity of slice i in N, A_i is the area of slice i in mm^2 and $fc_i(T)$ is the temperature-dependent compressive strength of slice i in $N \cdot mm^2$
- The total crushing load capacity of the cross-section is then calculated by summing the individual crushing loads of each slice as follows:

$$Cs = \sum_{1}^{n} A_i \, fc_i(T) \qquad \text{Eq. 27}$$

  Where Cs is the crushing load capacity of the cross-section in N.
- Parts of the cross-section that exceed 300 °C are assigned zero strength and eliminated.

2.2.2 Buckling Load Capacity

An important critical load for compression members is the buckling load. It can be defined as the lateral failure of a structural element subjected to compressive axial loads, and for

slender members, it is less than the crushing capacity of that member. The critical buckling load is given by the Euler buckling equation as:

$$\frac{\pi^2 EI}{cH^2} \qquad \text{Eq. 28}$$

Where E is the modulus of elasticity in MPa, I is the second moment of inertia of the cross-section in mm^4, c is a factor depending on the support conditions, H is the height of the member in m.

The second moment of inertia is given by:

$$I = \frac{b\,d^3}{12} \qquad \text{Eq. 29}$$

Where b, d are the dimensions of the cross-sections in mm and will depend on the axis.

For a CLT member, the layup of plies in a crosswise manner introduces a slight complexity when calculating I due to the different orientations parallel and perpendicular to span direction. The ratio of the elastic modulus of longitudinal layer to the crosswise layer can be taken as 30 [4], hence the crosswise layers must be transformed into equivalent depths of longitudinal layers before the second moment of inertia is calculated, hence buckling load can then be calculated. This procedure describes the calculation of buckling load of CLT members under ambient conditions.

In a fire however, the temperature induced reduction in elastic modulus must be considered. Each affected slice of the cross-section can be regarded as a different material (with different E) and must be transformed into an equivalent thickness of virgin timber resulting in a shift in the neutral axis of the whole cross-section. This therefore requires a stepwise procedure that calculates the reduction in elastic modulus of the heat affected zones, transformation to an equivalent depth of timber at ambient conditions, followed by calculating the second moment of area of the transformed cross-section while accounting for the shifts in the

neutral axis due to the transformation. Parts of the cross-section that reach temperatures of 300 °C and above are eliminated (since E = 0) and the residual cross-section is used for computation of the buckling load.

The procedure to compute the buckling load of a CLT compression member is given below :.

At each time step, the buckling load is calculated as follows:

- The temperature-dependent elastic modulus for each slice in the cross-section is computed using the corresponding temperature distribution obtained from the thermal analysis.
- The depth of the heat affected slices parallel to the weak axis (y-axis in this case) are transformed to an equivalent depth of virgin timber by:

$$d(x,t)_{C-T} = \frac{d}{n}$$

$$n = \frac{E_{amb}}{E(T)} \qquad \text{Eq. 30}$$

  where $d(x,t)_{C-T}$ is the transformed depth of the cross-section in mm at a distance x and time t, E_{amb} is the elastic modulus of virgin timber at ambient conditions in MPa and $E(T)$ is the temperature-dependent elastic modulus in MPa. For crosswise layers, E_{amb} is divided by 30 before n is computed.
- The coordinates of the transformed cross-section are computed and stored as shown in Figure 2-5
- Using the coordinates of the transformed cross-section, the transformed second moment of area of the entire cross-section is computed using an procedure outlined in [109] and is given as follows:
    - For an arbitrary shape idealized as a polygon of N sides, the integral over its area is given by:

$$H_{mn} = \int x^m y^n dA$$

Eq. 31

- Expressing the integral as a summation:

$$H_{mn} = \sum_{i=1}^{N} \Delta_i$$

Eq. 32

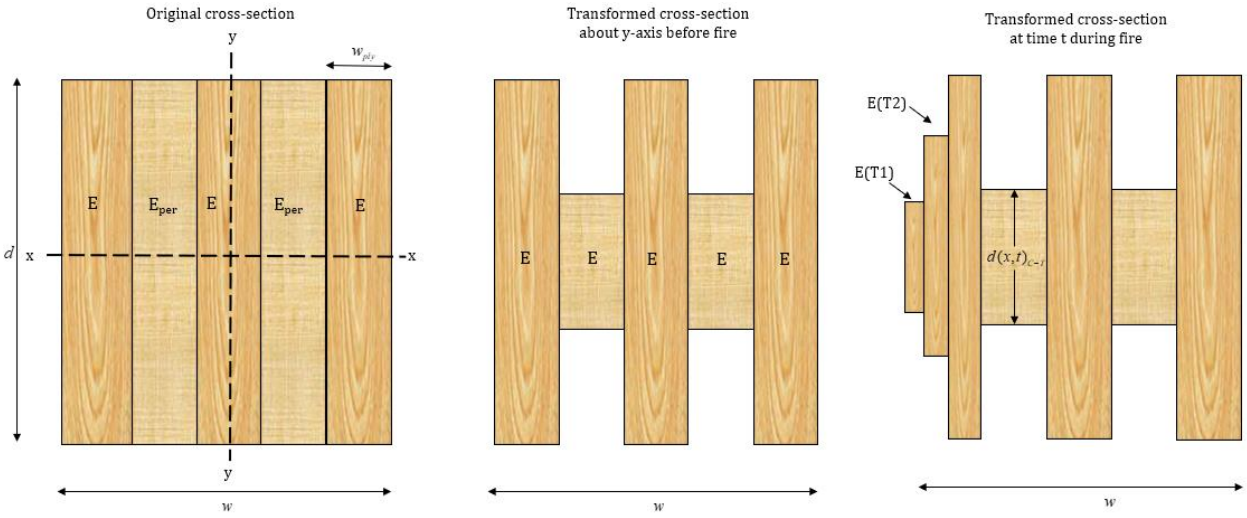

Figure 2-5 Original 5-ply CLT cross-section (left) and its transformed CLT cross-section (middle) at ambient temperature and transformed section during fire. E – ambient elastic modulus, E_{per} – perpendicular elastic modulus, E(T) – elastic modulus at temperature T.

- The value of the integral over the area between the x axis and the *i*th side of the perimeter is given by:

$$\Delta_i = \int_0^{\Delta x_i} \int_0^{y_i + \frac{\Delta y_i}{\Delta x_i}} (x_i + \bar{x})^m y^n dy d\bar{x}$$

Eq. 33

- Simplified to give:

$$\Delta_i = \frac{1}{n+1}\int_0^{\Delta x_i} (x_i + \bar{x})^m \left(y_i + \frac{\Delta y_i}{\Delta x_i}\bar{x} \right)^{n+1} d\bar{x} \qquad \text{Eq. 34}$$

- Where

$$\bar{x} = x - x_i$$

$$(y)_{ith\_side} = y_i + \frac{\Delta y_i}{\Delta x_i}\bar{x}$$

$$\Delta x_i = x_{i+1} - x_i ; \Delta y_i = y_{i+1} - y_i$$

- Substituting each of the two terms in eqn A7 by its binomial expansion and integrating gives:

$$\Delta_i = \frac{1}{n+1}\left\{ \sum_{j=0}^{m} \left[c_{mj} x_i^{m-j} (\Delta x_i)^{j+1} \left(\sum_{k=0}^{n+1} c_{(n+1)k} \frac{y_i^{n+1-k} (\Delta y_i)^k}{k+j+1} \right) \right] \right\} \qquad \text{Eq. 35}$$

  Where

$$c_{mj} = \frac{m!}{j!(m-j)!}$$

- Eq. 35 is incorporated into the computer model and calculates the area of the section by specifying $m = n = 0$, the second moment of area of the section about the x-axis (of the cartesian plane) when $m = 0; n = 2$ and the second moment of area of the section about the y-axis when $m = 2; n = 0$.

- The buckling load for that time step is then computed as follows:

$$\frac{\pi^2 E \sum_i^n I_{Tr,i}}{cH^2} \qquad \text{Eq. 36}$$

The procedure for calculating the buckling capacity is illustrated in Figure 2-6. An overview flow chart of the thermal and structural model is given in Figure 2-7.

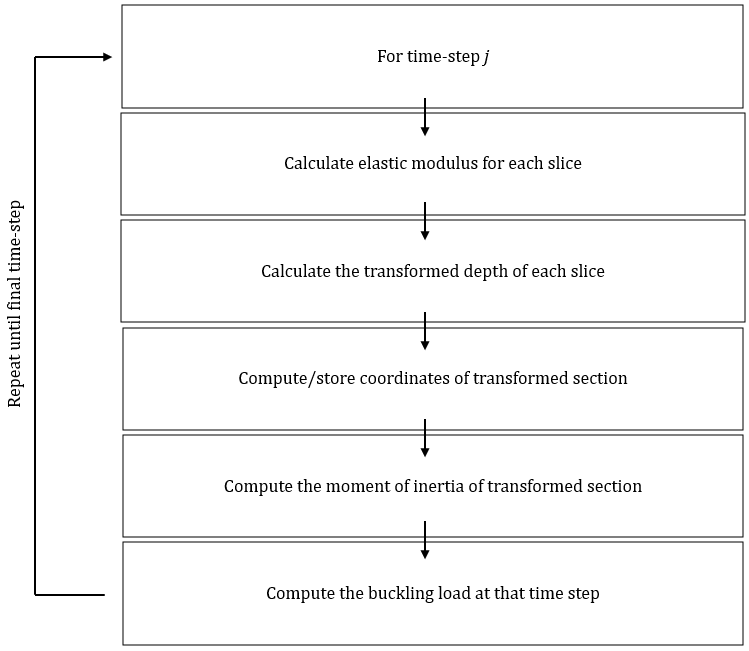

Figure 2-6 Calculation procedure for the buckling load capacity of a CLT cross-section

2.2.3 The Reduced Cross-section Method

The RCSM is incorporated into the model to compute the load carrying capacity of the member in question. This is done to compare the RCSM with the advanced method in EN 1995-1-2 [49]. Two models are defined based on the charring rate: the charring rate obtained directly from the thermal analysis, computed from the position of the 300 °C isotherm, and the predefined one-dimensional charring rate given in EN 1995-1-2 [49]. The procedure to determining the crushing and buckling load capacities is similar to the outlined methods above, however the effect of the thermally affected zone is only limited to a zero-strength layer equal to 7 mm, for both models.

The effective char depth under standard fire conditions is calculated as follows:

$$d_{char\_eff} = d_{char} + d_o,$$

For parametric fires β_{par} is calculated using $\beta_n = 0.7mm/\min$ as:

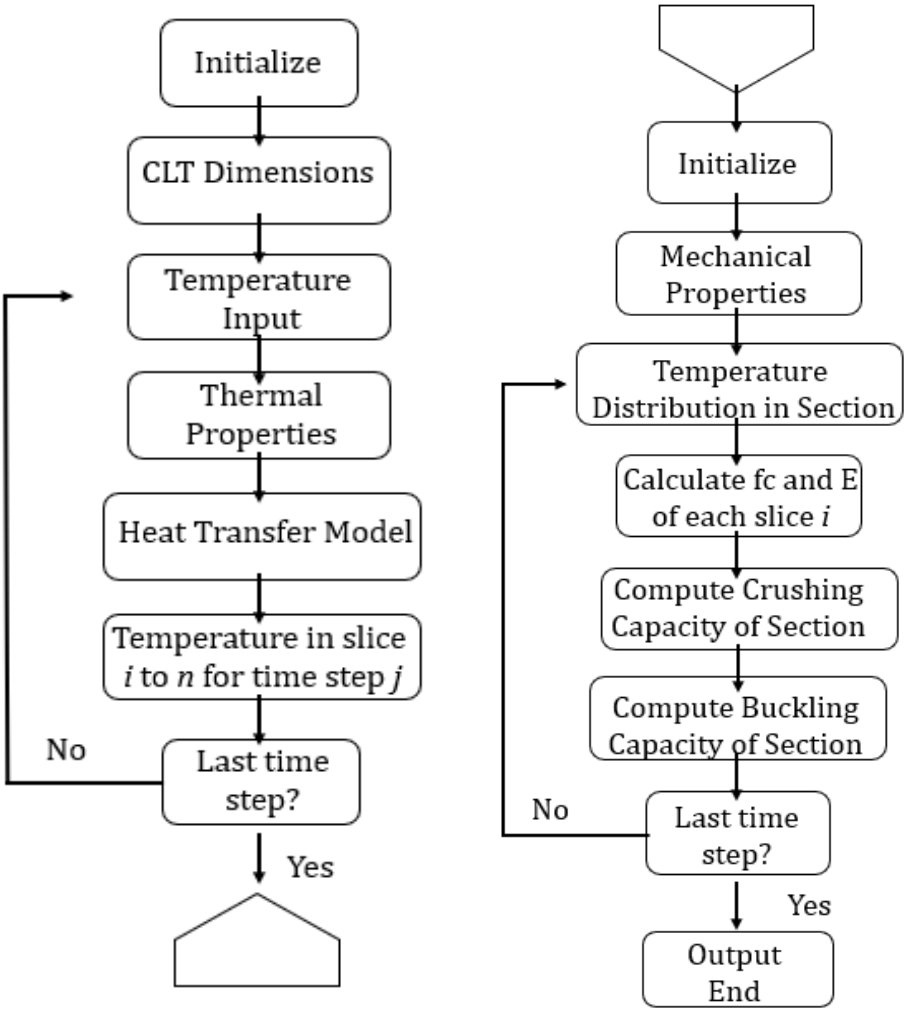

Figure 2-7 Model flow chart for thermal analysis (left) and structural analysis (right)

$$d_{char\_eff} = \begin{cases} \beta_{par} t + d_o & \text{for } t \le t_0 \\ \beta_{par}\left(1.5t - \dfrac{t^2}{4t_0} - \dfrac{t_0}{4}\right) + d_o & \text{for } t_0 < t < 3t_0 \\ 2\beta_{par} t_0 + d_o & \text{for } 3t_0 < t < 5t_0 \end{cases}$$

Where d_{char_eff} is the effective char depth, d_o is the zero-strength layer.

The residual cross-section depth is then given by:

$$d_{residual} = d - d_{char\_eff}$$

For the purpose of this study, the following notations are used for easier communication:

- Model 1 (M1) : refers to the advanced model outlined in EN 1995-1-2 [49].
- Model 2 (M2): refers to the advanced model with recoverability of properties.
- Model 3 (M3): refers to the RCSM using the 300 °C isotherm.
- Model 4 (M4): refers to the RCSM using EN 1995-1-2 [49] charring rate.

2.3 Model Input

Several input variables are required for carrying out the simulations. First, the cross-section and wood properties must be defined. Cross-section dimensions including number and thickness of lamellae, ambient compressive strength, ambient elastic modulus, ambient density, initial moisture content, support conditions and member height. Table 1 outlines the input parameters used. For all simulations, a unit length of wall is defined.

Table 1 Model input variables

Input Variable	Value
Cross-section dimensions	Varying (See below)
Compressive strength	24 MPa
Elastic Modulus	11000 MPa
Density	470 kg/m3
Moisture content	12%
Support condition	Varying
Member Height	3 or 4.8 m [1]

2.4 Study Cases

CLT being a new product, designers and manufacturers are still experimenting with different layup arrangements and thicknesses to achieve optimum strength. Under ambient conditions, checking the performance of these arrangements and thicknesses can easily be achieved through simple equations or by carrying out simple loading tests. In fire however, the performance of these new inventions requires a more in-depth analysis. The order and

thickness of layups will be investigated here to give designers and manufacturers a basic idea about what combination of layups and thicknesses will give the best performance in fire.

A survey of available CLT products for walls from various manufacturers such as Binderholz [110], Mayr Melnhof Holz [111], Stora Enso [112], KLH [113], Zueblin Timber [114] and Hasslacher Norica Timber [115] showed that 3-ply CLT walls range in overall thickness from 60 to 120mm, 5-ply range from 100 to 240mm and 7-ply range from 180 to 280mm. The arrangement and thickness of plies in these products differ between manufacturers and per manufacture's product range.

2.4.1 Fire Scenarios

Different fire curves will be employed to investigate the fire performance of the CLT members in this study. The temperature-time data from these curves is used as input for the model described above. The selection of the curves considered aims to analyze the effects of different heating phases (with different peak temperatures) and their duration as well as how the structural capacity declines during the decay phase due to the thermal wave that propagates through the cross-section. The fire curves implemented are briefly described below and are shown in Figure 2-8 . These curves were selected to analyze the effect of different heating scenarios such as

- 60-minute ISO Fire: Surviving a 60-minute ISO 834 fire [116] is the most basic requirement that has to be fulfilled by a structural element for it to be graded as a fire-resistant load bearing member, that is, the element must "survive" at least one hour of this curve, hence including this fire curve will investigate performance of CLT under this condition. After the heating phase, a cooling rate of 15.75 °C/min was applied until ambient to simulate the effects of burnout resistance. This cooling rate was selected at the author's discretion for academic purposes. A sensitivity of the cooling rate will be carried out in later sections.
- 120-minute ISO Fire: Similar to the 60-minute ISO fire curve [116], a two-hour curve is included here. Two hours is usually regarded as a maximum resistance that can be achieved [22]. Similarly, a cooling rate of about 16 °C/min is applied for 65 minutes until ambient.

- Short Parametric Fire: A short parametric fire curve was selected to mimic a short, intense natural fire with a prolonged cooling phase. This curve was constructed according to EN 1991-1-2 [117] for an office compartment with the following specifications as shown in Table 2.
- Long Parametric Fire: A long parametric fire curve will simulate a compartment fire with an extended heating duration followed by a gentle decay phase. Just as above, a library compartment will be used with specifications also shown in Table 2.

Table 2 Parametric fire curve details

Quantity	**Short Parametric Fire**	**Long Parametric Fire**
Room height (m)	3	3
Floor length (m)	10	10
Floor width	10	10
Opening factor	0.06	0.05
b $(J \cdot m^{-2} s^{-0.5} K^{-1})$	1160	1160
q_{fk} (MJ/m^2)	511	1824
q_{td} (MJ/m^2)	161.63	684

2.4.2 Parameter Study

Other than the fire scenarios, the effects of several parameters on the fire performance of CLT members will be analyzed. CLT products differ between countries and between manufacturers as well as within a manufacturer's product range. These products can also be custom made for a particular project by having specific ply layups and thicknesses. The parameters investigated here are:

- The number of plies,
- Member thickness,
- Individual layer thicknesses and arrangement,
- Influence of wall height
- Influence of support conditions

Simulations carried out for the parametric study are summarized in Table 3.

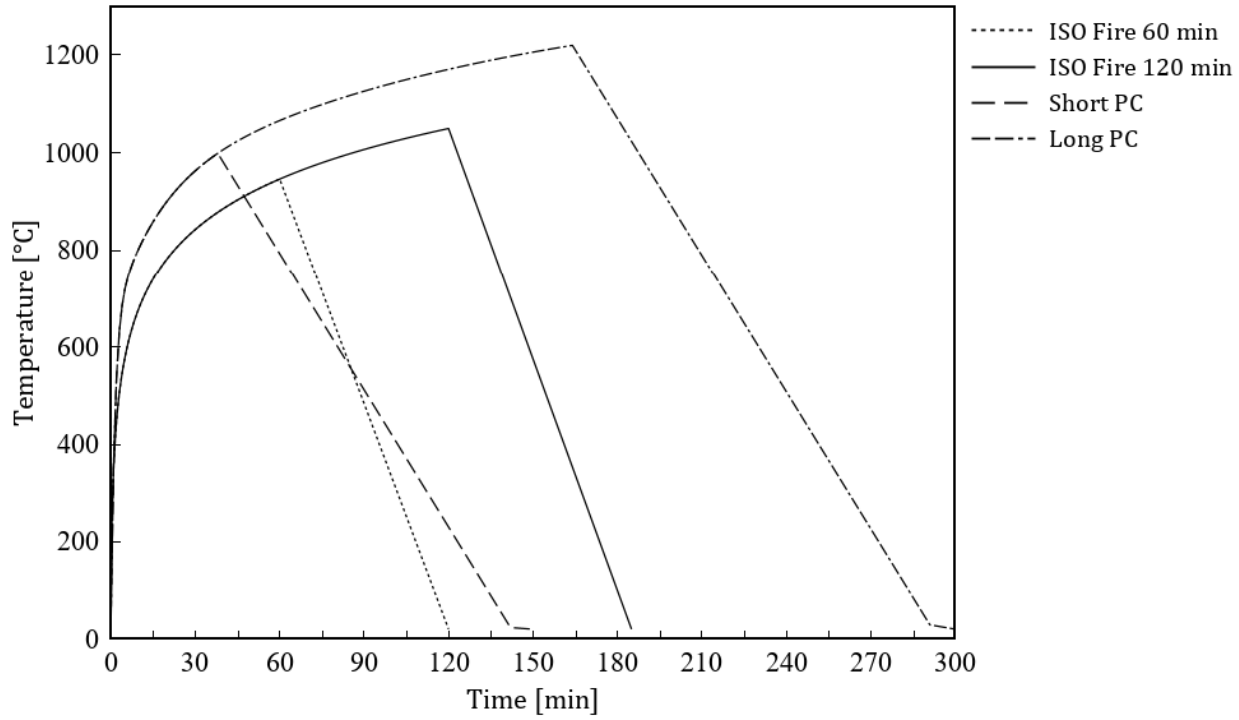

Figure 2-8 Fire curves investigated in this study.

Table 3 Simulations carried out in this study.

Ply Arrangement	Member Thickness (mm)	Ply Dimensions (mm)	Label
Uniform Plies	210 mm	3 Ply – 70 each	3-210-U
		5 Ply – 42 each	5-210-U
		7 Ply – 30 each	7-210-U
	105 mm	3 Ply – 35 each	3-105-U
		5 Ply – 21 each	5-105-U
		7 Ply – 15 each	7-105-U
Larger First/last Ply	210 mm	3 Ply – 85/40/85	3-210-FL
		5 Ply – 51/36/36/36/51	5-210-FL
		7 Ply – 40/26/26/26/26/26/40	7-210-FL

	105 mm	3 Ply – 42/21/42	3-105-FL
		5 Ply – 27/17/17/17/27	5-105-FL
		7 Ply – 20/13/13/13/13/13/20	7-105-FL
Larger Odd Plies (longitudinal layers)	210 mm	3 Ply – 85/40/85	3-210-O
		5 Ply – 50/30/50/30/50	5-210-O
		7 Ply – 36/22/36/22/36/22/36	7-210-O
	105 mm	3 Ply – 42/21/42	3-105-O
		5 Ply – 25/15/25/15/25	5-105-O
		7 Ply – 18/11/18/11/18/11/18	7-105-O
Larger Even Plies (crosswise layers)	210 mm	3 Ply – 60/90/60	3-210-E
		5 Ply – 30/60/30/60/30	5-210-E
		7 Ply – 24/38/24/38/24/38/24	7-210-E
	105 mm	3 Ply – 30/45/30	3-105-E
		5 Ply – 15/30/15/30/15	5-105-E
		7 Ply – 12/19/12/19/12/19/12	7-105-E

2.5 Development of a Tool for Capacity Checks

The models created above were used to create a simple tool with a graphical user interface (GUI) to enable its ease of use. A snapshot of the GUI is shown in Figure 2-9 and Figure 2-10 and a description on how to navigate it is given below.

Two tabs defining the thermal and structural analysis are outlined. The user begins by first going into the thermal analysis tab and defines the cross-sectional dimensions of the CLT member as well as the number and dimensions of plies. Up to 7 plies can be defined with the thickness of each ply inputted and comma separated. Properties such as the convective heat transfer coefficient, density, moisture content and emissivity can be defined by the user. Thermal conductivity and specific heat are however hard coded into the program and are according to the values provided in Annex B of EN 1995-2 [49]. The units of each input is shown next to the input box.

After defining the dimensions and properties, a temperature input file must be fed into the model which will be applied as thermal load onto the CLT member. The program can read CSV files with time in seconds, starting at time zero and temperature in Celsius, starting at ambient temperature.

Before running the thermal analysis, the user has the option of choosing between reversible and irreversible thermal properties by selecting the appropriate option from the dropdown list. Different data such as char depth, temperature at a particular depth, 300 °C isotherm and charring rate obtained from the thermal analysis can be plotted in the plot box located on the right by clicking on the 'plot' button. The 'copy' button copies the plotted data onto the user's system clipboard which can later be pasted for post processing purposes.

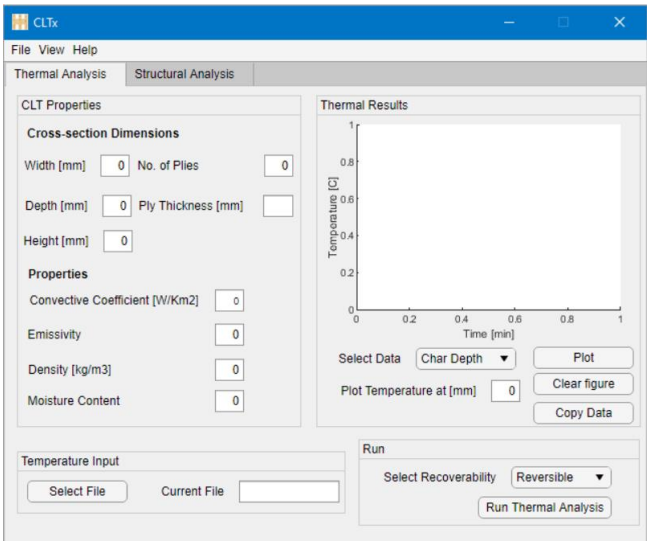

Figure 2-9 Snapshot of tool's GUI: thermal analysis tab

After running the thermal analysis, the next step is to head to the structural analysis tab. Variables such as the compressive strength, elastic modulus, charring rate, and zero-strength layer can be defined by the user. The user also has the option of selecting different support conditions from the dropdown list. The thermal and structural analyses are decoupled, meaning, for a particular thermal analysis, the user can run several structural analyses without needing to rerun the thermal analysis. This is especially important when the influence of a parameter such as the support condition is of interest. Similar to the thermal

analysis, the user can plot and copy the results from the different strength prediction models by selecting the desired model from the dropdown list.

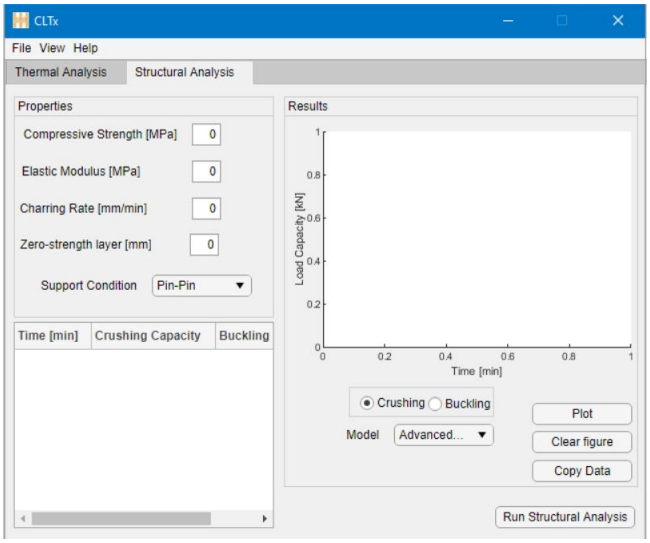

Figure 2-10 Snapshot of tool's GUI: structural analysis tab

3 RESULTS

In this section, results from the simulations will be presented and briefly discussed. Firstly, a validation of the heat transfer model presented above is carried out. This will be followed by an analysis of the different design models (M1-M4) after which a parametric study will be carried out. As outlined in section 2.4.1, different fire scenarios will be applied in this study, however, only the results for the 60-minute and short parametric fire curves will be presented in this section. Readers are referred to the appendix for results obtained for the 120-minute standard fire and long parametric fire curves.

Several other plots will also be included in the appendix as noted under each section.

This section contains the following subsections:

- Validation of heat transfer model
- Analysis of Strength Prediction Models Under Different Fire Conditions
- Effect of End Restraints
- Influence of Wall Height
- Effect of Number of Plies, Arrangement and Thickness

3.1 Validation of Heat Transfer Model

To accurately predict the load carrying capacity of the CLT cross-section, it is essential that the heat transfer model can capture with reasonable accuracy, the temperature evolution inside the exposed member. A small validation study of the heat transfer model outlined above is therefore carried out. The experiments carried out by Frangi and Fontana [39] on glulam and solid wood cross-sections are simulated and results compared with test data. Although solid wood is used in these experiments (instead of CLT), the heat transfer through the wood should be similar. They [39] carried out experiments on glulam and solid wood beams and slabs exposed to the standard fire curve on three sides and one side, respectively. Only data from the slab experiments are used since exposure is on one face, just as the model. As shown in Figure 3-1, simulation results agree well with experimental results. The model is able to accurately predict the temperature profile along the depth of the cross-section during the heating phase.

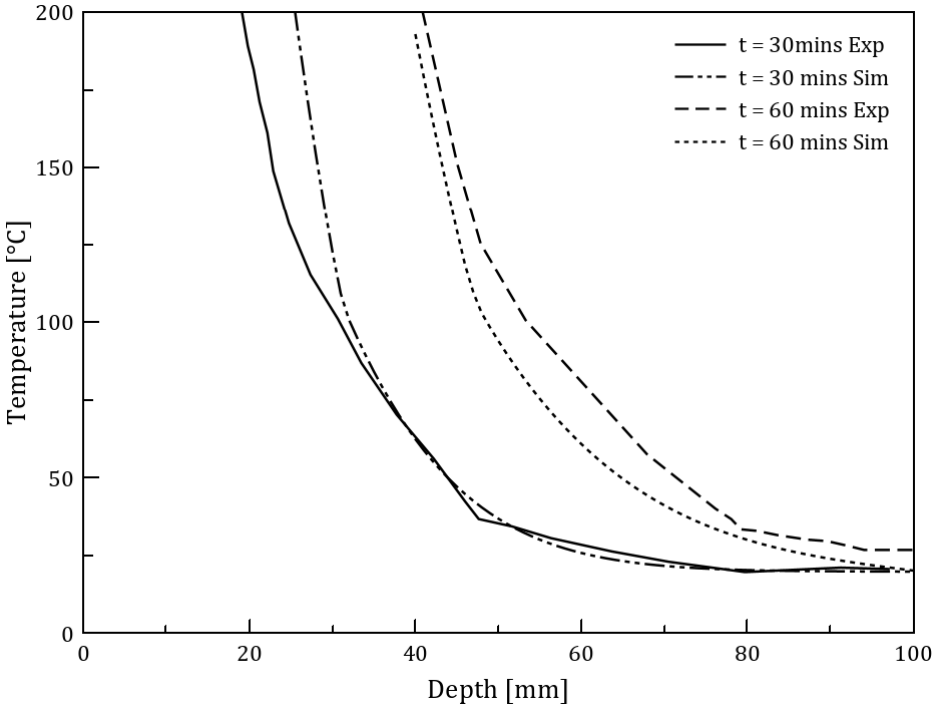

Figure 3-1 Validation of heat transfer model: simulation and experimental results

3.2 Analysis of Strength Prediction Models Under Different Fire Conditions

In this section, the different strength calculations models under the different fire curves as defined in the methodology will be analyzed. This analysis is carried out to check the adequacy of the RCSM (model M4) under standard and parametric fire curves using the one-dimensional and parametric charring rates respectively, as compared to other models (M1-M3) for CLT walls. The model(s) which give the most conservative results will be employed further to carry out a parametric study (see section 2.4.2).

Results are normalized to allow for the comparison of crushing and buckling load predictions of the different models. In later sections, a more critical look will be taken at the actual magnitudes of these loads and the implications of temperature-dependent strength reduction on the mode of failure.

Results will be presented for 3, 5 and 7-ply CLT for crushing and buckling strengths separately under the different fire curves.

3.2.1 60-Minute Standard Fire Curve

3.2.1.1 Results from Thermal Analysis: Charring Rate and Effective Charring Depth

The position of the 300 °C isotherm obtained from the thermal analysis is shown in Figure 3-2. The charring rate shown in Figure 3-2 is calculated based on the position of the 300 °C isotherm by dividing the depth of the 300 °C isotherm by the time taken to reach that depth. For comparison purposes, the one-dimensional charring rate as per EC 5 is also plotted on the same graph. The model is able to capture the behavior of a timber section in fire as outlined in section 1.4. During the initial stages of a fire, there is an initial spike in charring rate caused by the pyrolysis and char of the virgin timber surface. This occurs during the first 5.44 minutes (326.4 seconds) of fire exposure and results in a charring rate of 0.92 mm/min, equivalent to a char depth of 5 mm. As a thicker char layer forms, the insulating property of the char slows the conduction of heat through the cross-section. This is evident by the gradual change in slope of the position of the 300 °C isotherm and consequently the decline in the char rate. At the end of the heating phase, the achieved charring rate was 0.5 mm/min, considerably lower than the codified one-dimensional charring rate. Another interesting observation is the capability of the model to account for the thermal wave propagating through the section during the decay phase. There is a continued increase in the depth of the 300 °C isotherm beyond 60 minutes until 65 minutes followed by a plateau for the next 9 minutes. Subsequently, no more increase in depth is recorded and a sharp decline to zero follows. Similarly, charring rate gradually declines, and pyrolysis stops.

Figure 3-3 shows the effective charring depths computed based on the position of the 300 °C isotherm (long dash line) and according to the EC 5 method (short dash line) that will be employed later in models M3 and M4, respectively. The 300 °C effective char depth is a summation of the depth of the 300 °C isotherm and the zero-strength layer. At the beginning of the fire, the EC 5 effective char depth exceeds the 300 °C effective char depth. This is due to the 7 mm zero-strength layer that is immediately added at the smallest time step. With time, and as the timber front heats up and pyrolyzes, the 300 °C effective char depth exceeds that of the EC 5 until about 28 minutes where both depths are equal at 25.2 mm. This corresponds with the same time the char rate in Figure 3-2 crosses the EN char rate (0.65m). The EC 5 effective char depth continues to grow linearly until the end of the heating phase,

after which it seizes to increase. The 300 °C effective char depth however slightly increases beyond the heating phase until about 65 minutes as described above.

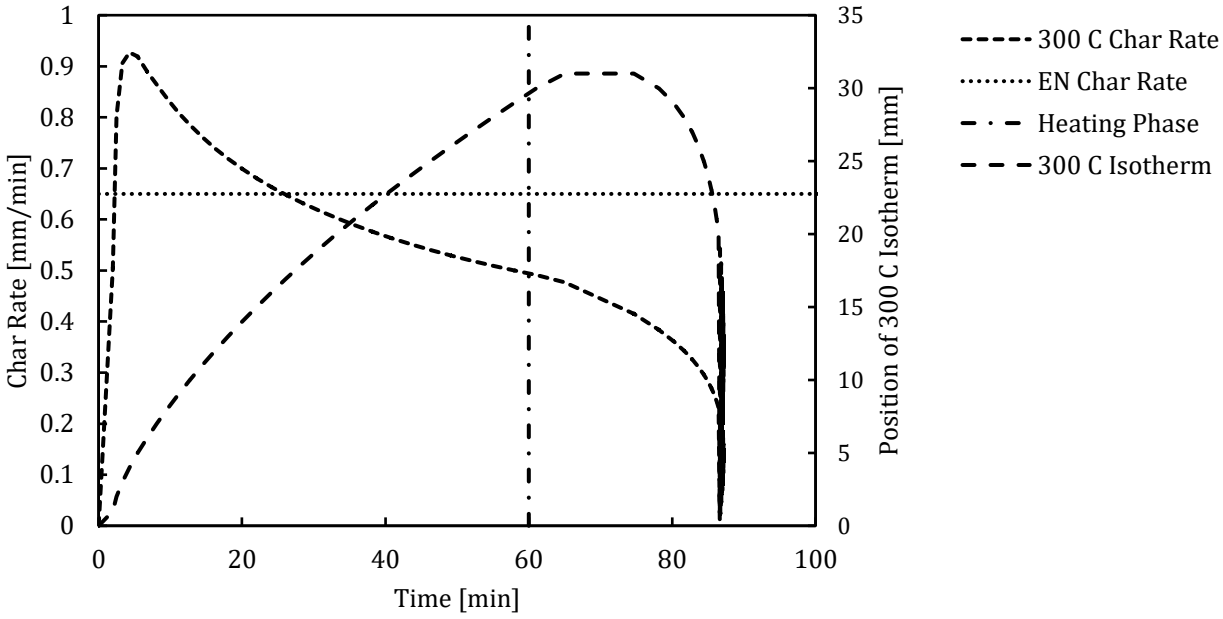

Figure 3-2 Position of 300 °C isotherm and corresponding char rate under [ISO-60]

3.2.1.2 3-Ply CLT -subtopic

Simulations were carried out for a 120 mm 3-ply CLT wall of equal ply thickness (40mm each) under a 60-minute standard fire with one-hour linear cooling to simulate burnout. Figure 3-4 shows the predicted losses in crushing (indicated as CS) and buckling strength (indicated as BS) capacities. The plot is shifted slightly to the left on the x-axis for clarity of presentation and to indicate the starting capacities for each of the models.

A general observation for all the models can be seen in the rate of strength reduction. All models predict a much steeper slope for the buckling load as compared to a more gentle reduction in crushing load. The buckling load is a function of the stiffness and second moment of area (Eq. 28). The moment of inertia is a function of the cross-sectional dimensions to the power four (Eq. 29), and hence the temperature induced reduction in the stiffness will result in a transformed cross-section (with smaller dimensions) leading to higher rates of buckling strength reductions.

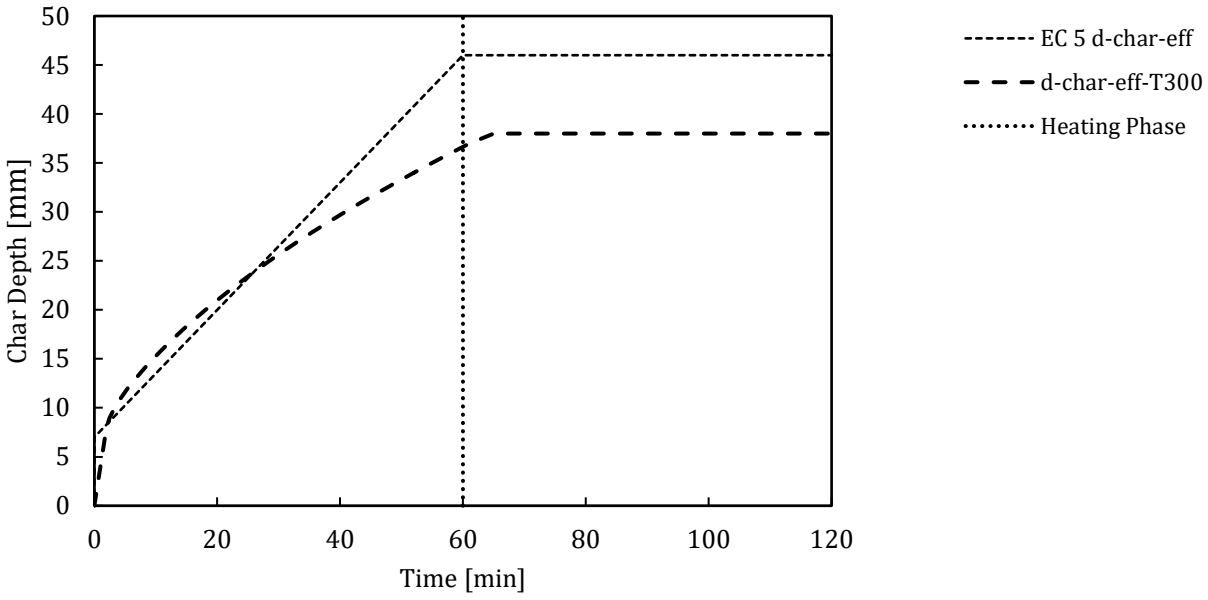

Figure 3-3 Effective char depth as per EC 5 and 300 °C isotherm for [ISO-60]

Almost all the strength and stiffness are provided by the longitudinal plies. During the early stages of the fire, the first lamella heats up resulting in a gradual loss of overall load carrying capacity of the cross-section. With time, and as the first lamella fails (approaches 300 °C, implying zero strength and stiffness), the residual load capacity will be determined from the second lamella and subsequent lamellae beneath it. The load capacity reduction obtained from the mechanical deterioration of this crosswise lamella contributes minimally to the overall loss in capacity of the remaining cross-section (since its initial contribution was already a small fraction). This can be observed for all the models, with M1 showing a gradual change in slope at the time of failure of the first lamella. Model M4 shows this more clearly with a gradual decrease in capacity for the first 50 minutes, followed by an almost constant plateau, indicating the failure of the first lamella. Subsequent heating up of the second lamella results in very limited strength reduction of the cross-section. It should be noted that for M4, after the duration of the heating phase (60 minutes in this case), no more change in strength occurs since the charring rate (and hence char depth) of EC 5 only accounts for the heating phase of a standard fire. Therefore, the constant line after 60 minutes does not mean the failure of a longitudinal ply but the end of applicability of the model itself.

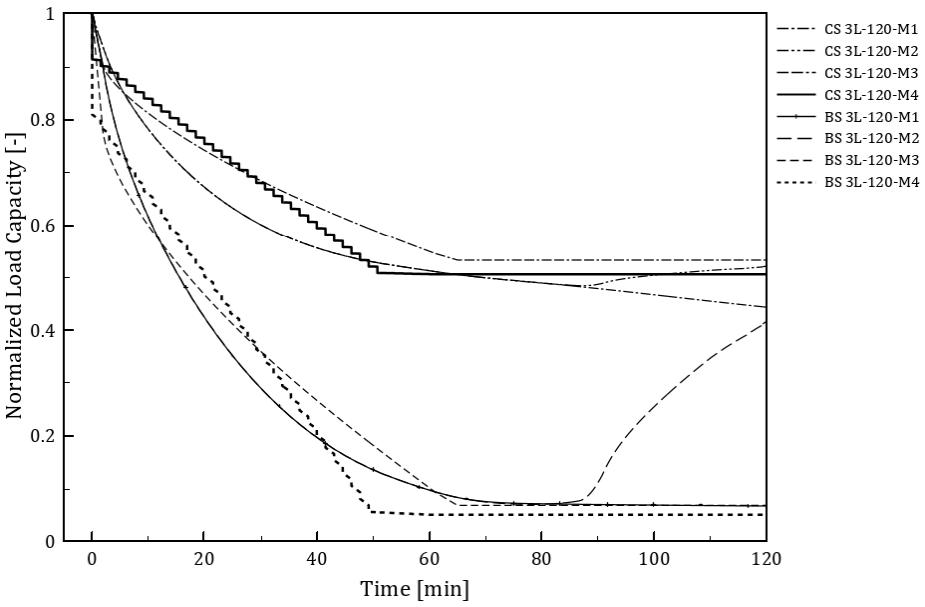

Figure 3-4 Normalized load carrying capacity for 120 mm 3-ply CLT under [ISO-60]

Immediately after the start of the simulation, it can be observed that there is a sudden drop in capacity for the crushing and buckling loads predicted according to the RCSM of the EC 5 (M4). This can be explained by the instantaneous disappearance of the zero-strength layer at the smallest time step when calculating the char depth, and hence effective cross-sectional dimensions. The loss in strength in terms of buckling is however more pronounced, with about 19% loss in capacity as compared to 9% for crushing (reasons as explained above). A stepwise reduction in strength can also be noticed and can be attributed to how the effective char depth is computed as shown in Figure 3-3.

A closer look at the crushing capacity reveals that at the end of the heating phase, similar strength predictions are obtained with the advanced model (M1) and the EC 5 RCSM model (M4), with M4 being slightly more conservative (0.68% less strength). The predictions by the 300 °C isotherm RCSM model (M3) followed closely that of M4 however underpredicted the strength reduction and gave the most unconservative results at 60 minutes. During the cooling phase however, the advanced model (M1) was able to account for further losses in capacity due to the existing thermal wave propagating through the cross-section resulting in 7% additional reduction in the crushing strength. The advanced recovery model (M2)

followed the same trend as M1 during the heating phase (as expected) and predicted approximately 8% recovery in strength during the cooling phase.

The most conservative strength prediction during the heating phase in terms of the buckling strength was obtained by M4, with a residual strength of about 5.1% at 60 minutes. Models M1 and M3 showed 9.8% and 9.3% residual strengths, respectively. Addition strength losses were recorded during the decay phase for M1 with the residual strength being 6.7% at 120 minutes. A 32% recovery in buckling strength was obtained by M2 during the cooling phase, indicating a very sharp recovery in buckling capacity. This makes sense since a higher rate of loss of strength will also imply a higher rate of strength recovery.

3.2.1.3 5-Ply CLT – subtopic

The results obtained for the crushing and buckling load carrying capacities for a 100 mm, equal ply (20mm each) CLT wall consisting of five layers subjected to a 60-minute ISO fire followed by linear cooling is shown in Figure 3-5. Similar to above, the plot is slightly shifted to the left on the x-axis for clarity of presentation and to indicate the starting capacities for each of the models.

As outlined above, all models predict a faster reduction in buckling strength as compared to crushing strength. The effect of the ply layup can be seen even more clearly in this case. Each ply is 20 mm thick, hence when exposed to the same fire, failure of the lamella will happen earlier as compared to a CLT with thicker lamellae. This is expected since for the same fire exposure, the temperature profile in the cross-section will be the identical regardless of the ply arrangements. A closer look at lines for M4 reveal that the first lamella failed at 20 minutes, shown by the sudden decline in capacity from time 0 to 20 minutes, corresponding to an effective char depth of 20 mm as shown in Figure 3-3. This is followed by an approximately constant change in capacity when the char depth is located in the second lamella. At roughly 50 minutes, the second lamella fails and the sharp decline in capacity commences until the end of the heating phase. The advanced model is able to capture this behavior, however it does so in a more subtle way with gradual change in slope in the capacities predicted.

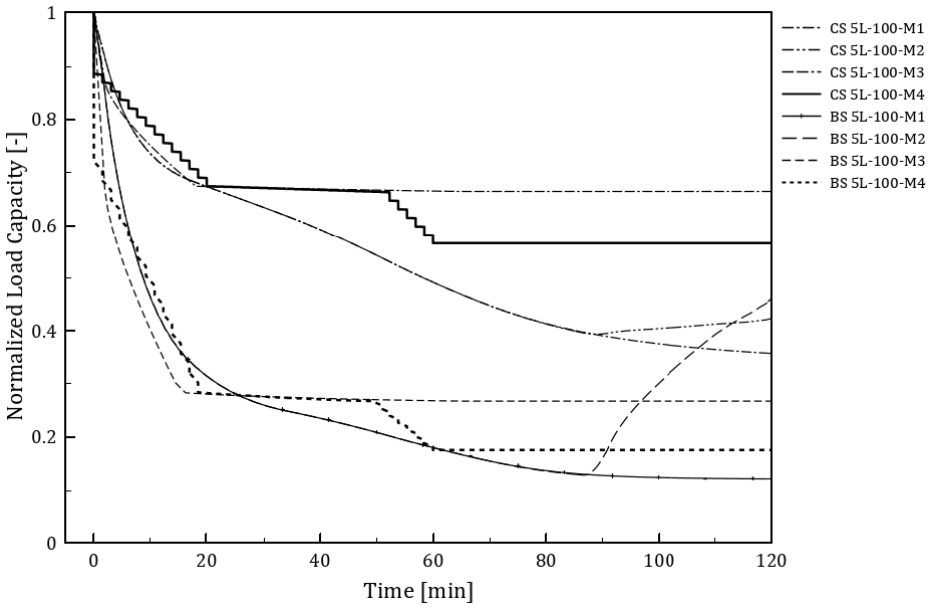

Figure 3-5 Normalized load carrying capacity for 100 mm 5-ply CLT under [ISO-60]

The sudden drop observed for the crushing and buckling loads obtained by M4 is more severe for this 5-ply CLT than for the 120mm 3-ply CLT. This is anticipated when we take a closer look at the ply layup, particularly the longitudinal plies. The overall thickness of the longitudinal layers (layers 1, 3 and 5) of the 5-ply CLT is 60 mm, thus the removal of the zero-strength layer (7 mm) will result in a more drastic loss in net capacity as against the removal of 7 mm from the 3-ply CLT which has a total of 80 mm of longitudinal layers. Nevertheless, the percentage loss in buckling capacity is still greater than the percentage loss in crushing capacity, with about 28% loss in buckling as opposed to 11% loss in crushing. A stepwise reduction in strength can also be noticed and can be attributed to how the effective char depth is computed, and hence the residual capacity.

While the crushing capacity predicted by the EC 5 RCSM model (M4) was more conservative at 60 minutes (peak of heating phase) for the 3-ply CLT above, the advanced model (M1) outperformed it, predicting more conservative results for the 5-ply CLT. The residual capacity at 60 minutes obtained from model M1 was 49.2% as opposed to 56.5% obtained by model M4. Model M3 also overpredicted the residual crushing capacity at 60 minutes with 66.5% of strength left. The explanation for this lies in how the residual capacity is calculated as well as the layer arrangement and their individual thicknesses.

For model M4, the charring rate is constant, and hence the effective char depth will be linear, increasing with time from 0 mm to 46 mm under a 60-minute standard (Figure 3-3). This would mean that the RCSM will predict higher losses in capacity when most of the effective char depth lies within a longitudinal layer(s). This is evidenced for the 3-ply CLT, where at about 50 minutes the entire first layer (40 mm) is disregarded when computing the residual capacity using the RCSM. For the 5-ply CLT however, each ply is 20 mm, thus after 60 minutes, only a total of 26 mm of longitudinal lamellae were 'consumed' (20 mm from the first ply and 6 mm from the third ply). Thusly, since most of the strength comes from plies arranged parallel to the grain, losing more longitudinal thickness will reflect higher loss in capacity. Likewise for model M3, the maximum depth of the 300 °C isotherm was found to be 31 mm (38 mm effective). Implying a total 38 mm of the longitudinal layer (first ply) was disregarded for the 3-ply CLT as opposed to 20 mm for the 5-ply CLT.

During the cooling phase, the advanced model (M1) was able to account for further losses in capacity due to the existing thermal wave traveling through the cross-section resulting in 13.5% additional reduction in the crushing strength to give a residual capacity at 35.7%. The advanced recovery model (M2) followed the same trend as M1 during the heating phase and predicted approximately 6.6% recovery in strength during the cooling phase.

Models M1 and M4 predicted similar buckling capacities at the 60-minute mark with 18% and 17.6% residual strength, respectively, making model M4 marginally more conservative. Model M3 overpredicted the residual buckling capacity at 26.9% of the ambient strength for reasons explained above. The importance of accounting for the cooling phase is reiterated here. As the thermal wave propagates through the cross-section, further loss in strength is recorded by M1 with only 12.1% residual buckling capacity at the end of the simulation. The residual buckling strength predicted by the recovery model at the 120-minute mark was 46.1%. This indicates a very sharp regain in buckling strength as compared to crushing strength. A similar observation was noted for the 3-ply CLT. It is worth mentioning that recovery of properties did not set in immediately after the end of the heating phase. It takes about 28 minutes until the first recovery in strength is observed. This can be ascribed to the thermal wave still heating up the cross-section.

3.2.1.4 7-Ply CLT – subtopic

The results obtained for the crushing and buckling load carrying capacities for a 140 mm, equal ply (20mm each) CLT wall consisting of seven layers subjected to a 60-minute ISO fire followed by linear cooling is shown in Figure 3-6. Similar to above, the plot is slightly shifted to the left on the x-axis for clarity of presentation and to indicate the starting capacities for each of the models.

The performance of the 7-ply CLT is akin to that of the 5-ply CLT. Buckling capacity is lost more rapidly in comparison to the crushing capacity. The decline in capacity predicted by model M4 at the beginning of the fire is of similar in magnitude to the 3-ply CLT. This is expected since both CLTs have 80 mm of longitudinal plies, thus the removal of the zero-strength layer (7 mm) will result in a similar reduction in strength. Approximately 22% loss was recorded in buckling strength as compared to 8.5% for crushing capacity.

The advanced model (M1) predicted the most conservative results at the end of both the heating and cooling phases for the crushing and buckling capacities alike. 61.9% residual crushing strength was predicted at the end of the heat phase by model M1 as compared to 67.5% by model M4. A further 12% loss in the crushing strength was captured by model M1 during the cooling phase resulting in 49.9% crushing capacity remaining. The RCSM computed using the position of the 300 °C isotherm (M3) predicted the least conservative crushing capacity with 50.2% of the initial strength remaining at the end of the simulation. Similar to the 3 and 5-ply CLTs the advanced recovery model (M2) followed the same trend as M1 during the heating phase and predicted approximately 4.9% recovery in strength during the cooling phase.

29.9% residual buckling capacity was predicted by model M1 as compared to 30.6% by M4 and 41.2% by M3 at the end of the heating phase. At the end of the cooling phase, only 21.9% of the initial buckling strength remained as predicted by model M1. Once more, the rate of recovery predicted by model M2 for the buckling capacity is much higher at 47.8% of the initial capacity.

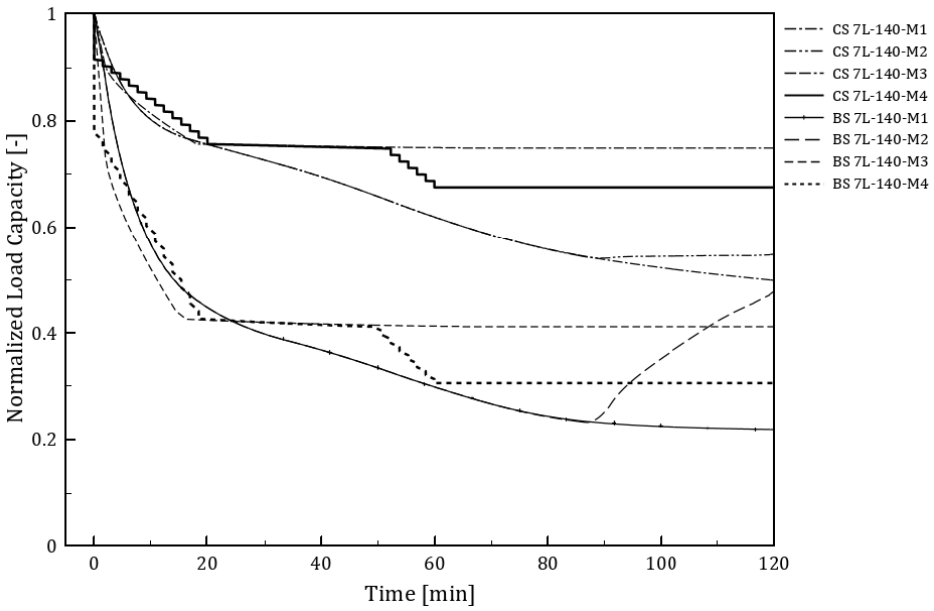

Figure 3-6 Normalized load carrying capacity for 140 mm 7-ply CLT under [ISO-60]

3.2.2 Short Parametric Fire Curve

3.2.2.1 Results from Thermal Analysis: Charring Rate, Effective Charring Depth

Under the short parametric fire, the heating phase is more intense as compared to the ISO fire curve the effect of which can be observed in Figure 3-7. This would mean the timber front will pyrolyze and char at a much faster rate due to the higher temperatures it is exposed to. The maximum charring rate obtained was approximately 1.2 mm/min and occurred during the first four minutes of the fire. As observed under the standard fires, the charring rate begins to slow down after reaching a maximum due to the protective layer provided by the already formed char layer. During the decay phase, the 300 °C isotherm continues to penetrate deeper into the cross-section from a depth of 25 mm to a depth of 30 mm in about 20 minutes and maintains a depth of 30 mm for the next 26 minutes.

The EC 5 effective parametric char depth rises at a much higher rate achieving 25 mm in the first 21 minutes as opposed to the effective one-dimensional char depth for standard fire which reaches 25 mm in approximately 28 minutes as shown in Figure 3-8. Another notable difference is that the EC 5 parametric char depth continues beyond the heating phase accounting for further charring during the decay phase.

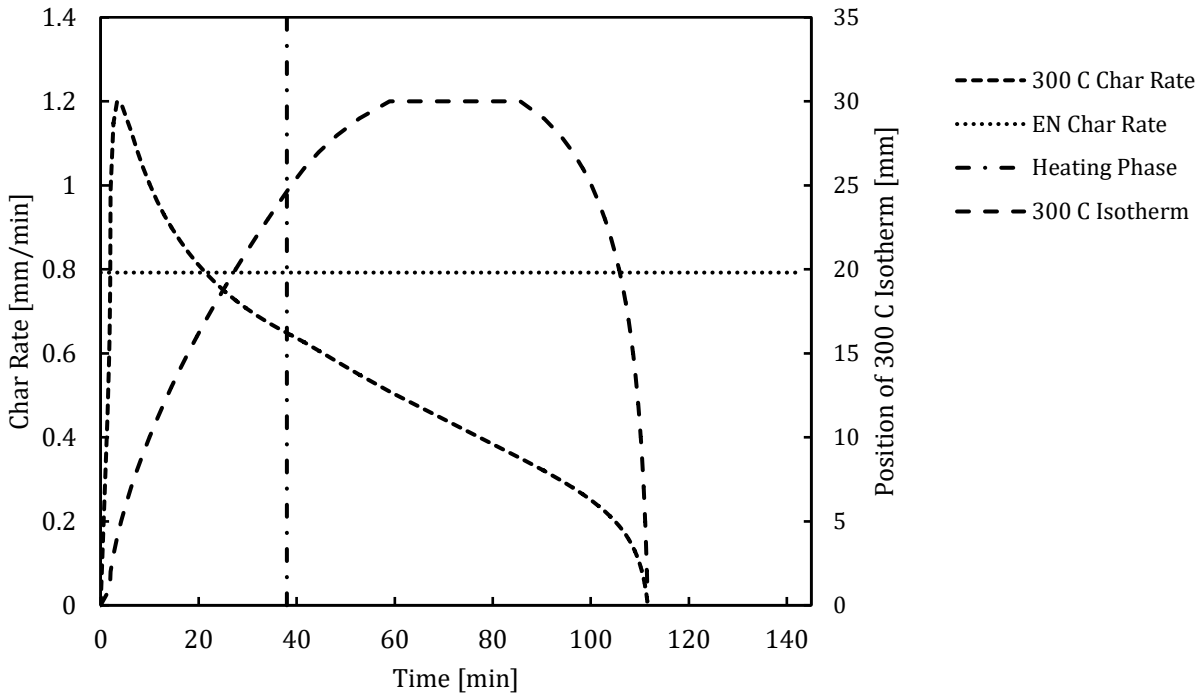

Figure 3-7 Position of 300 °C isotherm and corresponding char rate under short parametric fire

Similar to above, the char depth obtained from EC 5 is more conservative than the determined char depth from the 300 °C isotherm achieving an overall char depth of 56 mm as opposed to 37 mm.

3.2.2.2 Results from Structural Analysis

Simulations were carried out for a 120 mm 3-ply CLT wall of equal ply thickness (40mm each) under the short parametric curve shown in Figure 2-8. This fire curve had a heating phase equal to thirty-eight minutes after which cooling starts. Figure 3-9 shows the predicted losses in crushing and buckling strength capacities for the 3-ply CLT. The same general observations outlined previously for all models can be made here.

The immediate drop in capacity predicted by model M4 for all CLTs after the start of the simulation is identical to the values predicted for the 60-minute and 120-minute fire curves above.

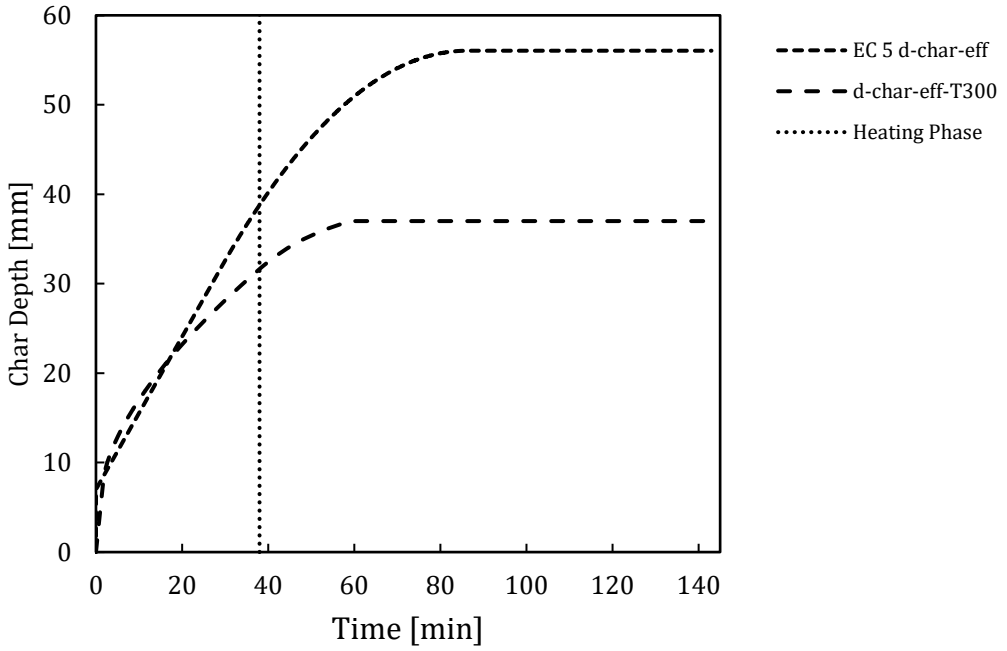

Figure 3-8 Effective char depth as per EC 5 and 300 °C isotherm for short parametric fire

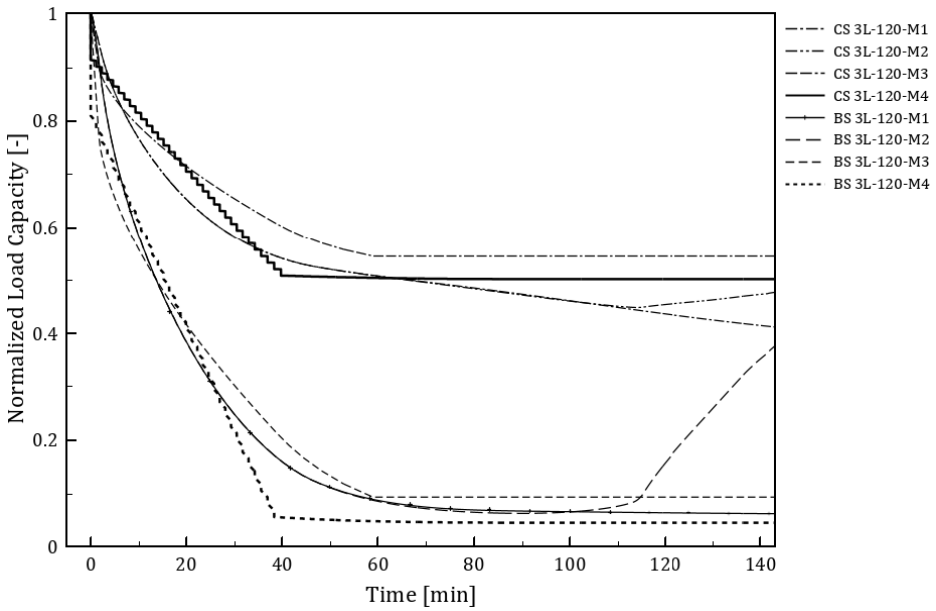

Figure 3-9 Normalized load carrying capacity for 120 mm 3-ply CLT under short parametric fire

A closer look at the crushing capacity for the 3-ply CLT (Figure 3-9) reveals that at the end of the heating phase (38 minutes), the Eurocode model (M4) is able to predict more conservative results with the residual strength being at 53.3%. This was followed closely by

the advanced model which predicted a residual strength of 54.7% and lastly by model M3 at 60.6%. At the end of the simulation, the advanced model (M1) predicted additional losses in capacity to become the most conservative at 41.2% residual strength followed by model M4 at 50.2% and model M3 at 54.5%.

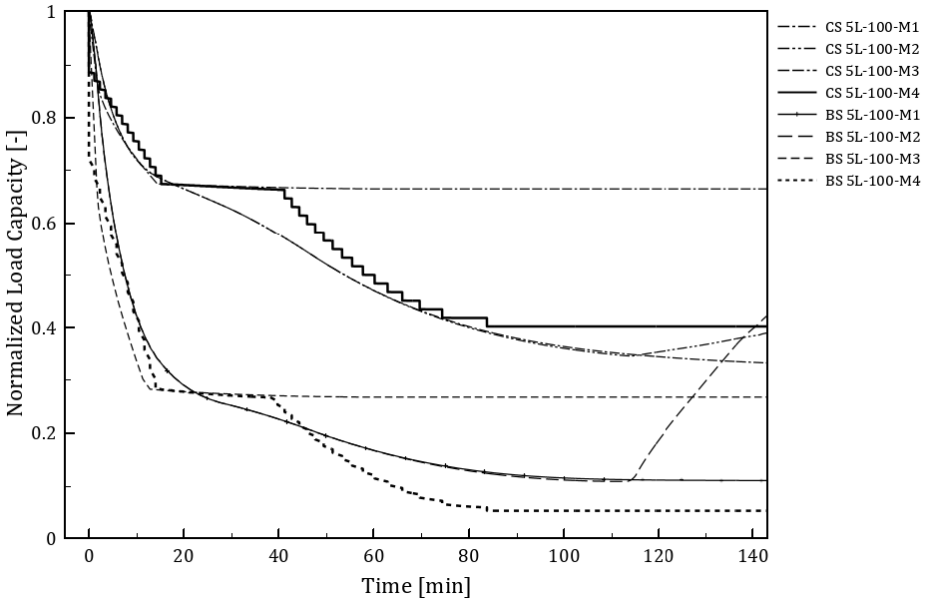

Figure 3-10 Normalized load carrying capacity for 100 mm 5-ply CLT under short parametric fire

The buckling strength predictions at the end of the heating phase were also more conservative for model M4 at 5.6% as compared to 17.2% for model M1 and 21.3% for model M3. At the end of the cooling phase, model M4 recorded additional losses to arrive at a residual capacity of 4.6%, as compared to 6.2% for model M1 and 9.3% for model M3.

For the 5-ply CLT (Figure 3-10), model M1 gave the most conservative results for the crushing and buckling capacities at the end of the heating phase predicting 58.7% and 23.2% for crushing and buckling, respectively. This was followed by model M4 at 66.4% and 26.8%, and 66.7% and 27.1% for model M3. The effect of using a charring rate in the cooling phase is seen here with model M4 being the most conservative model at the end of the cooling phase for buckling capacity. It predicted a residual buckling strength of 5.3% as opposed to 11% by model M1 and 26.8% by model M3. However, the advanced model was the most conservative in terms of crushing at 33.3% as opposed to 40.2% by model M4 and 66.5% by model M3.

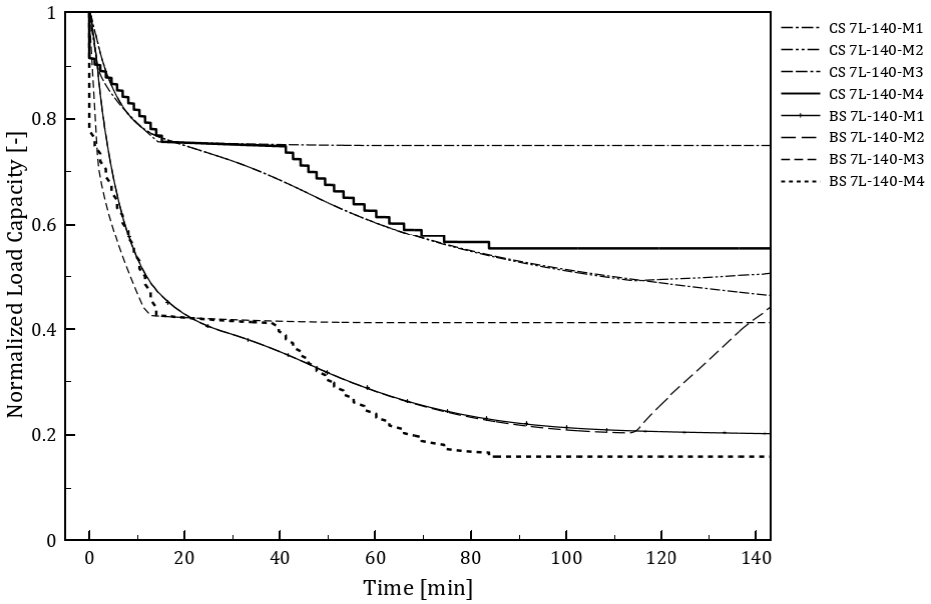

Figure 3-11 Normalized load carrying capacity for 140 mm 7-ply CLT under short parametric fire

Similar observations are made for the 7-ply CLT (Figure 3-11) with the advanced model (M1) being the most conservative at the end of the heating phase for crushing and buckling capacities predicting 69.2% and 36.4% for crushing and buckling, respectively. Model M4 predicted 74.9% and 41.2%, and 75.1% and 41.5% predicted by model M3. Again, the advanced model (M1) outperformed the EC 5 RCSM model in crushing at the end of the simulation with 46.4% residual crushing capacity as compared to 55.3% by model M4 and 74.9% by model M3. Predictions of the buckling capacity were more conservative for model M4 at 15.9% as compared to 20.2% for model M1 and 41.2% for model M3.

3.3 Effect of End Restraints

The effect of the end support conditions on the fire performance of a CLT wall is presented here. Previous results presented above are for walls pinned at both ends. In this section however, results for fixed-fixed and fixed-pinned support conditions are presented. Several simulations are run, but only the results for a 120 mm 3-ply CLT with equal thickness subjected to a 60-minute standard fire curve with one-hour linear cooling will be presented here. Readers are directed to the appendix for results on 5-ply and 7-ply CLTs. Nevertheless, similar observations can be made for all cases.

Figure 3-12 shows the true values of the buckling load capacity for a fixed-fixed end restraint, respectively. Results for the crushing capacity are not plotted since no changes will occur as one would expect. From Figure 3-12 it can be observed that the magnitude of the buckling capacity at ambient is double that of the same CLT with both ends pinned. Similarly, the buckling load for the CLT with fixed-pinned supports is approximately 1.4 times that with pinned-pinned supports.

This is logical and can be understood from the Euler buckling equation. Interestingly, all walls lose their buckling capacity in a similar manner. This can be attributed to the temperature distribution inside each cross-section being the same, hence the percentage loss in strength will be identical. It can also be noticed from Figure 3-12 that although changes to the support conditions improve the load carrying capacity of the wall at ambient conditions it contributes minimally to the improvement of its performance under fire conditions.

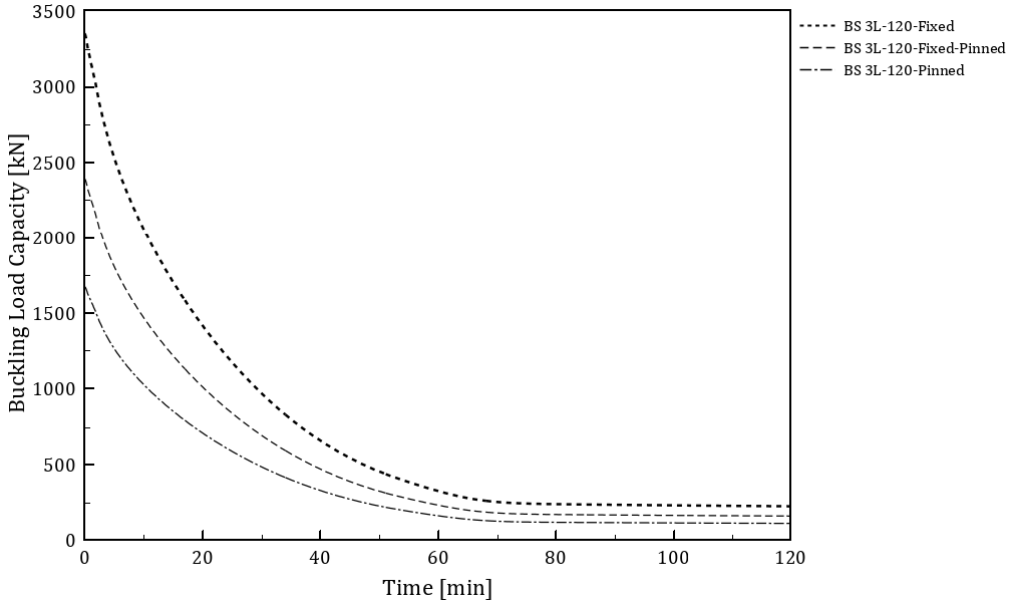

Figure 3-12 Buckling load capacity for 120 mm 3-ply CLT with varying end restraints [ISO – 60]

3.4 Influence of Wall Height

The effect of the height of a CLT wall on its behavior and performance when exposed to fire is presented here. Similar to above, only results for the buckling capacity of a 120 mm 3-ply

CLT subjected to a one-hour standard fire with linear cooling are presented here. Results for 5 and 7-ply CLTs are included in the appendix. Two different wall heights are simulated, that is 3 and 4.8 m.

Figure 3-13 shows the true values of the buckling load capacity for a 3 and 4.8 m CLT wall, respectively. As expected, the ambient capacity for a 3 m wall is much higher than for a 4.8 m wall (~2.5 times higher), however the rate at which the capacity is lost is identical as explained above. From Figure 3-13, the fire performance of both walls at the end of the simulation does not necessarily improve, with the 3 m wall having 112.84 kN of its capacity left as opposed to 44.08 kN for the 4.8 m wall.

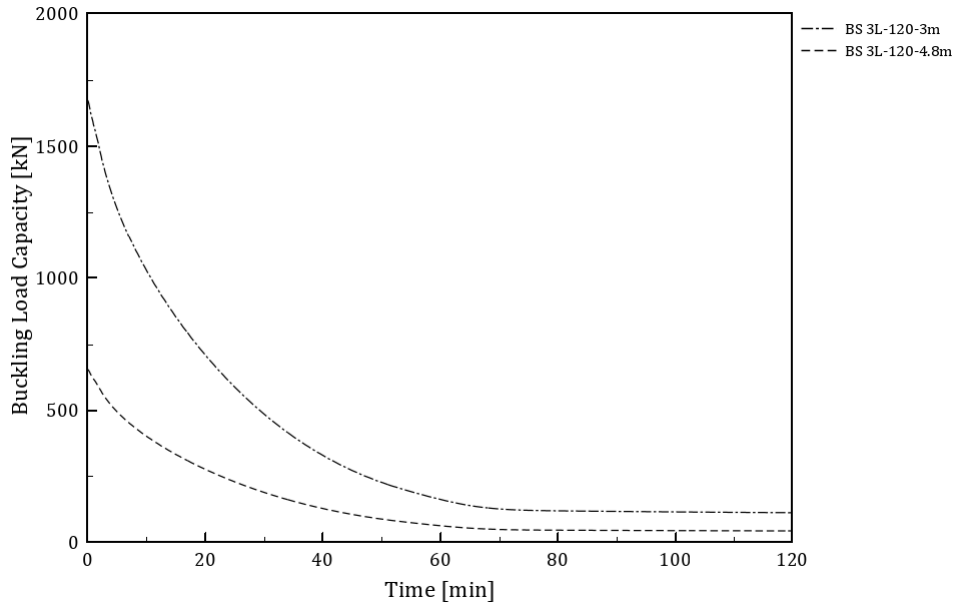

Figure 3-13 Buckling load carrying capacity for 3 and 4.8 m 120 mm 3-ply CLT wall [ISO-60]

3.5 Effect of Number of Plies, Arrangement and Thickness

This section is concerned with investigating the effects of different ply thicknesses and their arrangements (see section 2.4.2). Results for 3, 5 and 7 ply CLTs for crushing and buckling capacities will be presented separately. Only results for the 60-minute ISO fire exposure with cooling will be included herein, as similar trends are expected for the longer 120-minute exposure. Readers can however refer to the appendix for plots of 120-minute ISO fire exposure.

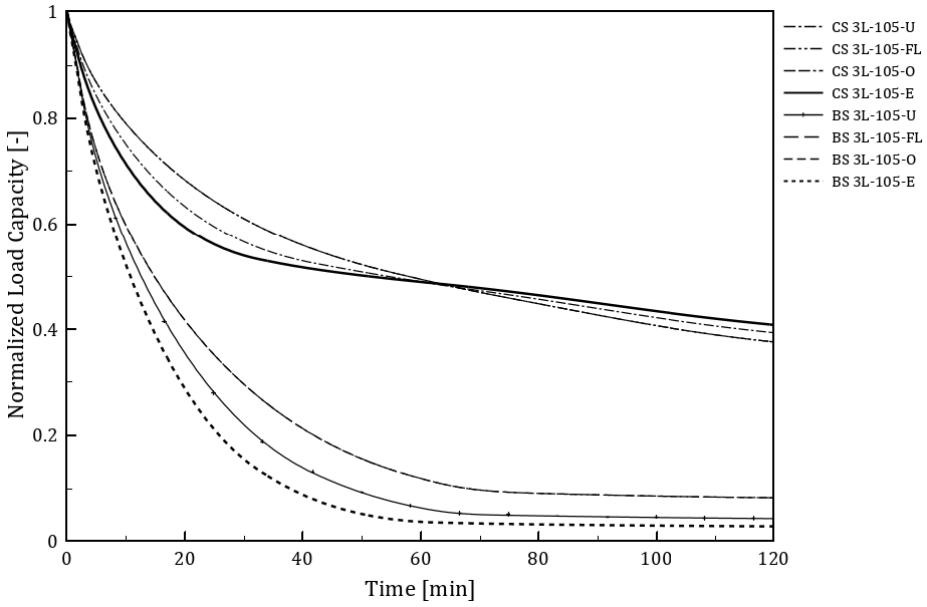

Figure 3-14 Normalized load capacity for 105mm 3-ply CLTs for varying ply arrangements [ISO-60]

Figure 3-14 and Figure 3-15 show the normalized load capacities for 105 and 210mm 3-ply CLTs with equal plies, thicker first and last plies, thicker longitudinal layers, and thicker crosswise layers subjected to a 60-minute ISO fire exposure with one-hour linear cooling. Although thicknesses may differ, normalizing allows comparison of the different ply arrangements. In terms of crushing capacities for the 105 mm 3-ply CLT, having thicker crosswise layers would appear to be the most favorable in a fire, with about 40.8% residual strength as compared to 37.6% for thicker longitudinal layers and 39.4% for equal layers.

However, having thicker crosswise layers also means that the initial capacity is lesser as compared to other ply arrangements. This is shown in Figure 3-16 where 3L-105-E exhibits the lowest crushing capacity while 3L-105-O has the highest residual capacity. For the 210mm 3-ply CLT, 3L-210-O (same as 3L-210-FL) had a higher residual crushing capacity than 3L-210-U and 3L-210-E, maintaining about 61% of its strength after the fire (Figure 3-17).

Similar trends are exhibited for buckling capacity, with 3L-105-O and 3L-210-O positively performing in fire, while 3L-105-E and 3L-210-E exhibited the worst behavior in fire. For the thinner CLTs, buckling appears to be more critical as compared to crushing, with the 105mm thick CLTs losing almost all their buckling strength very early during the fire, approximately

71-85% of their buckling capacity in the first 30 minutes (as compared to 50% for the 210mm CLTs).

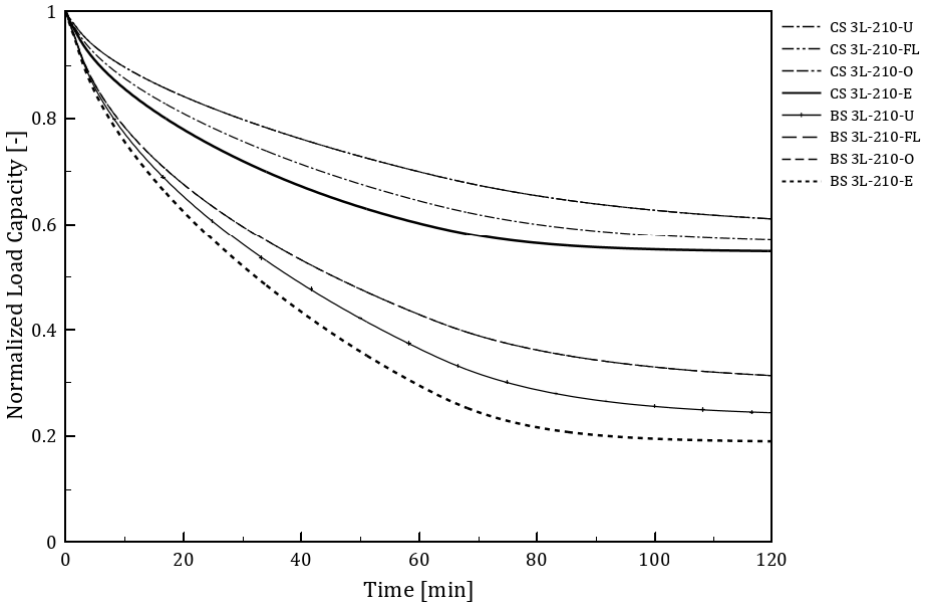

Figure 3-15 Normalized load capacity for 210mm 3-ply CLTs for varying ply arrangements [ISO-60]

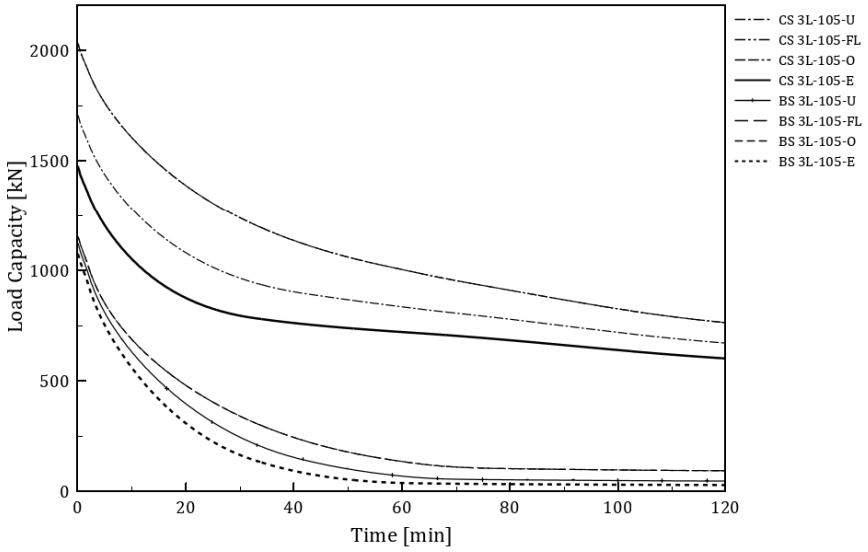

Figure 3-16 Load capacity for 105mm 3-ply CLTs for varying ply arrangements [ISO-60]

The heat affected first plies result in a sharp decline in stiffness leading to huge losses in buckling strength. This is more prominent in the thinner CLTs as heat is transferred through the section much quicker as compared to thicker CLTs.

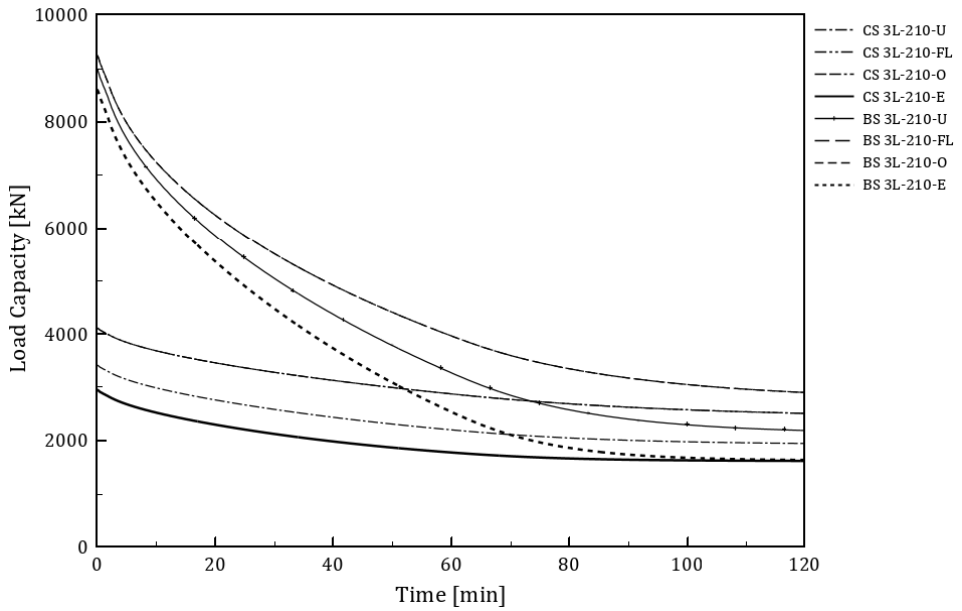

Figure 3-17 Load capacity for 210mm 3-ply CLTs for varying ply arrangements [ISO-60]

The crushing and buckling capacities for the 105 and 210 mm 5-ply CLTs are shown in Figure 3-18 and Figure 3-19 (normalized values), and, Figure 3-20 and Figure 3-21 (actual magnitudes). From Figure 3-18, it is observed that the reduction in crushing strength for all the 105 mm 5-ply CLTs appears to be similar, with residual capacities between 36-38% of initial strength. In terms of magnitude, 5L-105-O performed better, followed closely by 5L-105-FL. Identical to the 3-ply CLTs, the worst performance was the 5L-105-E, with 5L-105-U being slightly better.

The 210mm 5-ply CLTs followed a similar trend with residual capacities between 62-65%. Again, 5L-210-O exhibited the best performance, followed by 5L-210-FL, 5L-210-U and 5L-210-E. The reduction in buckling strength followed a similar trend just as the crushing strength, however, a more severe reduction is observed in the former much earlier. At 120 minutes, buckling capacities were at 10-13% for 105mm CLTs and 25-32% for 210mm CLTs. In both cases, CLTs with thicker longitudinal layers performed better, followed by thicker first and last layers, uniform layer thickness and finally thicker crosswise CLT.

The crushing and buckling capacities for the 105 mm and 210 mm 7-ply CLTs are shown in Figure 3-22, Figure 3-23 (normalized values) and Figure 3-24 and

Figure 3-25 (actual values), respectively. The same observations can be made as above for buckling and crushing capacities as 5-ply and 3-ply CLTs.

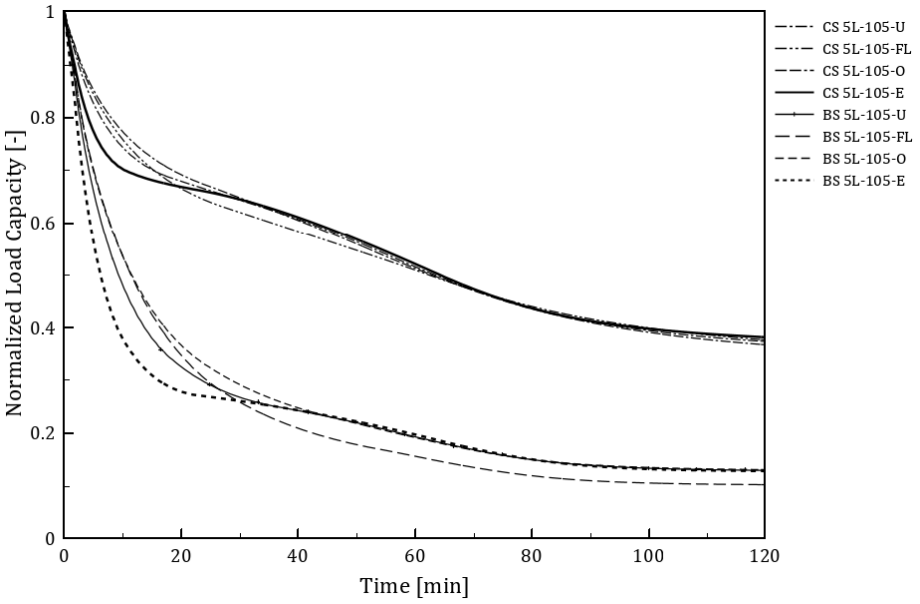

Figure 3-18 Normalized load capacity for 105mm 5-ply CLTs for varying ply arrangements [ISO-60]

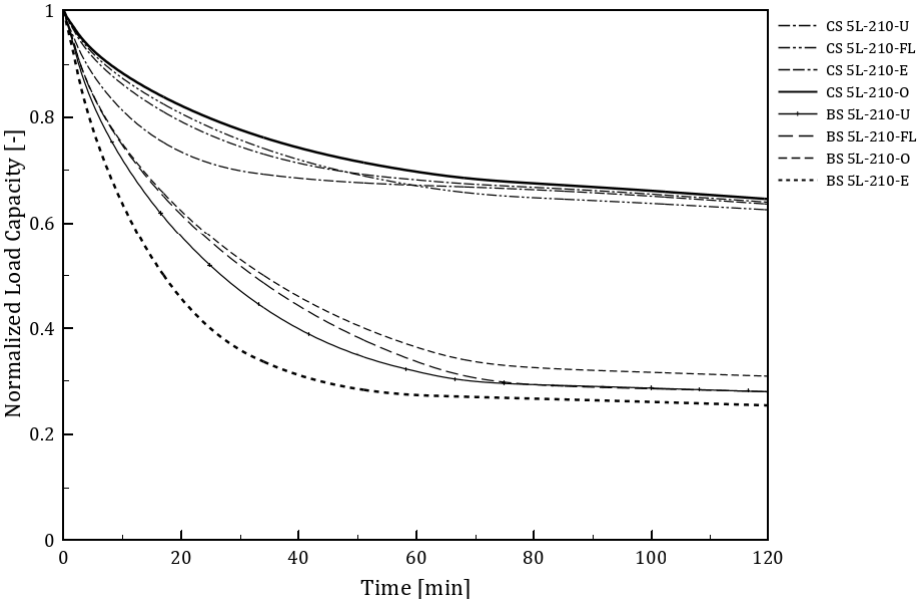

Figure 3-19 Normalized load capacity for 210mm 5-ply CLTs for varying ply arrangements [ISO-60]

When compared together, CLTs with uniform layer thicknesses had comparable residual crushing and buckling capacities (in magnitude) regardless of the number of plies. For CLTs

with thicker first and last layers (105-FL and 210-FL), the 3-ply CLTs had higher residual crushing capacity as compared to 5 and 7-ply CLTs which had similar capacities.

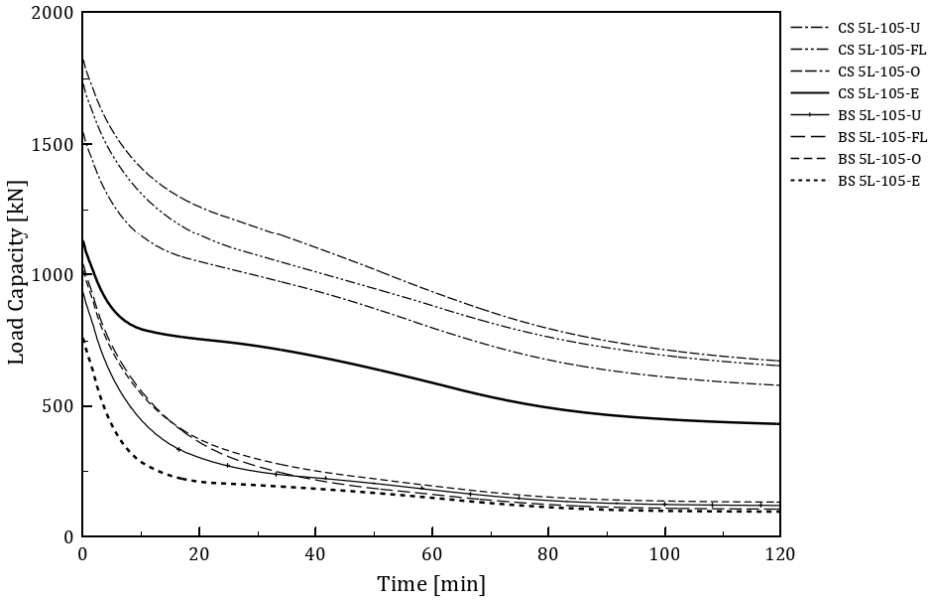

Figure 3-20 Load capacity for 105mm 5-ply CLTs for varying ply arrangements [ISO-60]

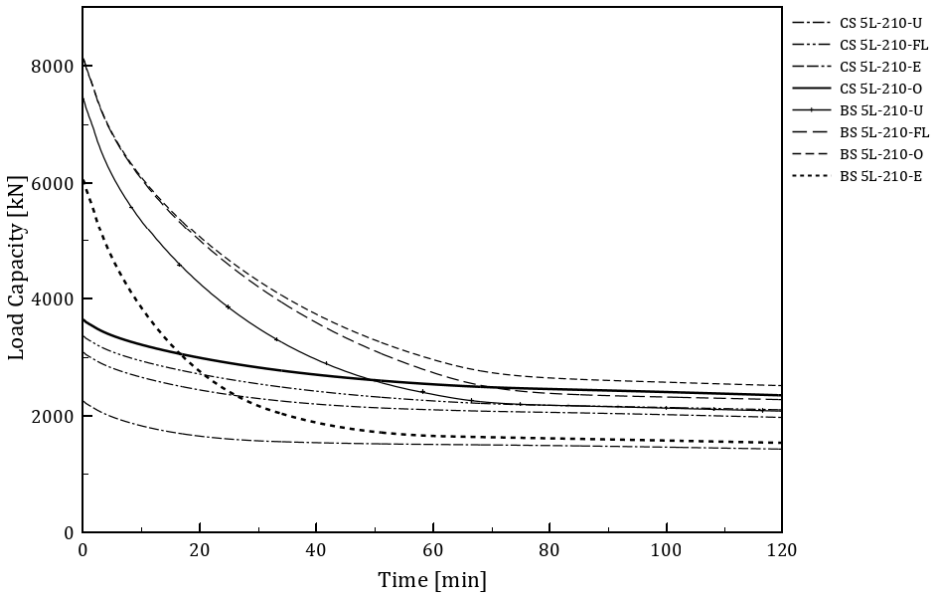

Figure 3-21 Load capacity for 210mm 5-ply CLTs for varying ply arrangements [ISO-60]

In terms of magnitude, buckling capacities for the 105mm thick CLTs had comparable buckling capacities at the end of the simulation irrespective of the number of plies. For the 210mm CLT however, the 3-ply CLTs had higher residual buckling capacities for the 210-U,

210-FL and 210-O ply arrangements, followed by the 5 and 7-plies. The 7-ply CLTs had greater buckling capacity for the case with thicker crosswise layers. 3-ply CLTs for 105mm

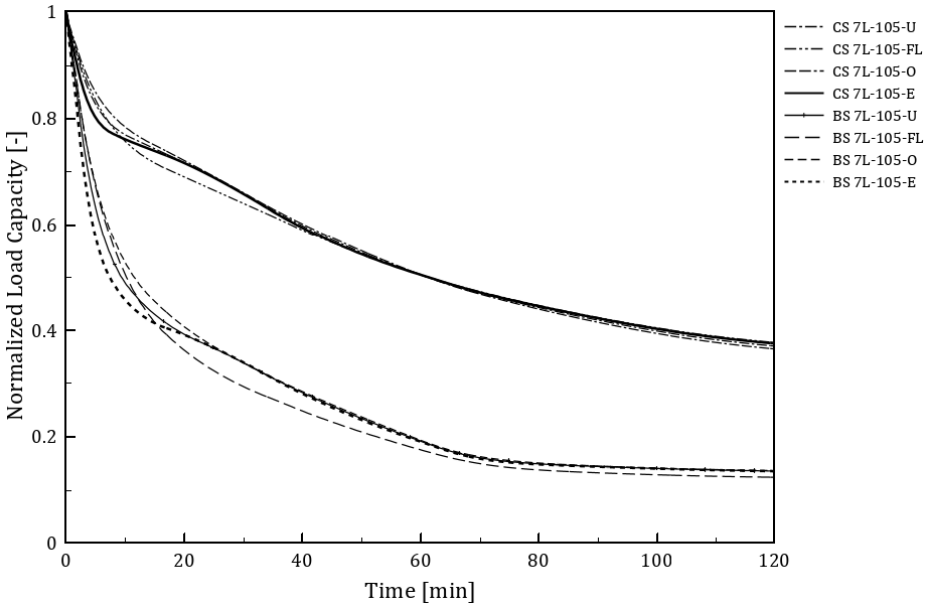

Figure 3-22 Normalized load capacity for 105mm 7-ply CLTs for varying ply arrangements [ISO-60]

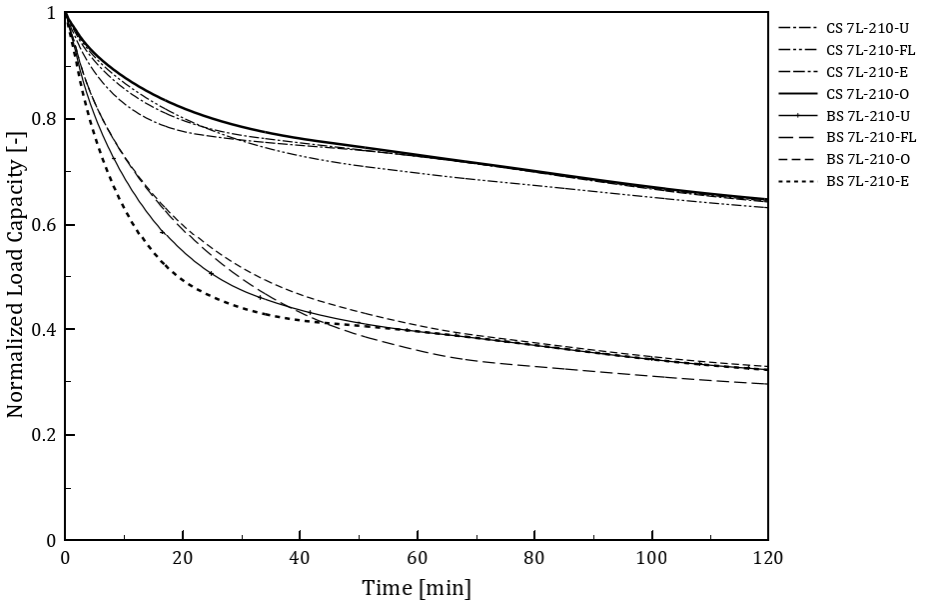

Figure 3-23 Normalized load capacity for 210mm 7-ply CLTs for varying ply arrangements [ISO-60]

and 210mm thicknesses had a greater residual crushing capacity followed by 5-ply CLT and then 7-ply CLT, except for the case with thicker crosswise plies where the 7-ply CLT had higher residual crushing capacity.

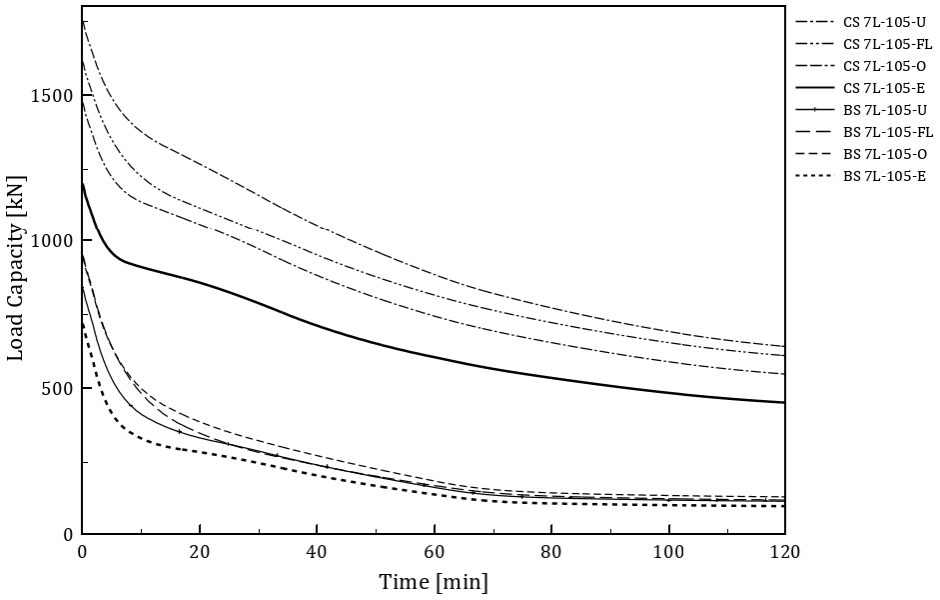

Figure 3-24 Load capacity for 105 mm 7-ply CLTs with different ply arrangements [ISO - 60]

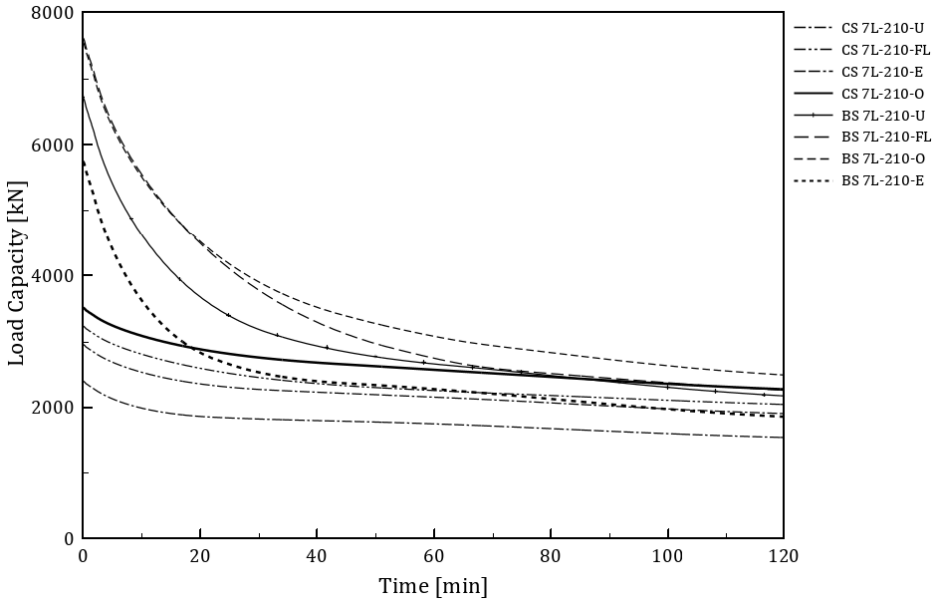

Figure 3-25 Load capacity for 210 mm 7-ply CLTs for varying ply arrangements [ISO-60]

From the figures showing the actual load capacities, it can be observed that the 210mm plies have higher initial capacities as compared to their corresponding 105mm plies. This makes sense as a thicker member will have more capacity. It can also be observed that the initial capacities for the 3-ply CLTs are higher than the 5-ply CLTs which are in turn higher than the

7-ply CLTs. This can be attributed to the fact that the overall thickness of longitudinal layers in a 3-ply CLT is higher than that of a 5-ply CLT or 7-ply CLT.

Unlike the 3-ply CLT, different behavior can be observed for the 5 and 7-ply CLTs. Having thicker longitudinal layers contributes positively to fire performance for crushing capacity. Thicker crosswise layer CLTs also performed reasonably well. Surprisingly, the worst performance is observed for CLTs with equal layer thickness, although they might show greater capacities at ambient conditions when compared to other ply arrangements.

4 DISCUSSION

4.1 The Methods for Design of CLT Walls in Fire

The complication with the use of the RCSM for CLT members (unlike solid timber or glulam) is the 'buffer zone' in strength reduction caused by the crosswise layers contributing almost no strength or stiffness to the cross-section. When the effective char depth is located in a crosswise layer, nearly no change in the predicted load carrying capacity is recorded. This can be readily observed by the predicted load capacities from model M4 as shown, for example in Figure 3-4 to Figure 3-6 by the plateaus. The resulting crushing and buckling capacities will consequently be unconservative. The occurrence of delamination, although not modeled here, will also result in further losses in capacity. Hence, the use of a constant zero-strength layer, either 7 mm or an increased value for that matter will be inadequate to give conservative results for all cases. A similar observation was made by Wiesner et al. [106] resulting from their experiment on CLT members in a compartment fire. The use of a time-dependent or fire load-dependent zero-strength layer coupled with an increased rate of charring rate (to account for delamination) is therefore imperative for the design of CLT.

Nonetheless, the RCSM predicted similar, and in some cases more conservative results to the advanced model for 3-ply CLTs in terms of buckling while crushing strength was still underpredicted. This is the case provided that the effective char depth penetrates beyond the first layer. For 5 and 7-ply CLTs however, the one-dimensional charring rate coupled with the 7 mm zero-strength layer only gave conservative residual buckling capacities under more severe standard fires and where the effective char depth penetrated beyond the first two layers.

The parametric charring rate when applied with the RCSM provided conservative results when compared to the advanced model for buckling only, regardless of the number of plies making up the CLT. This can be attributed to the continued increase in char depth after the heating phase simulating the propagation of the thermal wave. However, the advanced method was originally developed for standard fire curves and hence its applicability to parametric fires and hence, this comparison may not be entirely accurate. Also, the relevance of the parametric charring rate is limited to short parametric fires as outlined earlier (see

section 1.4). Additionally, most designers apply standard fire curves when designing a timber member since this is current requirement under the existing regulations to satisfy a particular fire rating.

Utilizing the position of the 300 °C isotherm with a constant zero-strength layer in determining the residual load carrying capacity of a CLT member is unconservative for use in design irrespective of the number of layers. This could however be due to the limitation in the heat transfer model itself which could be underpredicting the position of the 300 °C isotherm.

Unlike steel and in some cases concrete, assuming that the properties of timber revert back either partially or fully to their ambient values can be detrimental and will lead to underprediction of the residual strength of the cross-section. Wiesner el al. [106] suggest that the real value will lie between these two extremes. In design however, the most conservative result is of interest. A major reason for this is due to the fact that when exposed to high heat conditions, the constituent compounds of timber undergo irreversible chemical changes at much lower temperatures [4] as opposed to other construction materials like steel and concrete whose chemical composition remains fairly unchanged. Therefore, while it is safe to assume steel and concrete regain part of their ambient strength such supposition is largely invalid for timber and would require extensive research to prove otherwise.

The discussion presented above is based on the simulation results presented above and should not be regarded as sufficient in its own regard as prove of adequacy of the RCSM and further research and experiments are required to validate these observations.

4.2 Critical Load for CLT Walls

It is important to determine what type of load will be the governing mode of failure for CLT walls so that engineers can design against it. Although not exhaustive, results from the simulations carried out in this thesis suggest that the governing loads under ambient conditions might not necessarily govern when the wall is exposed to fire. This is particularly important for CLT walls with a thickness greater than or equal to 150 mm since for thinner cross-sections buckling is already the governing load of failure.

Taking for example the 210 mm 3-ply CLT with equal ply thickness subjected to a two-hour standard fire curve with linear cooling shown in Figure 4-1 below, it is apparent that at ambient conditions (time = 0), the crushing load is automatically the governing load for failure. That is, this wall would fail by crushing under normal conditions and designers will often design against that mode of failure. However, as the CLT member is exposed to fire, the mechanical degradation and charring of the wood material results in the cross-section suddenly losing a huge proportion of its buckling capacity to the point where buckling becomes the mode of failure.

This can be seen clearly in Figure 4-1 where at ambient conditions, the computed buckling capacity is 8975 kN as opposed to 3415 kN for the crushing capacity, making the buckling capacity about 2.6 times higher than the crushing capacity at ambient. The effects of the thermomechanical degradation can be observed to be more critical for buckling and the cross-section loses most of its buckling capacity at a much quicker rate than crushing capacity. At about the 95th minute, further losses in buckling result in it being more critical than crushing, and hence a transition in the governing critical load. Such transition can also be seen for 5 and 7-ply CLTs with the buckling capacity of the 7-ply CLT going below the crushing capacity during the cooling phase, reiterating the importance of accounting for the decay phase.

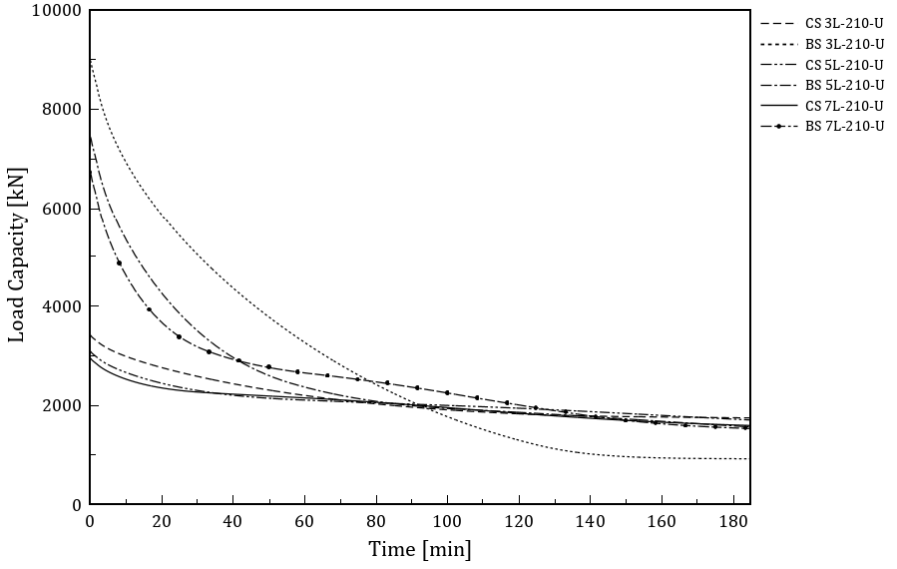

Figure 4-1 Load capacity for equal ply 210 mm 3, 5 and 7-ply CLTs [ISO - 120]

Although not modelled here, second order and P-delta effects as a consequence of geometric and material nonlinearities will introduce second moments which will in turn lead to further deflections and eccentricities that will result in even further bending and displacements. This would mean that the buckling load will be much lower than predicted by the model in this thesis, and in essence much lower than the crushing capacity.

4.3 Burnout Resistance

Accounting for the decay phase of a fire has been shown to be important to accurately predict the behavior of CLT walls in fire as further losses in load carrying capacity are recorded. For example, a 3-ply 210 mm CLT wall loaded with 25% of its capacity will appear not to fail if designed based on the heating phase only as shown in Figure 4-2. However, when cooling is considered, the propagation of the thermal wave leads to further losses in capacity, from 36.5% to 17.9% and eventually the wall will fail under that specific loading condition.

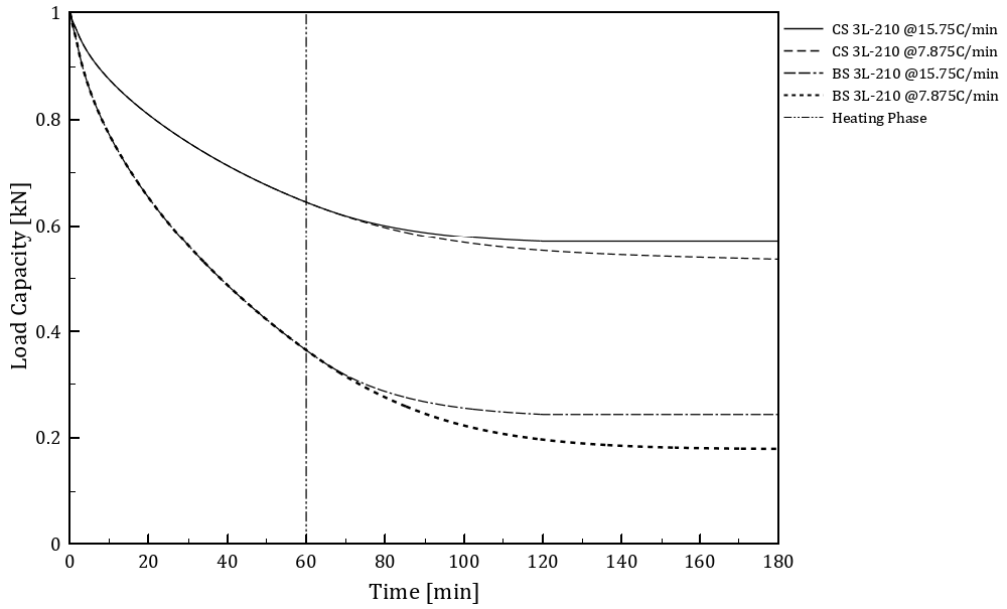

Figure 4-2 Load capacity for 210 mm 3-ply CLT (uniform plies) subjected to different cooling rates

The rate at which the member cools is also of importance and can result in even further reduction in capacity. A slower cooling rate will mean heat is lost more slowly to the ambient and the thermal wave will persist longer as compared to a faster cooling rate. This has also been demonstrated by Gernay [107] but for solid timber columns exposed on all sides. To illustrate this, simulations were carried out for a 210 mm 3-ply CLT with equal ply thickness

exposed to a 60-mintue standard fire followed by a cooling rate of 15.75 °C/min and 7.875 °C/min to ambient. From Figure 4-2, it can be observed that the cooling rate is more critical for the buckling capacity which recorded a further 6.5% reduction in capacity as compared with crushing capacity with only an additional 3.4% loss in capacity at the end of the simulation. Designers should therefore be aware that failure of the structural member is still possible during the decay phase. Apart from the parametric charring rate (which is limited in applicability), the effects of the decay phase are not considered by EN 1995-1-2 [49].

4.4 Optimum CLT Wall Design

The normalized and true values of the residual buckling capacities of the different ply arrangements for the 210 mm thick CLTs simulated in the parametric study under the 60 and 120-minute standard fire curves with cooling are shown in Figure 4-3 to Figure 4-6 below. Focus here will be on buckling load capacity since this is the governing mode of failure for CLT walls in fire. Similar plots for the crushing capacity are included in the appendix.

First, a closer look at the normalized residual capacity for each ply number and type under the different fire curves is taken. Under the shorter fire (Figure 4-3), the 3-ply CLT with uniform and larger crosswise layers lost most of their capacity with only 24.4% and 19.0% of the ambient capacity remaining, respectively. The 7-ply CLT retained the most strength in all cases, outperforming the 3 and 5-ply CLTs in terms retaining except for the case with thicker first and last layers (FL). The 5-ply CLT had comparatively medium performance, with the 5-ply CLT having larger longitudinal plies outperforming all other 5-ply arrangements at approximately 31% of its capacity.

Although from Figure 4-4 the 3-ply CLTs lost a larger percentage of its ambient capacity, in terms of true values, the 3-ply CLT performed much better than the 5 and 7-ply CLTs except for the case with larger crosswise layers where the 7-ply CLT had slightly higher capacity. Both 5 and 7-ply CLTs had similar capacities as can be seen in Figure 4-4.

When the same CLTs are subjected to a more severe fire, their performance changes. Figure 4-5 shows the normalized residual buckling capacities at the end of the simulation for all CLTs. As expected, the fraction of capacity left for each CLT is lesser as compared to the same CLTs under a shorter fire due to the increased thermal load and fire duration. All the 3-ply

CLTs lost a higher fraction of their ambient residual capacity relative to the 5 and 7-ply CLTs. The 3-ply CLT with thicker crosswise layers performed the worst with only 6.1% of its capacity left. The 7-ply CLTs lost approximately an additional 10% of their capacity when compared to the same CLTs under the shorter fire.

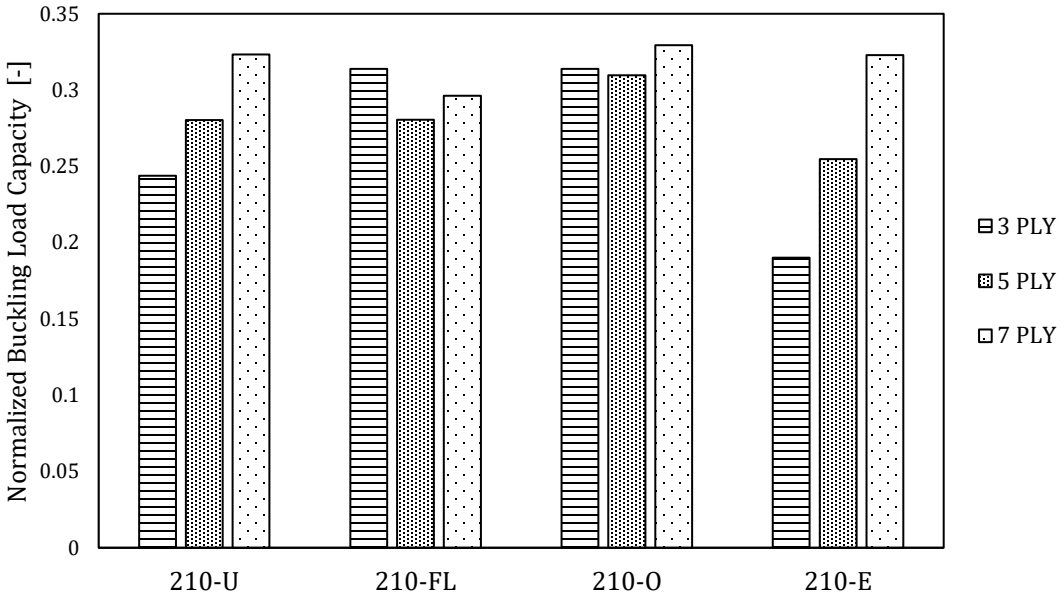

Figure 4-3 Comparison of the residual normalized buckling capacity of different CLTs [ISO - 60]

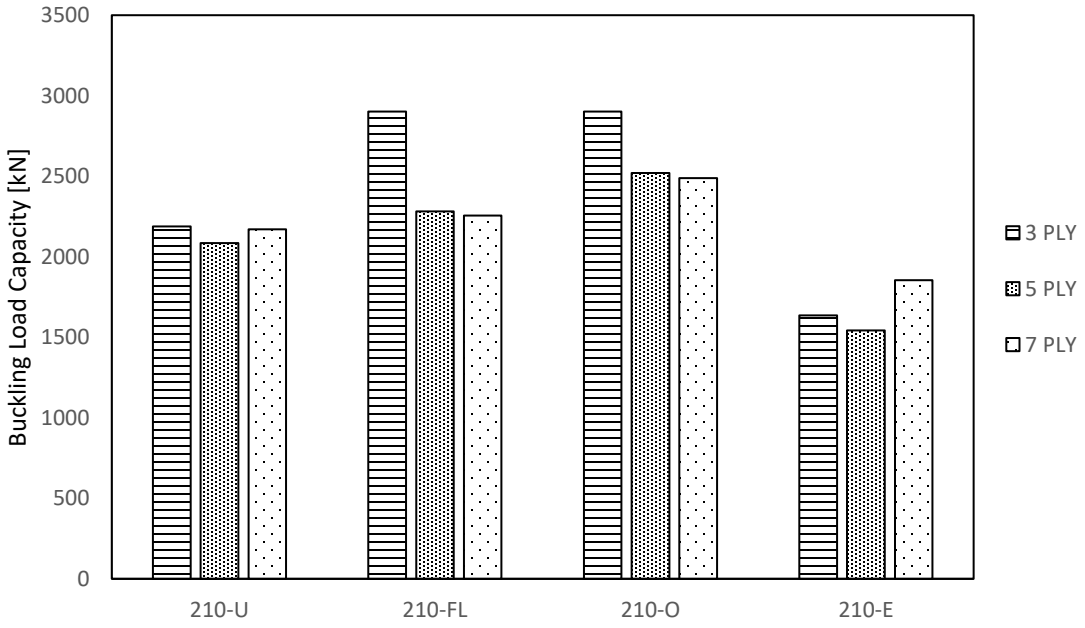

Figure 4-4 Comparison of the residual buckling capacities of different CLTs [ISO - 60]

With regards to the actual buckling capacity values (Figure 4-6), the 3-ply CLTs produced the worst performance with the exception of the case with thicker first and last layers where the 3 and 7-ply CLTs had similar capacities and the 5-ply CLT had the least capacity.

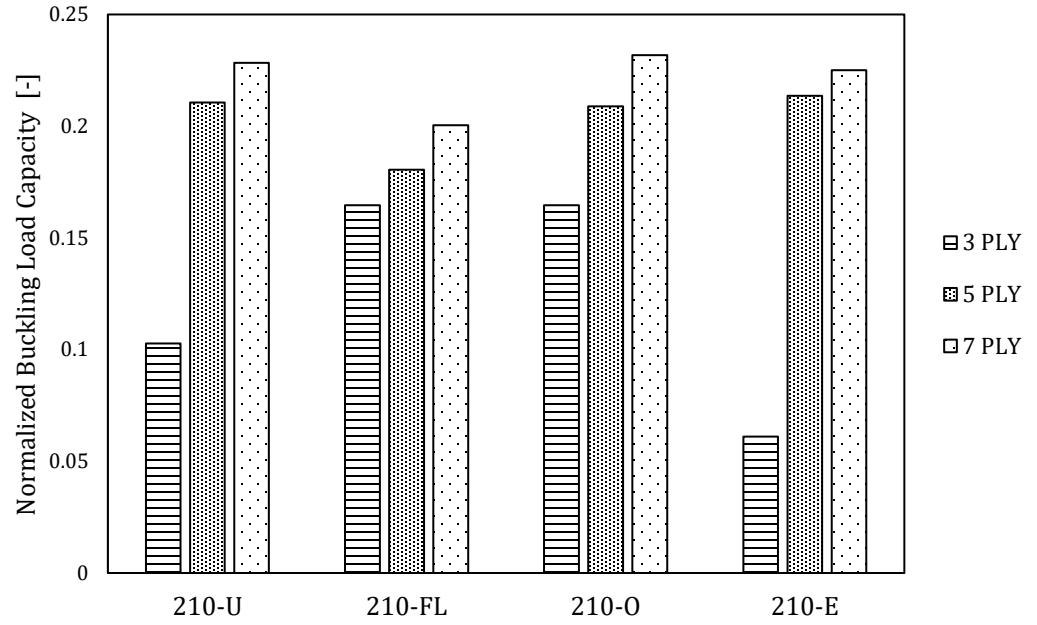

Figure 4-5 Comparison of the residual normalized buckling capacity of different CLTs [ISO - 120]

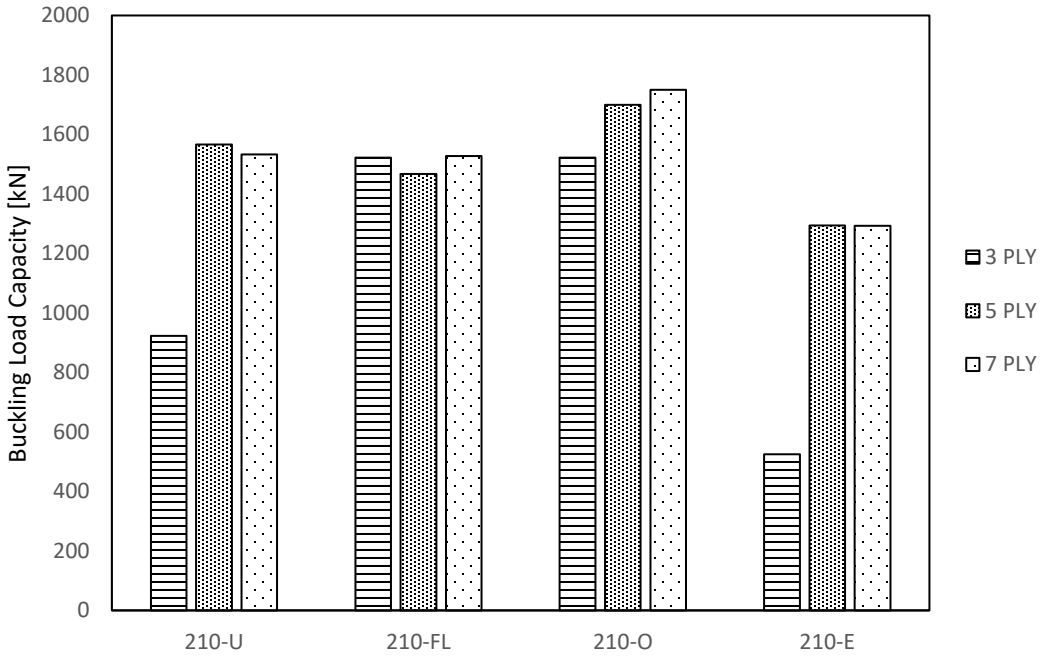

Figure 4-6 Comparison of the residual buckling capacities of different CLTs [ISO - 120]

The results and discussion presented above suggest that the fire behavior of a CLT is dependent upon the number, arrangement, and thickness of its individual plies as well as the fire load to which it is exposed to. This provides an interesting insight for designers and manufactures alike. Most CLT products in the market come in plies of equal thicknesses although such arrangement does not yield optimal performance. CLTs with thicker longitudinal plies have been found to have a greater initial capacity as well as perform better in a fire. It has been established in section 4.2 that buckling is the governing mode of failure for CLT walls in fire. Therefore, for designers interested in achieving an optimum ply number and arrangement for a 60-minute fire rating, these results suggest that designing and installing 3-ply CLT walls with larger longitudinal layers will yield the best result in buckling as compared to using other ply arrangements or number of plies.

On the contrary, for the same desired wall thickness, and under a more severe fire, opting for a 7-ply CLT with thicker longitudinal layers will guarantee a better performance as compared to 3 and 5-ply CLTs with the same arrangement. If due to design constraints or the available products in the market are limited to CLTs with uniformly thick layers, selecting a 5-ply CLT will then be more favorable.

CLTs with thicker longitudinal layers perform better in fire. However, for a particular wall thickness, how thick they should be with respect to the crosswise layers would require further investigation through experiments. Theoretically, the larger the longitudinal plies, the better the performance, howbeit in reality, failure modes such as slip or rolling shear may occur if the bond between layers is not strong enough. It is therefore imperative to carry out experiments in this regard.

As presented earlier, while changes in the end restraints or wall height may affect the buckling capacity at ambient conditions, such modifications do not enhance the performance of a wall in a fire and the rate at which buckling capacity is lost is still the same. For example, designing a CLT wall with fixed-pinned supports increases the overall buckling capacity approximately 1.4 times as compared to a pinned-pinned support at normal conditions. In a fire, the residual buckling capacities are identical.

5 CONCLUSION

CLT is an inventive engineered timber product that has revamped the timber construction industry due to its many advantages over the more traditional building materials such as steel and concrete. However, just as with any timber product, its combustibility limits its application in the built environment especially to tall timber buildings. The study carried out in this thesis is aimed at engineers and designers to provide them with helpful insight on the different factors that contribute to the structural performance of CLT walls in fire.

A one-dimensional transient heat transfer model was created to predict the temperature distribution in-depth of a CLT cross-section while accounting for temperature dependent thermal properties modeled according to the advanced method outlined in Annex B of EN 1995-1-2. By utilizing the simulated cross-section temperatures, a structural model was created to account for the reduction in strength and stiffness based on the thermomechanical properties for compressive strength and elastic modulus given in EN 1995-1-2 to predict the crushing and buckling load carrying capacity of the section with time. The structural model also computes the evolution of crushing and buckling capacities according to the reduced cross-section method based on the one-dimensional charring rate and the charring rate obtained from the position of the 300 °C isotherm. The above models also considered the reversibility of thermal and mechanical properties to simulate the recoverability of load carrying capacity during cooling. First an analysis of the different structural models was carried out under different standard and parametric fire exposures after which a parametric study was carried out. The following conclusions can be drawn:

- As expected, the thermal load and exposure time influence the temperature distribution in the cross-section and hence the extent of mechanical degradation. The effect of the decay phase and the rate of cooling has also been demonstrated to be very crucial in accounting for further reduction in crushing and buckling strength.
- The RCSM was unable to predict conservative crushing capacities for all the simulations ran. However, for buckling, the RCSM should be applied carefully in design as it might not always provide conservative results relative to the advanced method. Conservative results were obtained for 3-ply CLTs when the effective char

depth penetrated the second ply. For 5 and 7-ply CLTs, conservative results were obtained when the effective char depth penetrated the third ply. An increased zero-strength layer should therefore be used in designing CLT members to account for the influence of the ply layup on capacity predictions. Assuming recoverability of properties leads to overestimation of the load carrying capacity of CLT walls.

- In fire, the loss in buckling strength is more sudden as compared to crushing strength.
- For thicker CLT walls, crushing appears to be the governing critical load under ambient conditions. There is however a transition in the governing load from crushing to buckling and this may occur during or after the heating phase of a fire.
- In terms of buckling, varying the end support conditions or wall height only affects the buckling capacity of a CLT wall at ambient conditions with little effect on its residual capacity after a fire.
- The number, arrangement and thickness of the individual layers making up the CLT wall influence its residual capacity to a greater extent. CLTs with thicker longitudinal layers perform better in fire as opposed to equally thick plies, CLTs with larger crosswise layers and CLTs with thicker first and last layers. For the same wall thickness and under a short fire, 3-ply CLT walls with thicker longitudinal layers outperformed all other CLT arrangements. Similarly, under a more severe fire curve, 7-ply CLTs with thicker longitudinal layers performed better than other CLTs.

Further research

- Experimental tests investigating the results obtained from the numerical modeling carried out in this thesis are essential to validate the observations made here.
- A major setback of CLT is the phenomena of delamination. The model outlined in this thesis assumes the glue lines remain intact and hence delamination does not occur. This may lead to underestimation of in-depth temperatures and charring rates for cases where delamination occurs. Future models should therefore attempt at accounting for char fall off.
- Modeling of second order and P-delta effects to account for material and geometric nonlinearities should be included in future models to accurately capture failure modes such as instability failure.

References

[1] R. Brandner, G. Flatscher, A. Ringhofer, G. Schickhofer, and A. Thiel, "Cross laminated timber (CLT): overview and development," *Eur. J. Wood Wood Prod.*, vol. 74, no. 3, pp. 331–351, 2016, doi: 10.1007/s00107-015-0999-5.

[2] D. A. Weiss, *The Great Fire of London.* Trafford Publishing, 2012.

[3] Y. Hasemi, "Fire Research: Yesterday, Today, and Tomorrow Focusing on Japan.," *Fire Sci. Technol.*, vol. 23(4), pp. 262–268, 2004.

[4] F. Wiesner, "Structural behaviour of cross-laminated timber elements in fires," PhD Dissertation, The University of Edinburgh, 2019.

[5] A. Atreya, "Pyrolysis, ignition and fire spread on horizontal surfaces of wood," *Pyrolysis, Ignition Fire Spread Horiz. Surfaces Wood*, 1983, [Online]. Available: http://www.scopus.com/inward/record.url?eid=2-s2.0-0003600043&partnerID=tZOtx3y1.

[6] B. A. Bodig, J. and Jayne, *Mechanics of wood and wood composites.* 1982.

[7] M. H. Ramage *et al.*, "The wood from the trees: The use of timber in construction," *Renew. Sustain. Energy Rev.*, vol. 68, no. October 2015, pp. 333–359, 2017, doi: 10.1016/j.rser.2016.09.107.

[8] W. F. Kollmann, F.P. and Côté, "Solid wood. Principles of Wood Science and Technology, Reprint," *Springer-Verlag, Tokyo*, no. 1, p. p.180, 1984.

[9] R. Stürzenbecher, K. Hofstetter, and J. Eberhardsteiner, "Structural design of Cross Laminated Timber (CLT) by advanced plate theories," *Compos. Sci. Technol.*, vol. 70, no. 9, pp. 1368–1379, 2010, doi: 10.1016/j.compscitech.2010.04.016.

[10] R. M. Foster and M. H. Ramage, "Briefing: Super tall timber - Oakwood Tower," *Proc. Inst. Civ. Eng. Constr. Mater.*, vol. 170, no. 3, pp. 118–122, 2017, doi: 10.1680/jcoma.16.00034.

[11] R. E. Smith, G. Griffin, T. Rice, and B. Hagehofer-Daniell, "Mass timber: evaluating

construction performance," *Archit. Eng. Des. Manag.*, vol. 14, no. 1–2, pp. 127–138, 2018, doi: 10.1080/17452007.2016.1273089.

[12] I. Smith and A. Frangi, "Overview of design issues for tall timber buildings," *Struct. Eng. Int. J. Int. Assoc. Bridg. Struct. Eng.*, vol. 18, no. 2, pp. 141–147, 2008, doi: 10.2749/101686608784218833.

[13] J. W. G. Van De Kuilen, A. Ceccotti, Z. Xia, and M. He, "Very tall wooden buildings with Cross Laminated Timber," *Procedia Eng.*, vol. 14, pp. 1621–1628, 2011, doi: 10.1016/j.proeng.2011.07.204.

[14] M. F. L. Mallo and O. Espinoza, "Cross-Laminated Timber vs. Concrete/steel: Cost comparison using a case study," *WCTE 2016 - World Conf. Timber Eng.*, no. October, 2016.

[15] J. Zumbrunnen, P. and Fovargue, "MID RISE CLT BUILDINGS 2 THE UK· s EXPERIENCE AND POTENTIAL FOR AUS AND NZ," *World*, vol. 15, p. 19, 2012.

[16] E. Green, M. and Karsh, "The case for tall wood buildings," *Can. Wood Counc. behalf Wood Enterp. Coalit. by For. Innov. Investment, North Vancouver, BC, Canada.*, 2012.

[17] "World Green Building Council," *Swedish Council for Building Research*. https://www.worldgbc.org/news-media/WorldGBC-embodied-carbon-report-published.

[18] R. Jonsson and O. Pettersson, *Timber Structures and Fire. a Review of the Existing State of Knowledge and Research Requirements.* Swedish Council for Building Research, 1985.

[19] J. D. Barrett, F. Lam, and W. Lau, "Size Effects in Visually Graded Softwood Structural Lumber," *J. Mater. Civ. Eng.*, vol. 7, no. 1, pp. 19–30, 1995, doi: 10.1061/(asce)0899-1561(1995)7:1(19).

[20] J. M. Dinwoodie, *Timber: its nature and behaviour.* CRC Press, 2000.

[21] S. A. Young and P. Clancy, "Compression mechanical properties of wood at temperatures simulating fire conditions," *Fire Mater.*, vol. 25, no. 3, pp. 83–93, 2001,

doi: 10.1002/fam.759.

[22] J. Schmid, M. Klippel, A. Just, A. Frangi, and M. Tiso, “Simulation of the Fire Resistance of Cross-laminated Timber (CLT),” *Fire Technol.*, vol. 54, no. 5, pp. 1113–1148, 2018, doi: 10.1007/s10694-018-0728-9.

[23] M. He, X. Sun, and Z. Li, “Bending and compressive properties of cross-laminated timber (CLT) panels made from Canadian hemlock,” *Constr. Build. Mater.*, vol. 185, pp. 175–183, 2018, doi: 10.1016/j.conbuildmat.2018.07.072.

[24] M. Klippel and J. Schmid, “Design of cross-laminated timber in fire,” *Struct. Eng. Int.*, vol. 27, no. 2, pp. 224–230, 2017, doi: 10.2749/101686617X14881932436096.

[25] A. I. Bartlett, R. M. Hadden, and L. A. Bisby, “A Review of Factors Affecting the Burning Behaviour of Wood for Application to Tall Timber Construction,” *Fire Technol.*, vol. 55, no. 1, pp. 1–49, 2019, doi: 10.1007/s10694-018-0787-y.

[26] L. Lowden and T. Hull, “Flammability behaviour of wood and a review of the methods for its reduction,” *Fire Sci. Rev.*, vol. 2, no. 1, p. 4, 2013, doi: 10.1186/2193-0414-2-4.

[27] S. Poncsák, D. Kocaefe, M. Bouazara, and A. Pichette, “Effect of high temperature treatment on the mechanical properties of birch (Betula papyrifera),” *Wood Sci. Technol.*, vol. 40, no. 8, pp. 647–663, 2006, doi: 10.1007/s00226-006-0082-9.

[28] F. L. Browne, *Theories of the combustion of wood and its control.* 1958.

[29] E. Mikkola, “Charring of wood based materials,” *Fire Saf. Sci. Proc. Third Int. Symp.*, pp. 547–556, 2006, doi: 10.4324/9780203973493.

[30] J. König, “Effective thermal actions and thermal properties of timber members in natural fires.,” *Fire Mater. An Int. J.*, vol. 30(1), p. pp.51-63, 2006.

[31] A. Bartlett *et al.*, “Needs for total fire engineering of mass timber buildings,” *WCTE 2016 - World Conf. Timber Eng.*, 2016.

[32] X. Li, X. Zhang, G. Hadjisophocleous, and C. McGregor, “Experimental Study of Combustible and Non-combustible Construction in a Natural Fire,” *Fire Technol.*, vol.

51, no. 6, pp. 1447–1474, 2015, doi: 10.1007/s10694-014-0407-4.

[33] A. Frangi and M. Fontana, “Fire performance of timber structures under natural fire conditions,” *Fire Saf. Sci.*, pp. 279–290, 2005, doi: 10.3801/IAFSS.FSS.8-279.

[34] R. M. Hadden *et al.*, “Effects of exposed cross laminated timber on compartment fire dynamics,” *Fire Saf. J.*, vol. 91, no. February, pp. 480–489, 2017, doi: 10.1016/j.firesaf.2017.03.074.

[35] S. L. Zelinka, L. E. Hasburgh, K. J. Bourne, D. R. Tucholski, and J. P. Ouellette, “Compartment Fire Testing of a Two-Story Mass Timber Building,” *Fpl–Gtr–247*, no. 2018, p. 476, 2018, [Online]. Available: https://www.awc.org/pdf/codes-standards/fire/WCTE-2018_Fire-Tests.pdf.

[36] J. Su, P. Lafrance, M. Hoehler, and M. Bundy, “Fire Safety Challenges of Tall Wood Buildings – Phase 2: Task 2 & 3 – Cross Laminated Timber Compartment Fire Tests,” *Natl. Res. Counc. Canada*, no. February, p. 396, 2018.

[37] C. J. Bateman, A. I. Bartlett, L. Rutkauskas, and R. M. Hadden, “Effects of fuel load and exposed clt surface configuration in reduced-scale experiments,” *WCTE 2018 - World Conf. Timber Eng.*, no. May, 2018.

[38] R. Emberley *et al.*, “Description of small and large-scale cross laminated timber fire tests,” *Fire Saf. J.*, vol. 91, no. February, pp. 327–335, 2017, doi: 10.1016/j.firesaf.2017.03.024.

[39] A. Frangi and M. Fontana, “Charring rates and temperature profiles of wood sections,” *Fire Mater.*, vol. 27, no. 2, pp. 91–102, 2003, doi: 10.1002/fam.819.

[40] R. Emberley, A. Inghelbrecht, Z. Yu, and J. L. Torero, “Self-extinction of timber,” *Proc. Combust. Inst.*, vol. 36, no. 2, pp. 3055–3062, 2017, doi: 10.1016/j.proci.2016.07.077.

[41] H. Röll, “Untersuchungen über das Abbrandverhalten von Fichten-und Eichenholz, in Abhängigkeit von Rohdichte, Jahrringorientierung und Zeit.,” 1984.

[42] J. ichi Suzuki, T. Mizukami, T. Naruse, and Y. Araki, “Fire Resistance of Timber Panel Structures Under Standard Fire Exposure,” *Fire Technol.*, vol. 52, no. 4, pp. 1015–

1034, 2016, doi: 10.1007/s10694-016-0578-2.

[43] P. Reszka, “In-Depth Temperature Profiles in Pyrolyzing Wood,” *Sch. Civ. Eng.*, vol. Doctor of, no. June, p. 193, 2008, [Online]. Available: http://hdl.handle.net/1842/2602.

[44] A. Frangi, M. Fontana, M. Knobloch, and G. Bochicchio, “Fire behaviour of cross-laminated solid timber panels,” *Fire Saf. Sci.*, pp. 1279–1290, 2008, doi: 10.3801/IAFSS.FSS.9-1279.

[45] J. König, “Structural fire design according to Eurocode 5 - Design rules and their background,” *Fire Mater.*, vol. 29, no. 3, pp. 147–163, 2005, doi: 10.1002/fam.873.

[46] J. König and L. Walleij, “Timber frame assemblies exposed to standard and parametric fires Part 2: A design model for standard fire exposure,” *Institutet f¨or Tr¨ateknisk Forsk.*, no. issn: 1102-1071, pp. 1–76, 2000.

[47] R. H. White and M. A. Dietenberger, “Wood Products: Thermal Degradation and Fire,” *Encycl. Mater. Sci. Technol.*, pp. 9712–9716, 2001, doi: 10.1016/b0-08-043152-6/01763-0.

[48] T. . Lie, “A method for assessing the fire resistance of laminated timber beams and columns,” *Can. J. Civ. Eng.*, vol. 4, no. 2, pp. 161–169, 1977.

[49] EN1995-1-2., “Eurocode5: Design of Timber Structures Part 1–2: General Structural Fire Design,” *CEN, Eur. , Comm. Stand. Brussels*, 2004.

[50] E. Johansson and A. Svenningsson, “Delamination of Cross-laminated timber and its impact on fire development: Focusing on different types of adhesives,” 2018.

[51] M. Goina, “Resistenza al fuoco di pareti compresse in legno lamellare incrociato (Fire resistance of cross-laminated timber wall panels),” *Univ. Trieste, Trieste, Italy.*, 2010.

[52] K. L. Friquin, M. Grimsbu, and P. J. Hovde, “Charring rates for cross-laminated timber panels exposed to Standard and Parametric fires,” *11th World Conf. Timber Eng. 2010, WCTE 2010*, vol. 4, no. October, pp. 3293–3301, 2010.

[53] L. Osborne and C. Dagenais, “Preliminary CLT Fire Resistance Testing Report,” *FP Innov. Rep.*, no. 301006155, 2012.

[54] B. Östman *et al.*, “Fire safety in timber buildings,” *Tech. Guidel. Eur. SP, 19.*, pp. 39–48, 2013.

[55] R. Emberley, T. Do, J. Yim, and J. L. Torero, “Critical heat flux and mass loss rate for extinction of flaming combustion of timber,” *Fire Saf. J.*, vol. 91, no. February, pp. 252–258, 2017, doi: 10.1016/j.firesaf.2017.03.008.

[56] R. Crielaard, J. W. van de Kuilen, K. Terwel, G. Ravenshorst, and P. Steenbakkers, “Self-extinguishment of cross-laminated timber,” *Fire Saf. J.*, vol. 105, no. January, pp. 244–260, 2019, doi: 10.1016/j.firesaf.2019.01.008.

[57] A. Frangi, M. Fontana, E. Hugi, and R. Jübstl, “Experimental analysis of cross-laminated timber panels in fire,” *Fire Saf. J.*, vol. 44, no. 8, pp. 1078–1087, 2009, doi: 10.1016/j.firesaf.2009.07.007.

[58] D. Nicolaidis, A., Emberley, R., Fernando and J. Torero, “Thermally driven failure mode changes in bonded timber joints,” in *In WCTE 2016-World Conference on Timber Engineering*, pp. 5243–5251.

[59] R. Emberley and J. L. Torero, “Cross-laminated timber failure modes for fire conditions,” 2015.

[60] H. L. Malhotra, “Fire Resistance of Laminated Timber Columns,” 1967.

[61] K. Odeen, “Fire resistance of glued laminated timber structures.,” *Fire Struct. Use Timber Build.*, p. pp.7-15, 1970.

[62] L. Hasburgh, K. Bourne, C. Dagenais, L. Ranger, and A. Roy-Poirier, “Fire performance of mass-timber encapsulation methods and the effect of encapsulation on char rate of cross-laminated timber,” *WCTE 2016 - World Conf. Timber Eng.*, 2016.

[63] F. Wiesner and L. Bisby, “The structural capacity of laminated timber compression elements in fire: A meta-analysis,” *Fire Saf. J.*, vol. 107, no. May 2018, pp. 114–125, 2019, doi: 10.1016/j.firesaf.2018.04.009.

[64] J. König and B. Källsner, “Cross-section properties of fire exposed rectangular timber members.”

[65] E. Schaffer, C. Marx, D. Bender, and F. Woeste, “Strength validation and fire endurance of glued-laminated timber beams,” *Res. Pap. FPL 467. For. Prod. Lab. Madison*, 1986.

[66] S. A. Lineham, D. Thomson, A. I. Bartlett, L. A. Bisby, and R. M. Hadden, “Structural response of fire-exposed cross-laminated timber beams under sustained loads,” *Fire Saf. J.*, vol. 85, pp. 23–34, 2016, doi: 10.1016/j.firesaf.2016.08.002.

[67] D. J. Hopkin, J. El-Rimawi, T. Lennon, and V. V. Silberschmidt, “Effect of fire-induced damage on the uniaxial strength characteristics of solid timber: A numerical study,” *J. Phys. Conf. Ser.*, vol. 305, no. 1, 2011, doi: 10.1088/1742-6596/305/1/012039.

[68] J. Schmid, A. Menis, M. Fragiacomo, I. Clemente, and G. Bochicchio, “Behaviour of Loaded Cross-Laminated Timber Wall Elements in Fire Conditions,” *Fire Technol.*, vol. 51, no. 6, pp. 1341–1370, 2015, doi: 10.1007/s10694-015-0516-8.

[69] J. Schmid, A. Just, M. Klippel, and M. Fragiacomo, “The Reduced Cross-Section Method for Evaluation of the Fire Resistance of Timber Members: Discussion and Determination of the Zero-Strength Layer,” *Fire Technol.*, vol. 51, no. 6, pp. 1285–1309, 2015, doi: 10.1007/s10694-014-0421-6.

[70] F. Wiesner, F. Randmael, W. Wan, L. Bisby, and R. M. Hadden, “Structural response of cross-laminated timber compression elements exposed to fire,” *Fire Saf. J.*, vol. 91, pp. 56–67, 2017, doi: 10.1016/j.firesaf.2017.05.010.

[71] J. Schmid, M. Klippel, A. Just, and A. Frangi, “Review and analysis of fire resistance tests of timber members in bending, tension and compression with respect to the Reduced Cross-Section Method,” *Fire Saf. J.*, vol. 68, pp. 81–99, 2014, doi: 10.1016/j.firesaf.2014.05.006.

[72] B. Fredlund, “A model for heat and mass transfer in timber structures during fire: a theoretical, numerical and experimental study.,” 1988.

[73] G. Thomas, “Fire resistance of light timber framed walls and floors.,” University of Canterbury, 1996.

[74] A. Frangi, *Brandverhalten von Holz-Beton-Verbunddecken*, vol. 269. 2001.

[75] J. R. Mehaffey, P. Cuerrier, and G. Carisse, “A model for predicting heat transfer through gypsum-board/wood-stud walls exposed to fire,” *Fire Mater.*, vol. 18, no. 5, pp. 297–305, 1994, doi: 10.1002/fam.810180505.

[76] M. Janssens, “Thermo-physical properties for wood pyrolysis models.”

[77] A. . Knudson, R.M Schniewind, “Performance of structural wood members exposed to fire,” 1975.

[78] S. Hadvig, “Charring of Wood in Building Fires,” Technical University of Denmark: Lyngby., 1981.

[79] P. Clancy, “Time and probablity of failure of timber framed walls in fire,” Doctoral dissertation, Victoria University of Technology, 1999.

[80] P. Clancy, “A parametric study on the time-to-failure of wood framed walls in fire,” *Fire Technol.*, vol. 38, no. 3, pp. 243–269, 2002, doi: 10.1023/A:1019882131985.

[81] D. J. Barber and A. . Buchanan, “Fire resistance of epoxied steel rods in Glulam timber.,” *Dep. Civ. Eng. Univ. Canterbury.*, 1994.

[82] W. Klingsch, M. Tavakkol-Khah, J. Wesche, and M. Kersken-Bradley, “Temperaturentwicklung in brandbeanspruchten Holzquerschnitten Technical report,” 1993.

[83] D. J. Hopkin, J. El-Rimawi, V. Silberschmidt, and T. Lennon, “An effective thermal property framework for softwood in parametric design fires: Comparison of the Eurocode 5 parametric charring approach and advanced calculation models,” *Construction and Building Materials*, vol. 25, no. 5. pp. 2584–2595, 2011, doi: 10.1016/j.conbuildmat.2010.12.002.

[84] J. König, “Fire Resistance of Timber Joists and Load Bearing Wall Frames,” *SP Rep.*,

1995.

[85] J. König, J. Norén, F. B. Olesen, and F. T. Hansen, “Timber Frame Assemblies Exposed to Standard and Parametric Fires: Part 1, Fire Tests.,” 1997.

[86] C. . Gerhards, “Effect of Moisture Content and Temperature on the Mechanical Properties of Wood: An Analysis of Immediate Effects,” *Wood Fiber Sci.*, vol. 14, no. 1, pp. 4–36, 1982, [Online]. Available: http://wfs.swst.org/index.php/wfs/article/viewFile/501/501.

[87] I. M. Van Zeeland, J. J. Salinas, and J. R. Mehaffey, “Compressive strength of lumber at high temperatures,” *Fire Mater.*, vol. 29, no. 2, pp. 71–90, 2005, doi: 10.1002/fam.871.

[88] E. Sano, “Effects of temperature on the mechanical properties of wood. I. Compression parallel-to-grain.,” *Japan Wood Res. Soc*, vol. 7(5), p. pp.147-150, 1961.

[89] M. J. Manríquez Figueroa and P. Dias De Moraes, “Temperature reduction factor for compressive strength parallel to the grain,” *Fire Saf. J.*, vol. 83, pp. 99–104, 2016, doi: 10.1016/j.firesaf.2016.05.005.

[90] H. D. Tiemann, *Effect of moisture upon the strength and stiffness of wood*. US Department of Agriculture, Forest Service, 1906.

[91] R. I. Rykov, “Strength Characteristics of Timber at High Temperature Heating,” *In Fire Resistance of Wood Structures VTT Symposium*. p. (Vol. 9, pp. 157-159)., 1980.

[92] D. Hosser, T. Dorn, and O. El-Nesr, “Experimental and numerical studies of composite beams exposed to fire,” *J. Struct. Eng.*, vol. 120, no. 10, p. pp.2871-2892., 1994.

[93] G. Thomas and A. Buchanan, “In Proceedings of the Fourth International Fire and Materials Conference; Marriot Hotel, Crystal City Virginia, USA,” 1995.

[94] C. Gerhards, “Wood Fiber,” vol. 4, no. 1, pp. 4–36, 1984.

[95] B. Moghtaderi, “The state-of-the-art in pyrolysis modelling of lignocellulosic solid fuels,” *Fire Mater.*, vol. 30, no. 1, pp. 1–34, 2006, doi: 10.1002/fam.891.

[96] F. Jong and P. Clancy, “Compression properties of wood as functions of moisture, stress and temperature,” *Fire Mater.*, vol. 28, no. 2–4, pp. 209–225, 2004, doi: 10.1002/fam.859.

[97] R. White, “In The SFPE Handbook of Fire Protection Engineering. National Fire Protection Association: Quincy, MA,USA,” 1988.

[98] C. H. Bamford, J. Crank, and D. H. Malan, “The combustion of wood. Part I,” *Math. Proc. Cambridge Philos. Soc.*, vol. 42, no. 2, pp. 166–182, 1946, doi: 10.1017/S030500410002288X.

[99] P. . Thomas, “On the rate of burning of wood,” *Fire Saf. Sci.*, vol. 446, no. I, p. pp.1-1., 1960.

[100] H. C. Kung, “A mathematical model of wood pyrolysis,” *Combust. Flame*, vol. 18, no. 2, pp. 185–195, 1972, doi: 10.1016/S0010-2180(72)80134-2.

[101] F. Richter and G. Rein, “A multiscale model of wood pyrolysis in fire to study the roles of chemistry and heat transfer at the mesoscale,” *Combust. Flame*, vol. 216, pp. 316–325, 2020, doi: 10.1016/j.combustflame.2020.02.029.

[102] C. Lautenberger and C. Fernandez-Pello, “A model for the oxidative pyrolysis of wood,” *Combust. Flame*, vol. 156, no. 8, pp. 1503–1513, 2009, doi: 10.1016/j.combustflame.2009.04.001.

[103] C. Lautenberger and C. Fernandez-Pello, “Generalized pyrolysis model for combustible solids,” *Fire Saf. J.*, vol. 44, no. 6, pp. 819–839, 2009, doi: 10.1016/j.firesaf.2009.03.011.

[104] P. Reszka and J. L. Torero, “In-depth temperature measurements in wood exposed to intense radiant energy,” *Exp. Therm. Fluid Sci.*, vol. 32, no. 7, pp. 1405–1411, 2008, doi: 10.1016/j.expthermflusci.2007.11.014.

[105] T. Gernay, “Defining a burnout resistance rating to compare structural components under real fires.pdf.”

[106] F. Wiesner *et al.*, “Structural capacity in fire of laminated timber elements in

compartments with exposed timber surfaces," *Eng. Struct.*, vol. 179, no. October 2018, pp. 284–295, 2019, doi: 10.1016/j.engstruct.2018.10.084.

[107] T. Gernay, "Fire resistance and burnout resistance of timber columns," *Fire Saf. J.*, vol. 122, p. 103350, 2021, doi: 10.1016/j.firesaf.2021.103350.

[108] Mathworks, "MATLAB." https://www.mathworks.com.

[109] M. Kawakami and A. Ghali, "Time-dependent stresses in prestressed concrete sections of general shape," *PCI J.*, vol. 41, no. 3, pp. 96–102, 1996, doi: 10.15554/pcij.05011996.96.105.

[110] "Binderholz CLT." https://www.binderholz.com/.

[111] "Mayr Melnhof Holz." http://www.mm-holz.com/.

[112] "Stora Enso." https://www.storaenso.com.

[113] "KLH." https://www.klhuk.com.

[114] "Zueblin Timber." https://www.zueblin-timber.com.

[115] "Hasslacher Norica." https://www.hasslacher.com.

[116] ISO834-1, "Fire-reseistance tests—Elements of building construction—Part 1: General requirements.," *Int. Organ. Stand. ISO. Geneva, Switz.*, 1999.

[117] EN1991-1-2, "Eurocode 1: Actions on structures - Part 1-2."

A. Appendix A: Results for 120-Minute Standard Fire Curve

Results from Thermal Analysis: Charring Rate, Charring Depth and Effective Charring

The position of the 300 °C isotherm and the charring rate obtained from the thermal analysis are shown in Figure A-1. A similar trend is observed for the charring rate and position of the 300 °C isotherm as with the 60-minute standard fire. The maximum charring rate obtained was still 0.92 mm/min and occurred at 5.44 minutes. This was expected since both fire curves have identical thermal loads during that period. Due to the increased thermal load, more heat will be conducted through the timber section implying the pyrolysis and char of a larger depth of timber. This would in turn slow down thermal penetration from the surface to the timber underneath owing to the reduced thermal conductivity of the char layer. This is apparent from Figure A-1, where the initial increased rate of rise in the depth of the 300 °C isotherm slowly reduces with time. At the end of the heating phase, the achieved charring rate was 0.38 mm/min.

A higher thermal load will also connote a more severe thermal wave travelling through the timber section during the decay phase. Beyond the heating phase, the depth of the 300 °C isotherm continues to increase for next 14 minutes after which it remains constant at 49 mm until the 160th minute. Subsequently, no more increase in depth is recorded and a sharp decline to zero follows.

Figure A-2 shows the effective charring depths computed based on the position of the 300 °C isotherm and according to the EC 5 method. Similar observations are made during the first few minutes of the fire. At about 28 minutes, the two effective char depths overlap, and this corresponds to the time the char rate in Figure A-1 meets the EN char rate as outlined earlier. The final effective char depth computed using the position of the 300 °C isotherm equal to 56 mm is considerably lower than the calculated depth as per EC 5 equal to 85 mm. This could be related to the heat protection provided by the char layer which prevented much adverse thermal penetration and hence limited the charring rate.

Simulations were carried out for a 120 mm and 150 mm 3-ply CLT wall of equal ply thickness (40mm and 50 mm each) under a 120-minute standard fire with 65 minutes linear cooling

to simulate burnout. Figure A-3 shows the predicted losses in crushing (indicated as CS) and buckling strength (indicated as BS) capacities.

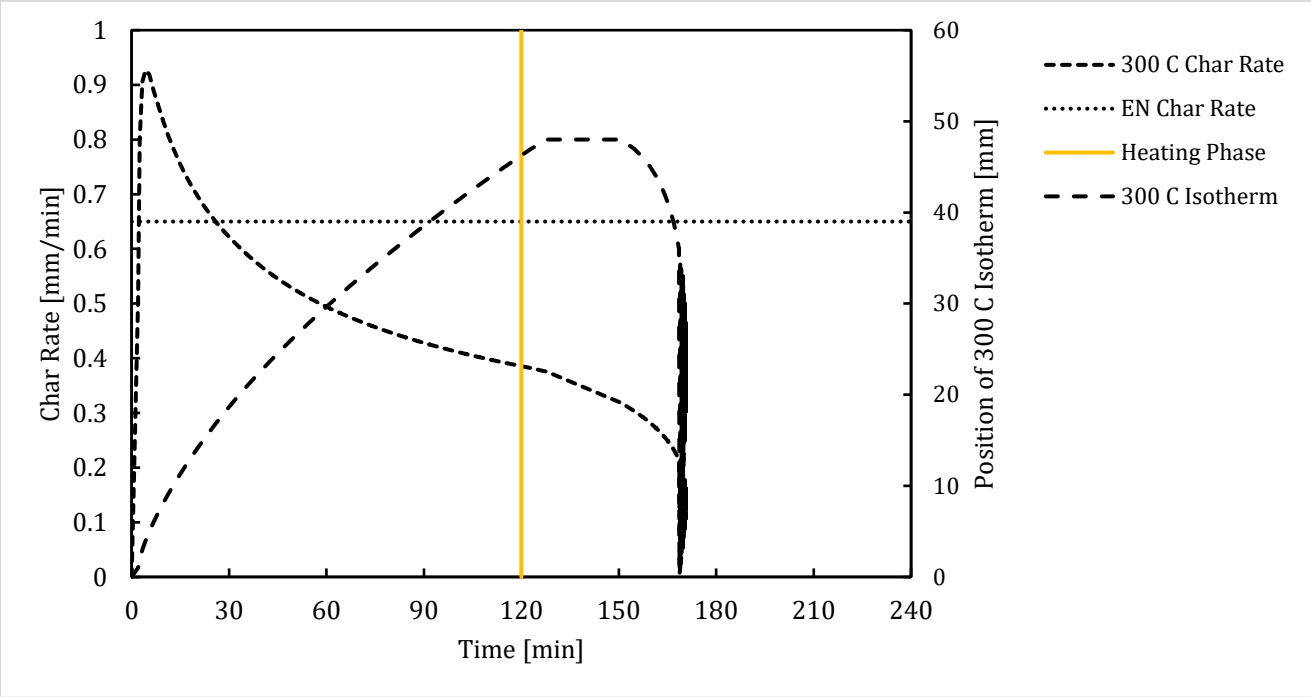

Figure A-1 Position of 300 °C isotherm and corresponding char rate under [ISO-120]

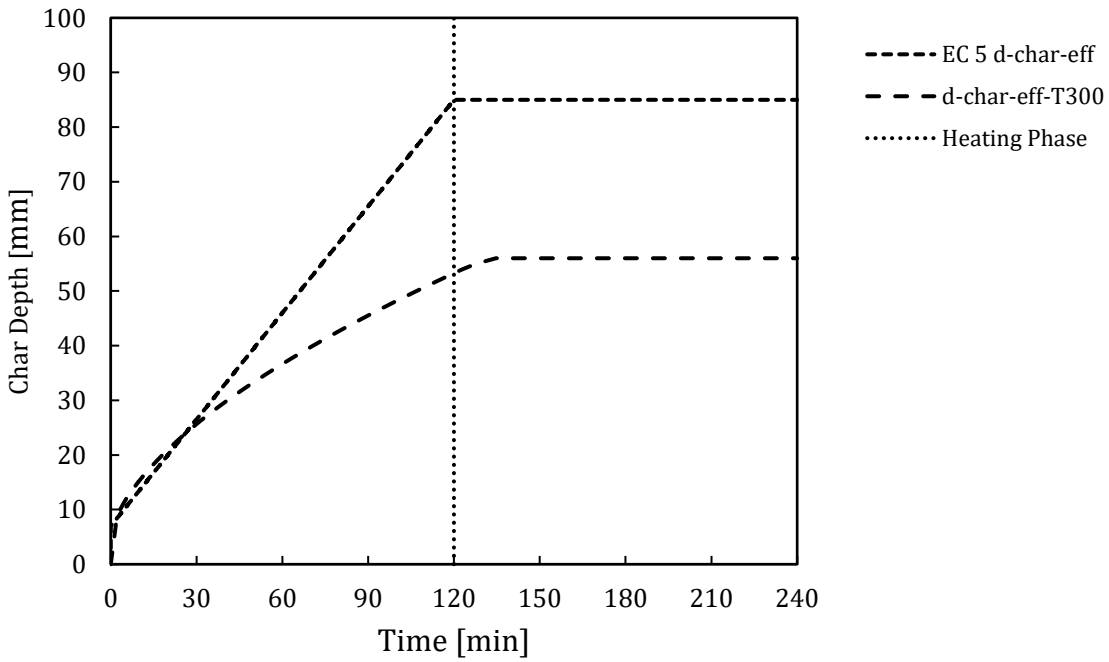

Figure A-2 Effective char depth as per EC 5 and 300 °C isotherm for [ISO-120]

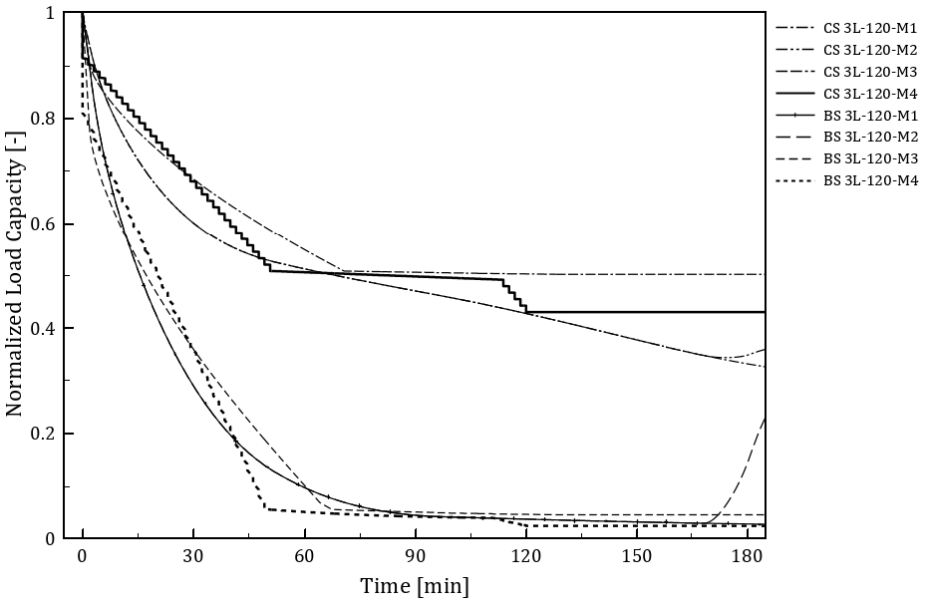

Figure A-3 Normalized load carrying capacity for 120 mm 3-ply CLT under [ISO-120]

Results from Structural Analysis

Results for the 3, 5 and 7-ply CLTs show similar trends when subjected to a more severe standard fire curve as was presented above. However, the higher thermal load and prolonged fire duration will imply a more adverse thermal wave and deeper thermal penetration depths, consequently further degradation of the mechanical properties (and hence load capacity) will occur. Taking the buckling strength predictions of model M1 for the 140 mm 7-ply CLT for example, the residual capacity at the end of the simulation of the 60-minutes standard fire with cooling is 21.9% as opposed to only 8.4% capacity when the same CLT is subjected to the 120-minute standard fire. The same observations can be made for the crushing capacity as well as the capacities predicted for other CLTs investigated under both fires.

The calculated effective char depth (Figure A-2) under a 120-minutes standard fire is 85 mm. Therefore, for the CLTs under consideration, the char depth will penetrate more longitudinal plies inducing more losses in capacity. This is evident in Figure A-3, Figure A-4 and Figure A-5 where the first two plies have failed for the 3-ply CLT and the first four plies have failed for both the 5 and 7-ply CLTs.

The predicted capacity by model M4 and in some cases M3 at the point of failure of a longitudinal lamella generally results in a more significant loss in strength at that point (in time) as compared to Model M1. This has to do with the addition of a zero-strength layer at each time step for models M3 and M4 resulting in a sudden transition from a longitudinal ply to a crosswise ply. M1 uses the simulated temperature distribution in depth at each time step to determine the reduced mechanical properties and compute the loss in strength in a more progressive manner.

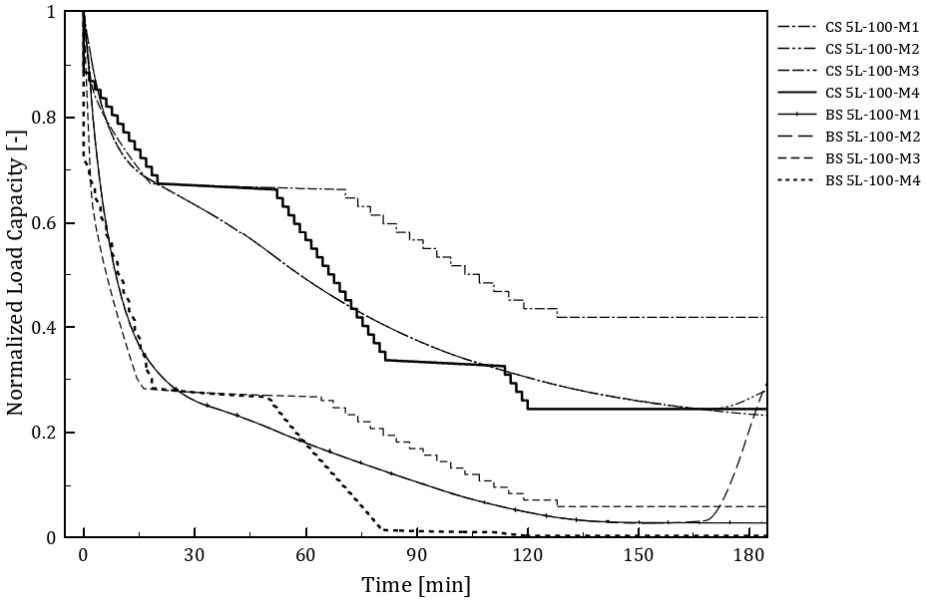

Figure A-4 Normalized load carrying capacity for 100 mm 5-ply CLT under [ISO-120]

All models showed comparable trends for the buckling capacity predictions throughout the simulation with model M3 again being the least conservative. Model M4 produced the most conservative results at the end of the heating phase for all CLTs. At the end of the simulation, additional losses in capacity were recorded by model M1, even so, the predictions by model M4 were still the most conservative.

Similarly for crushing capacity, model M4 gave the most conservative results at the 120-minute mark for all CLTs. However, further losses in capacity accounted for by model M1 make the advanced model more conservative than model M4.

Model M4 marginally outperformed the advanced model in predicting the buckling capacity and hence a further analysis is carried out on slightly thicker CLTs to investigate the

performance of model M1 and M4. Interest here is concerned with the buckling strength predicted by models M1 and M4. Simulations for 150 mm 3-ply, 225 mm 5-ply and 315 mm 7-ply CLTs were carried out under the same fire scenario. These new thicknesses were selected such that the thickness of any two layers is greater than the effective char depth (85 mm). As can be observed in Figure A-6, apart from the 3-ply CLT, model M1 outperforms M4 giving more conservative results at the end of the heating phase for the 5 and 7-ply CLTs. With the further loss of strength during the cooling phase, model M1 outperforms model M4 for all CLTs. For the 3, 5 and 7-ply CLTs, M4 underpredicts the residual buckling strength by 0.7%, 6.2% and 8.3%, respectively.

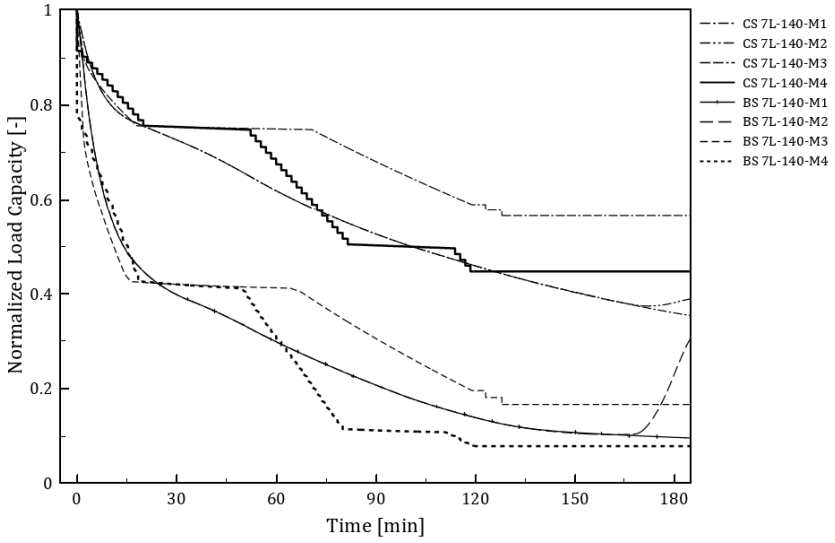

Figure A-5 Normalized load carrying capacity for 140 mm 7-ply CLT under [ISO-120]

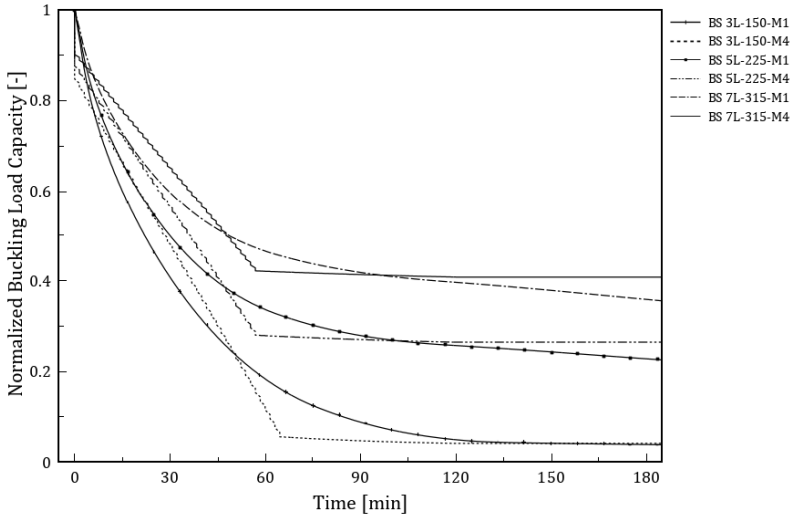

Figure A-6 Normalized buckling load capacity for models M1 and M4 for 3, 5 and 7-ply CLTs under [ISO-120]

B. Appendix B: Results for Long Parametric Curve

Results from Thermal Analysis: Charring Rate and Effective Charring Depth

The long parametric curve has the most intense fire load and duration. As expected, the 300 °C isotherm reached far deeper into the cross-section as compared to the other fire curves with a maximum depth of 66 mm as shown in Figure B-1. Even though the long parametric fire curve is more severe than the shorter parametric curve, they both have identical fire load for the first 38 minutes. This resulted in a similar maximum charring rate of 1.22 mm/min during the first four minutes of the fire. The trend in the reduction of the charring rate is similar as explained above. During the decay phase, the 300 °C isotherm propagated deeper into the cross-section from a depth of 62 mm to a depth of 66 mm in about 27 minutes and maintains this depth of for the next 31 minutes.

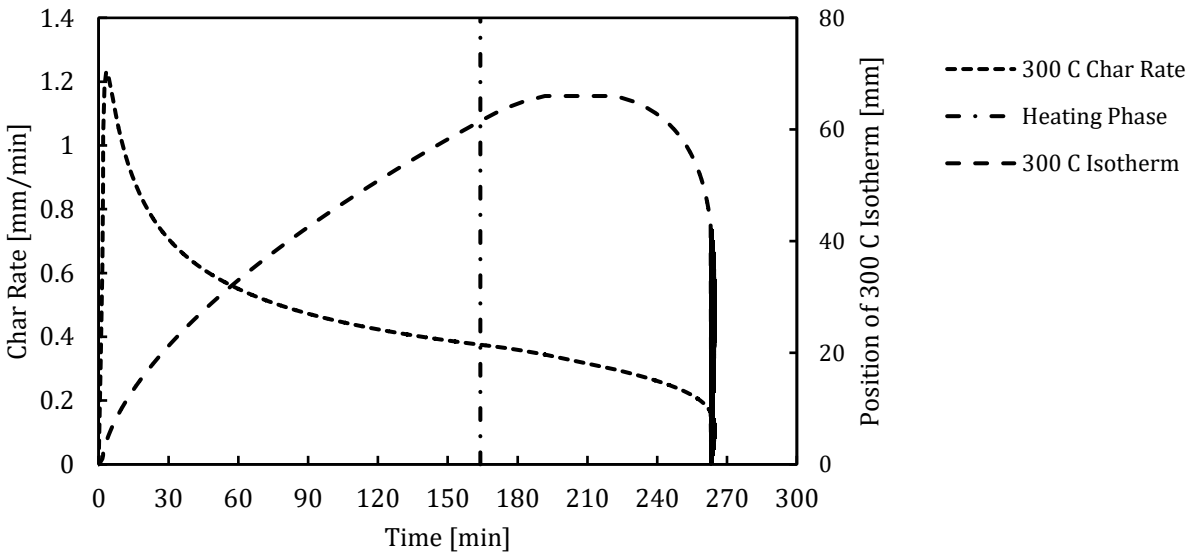

Figure B-1 Position of 300 °C isotherm and corresponding char rate under long parametric fire

The parametric charring rate given in annex A of EC 5 is not applicable to parametric fires with t_0 > 40 minutes (see section 1.4) and hence Figure B-2 shows the effective charring depths computed based on the position of the 300 °C isotherm only. This would also imply

that the RCSM based on the parametric charring rate and hence model M4 will not be applicable here. The maximum effective char depth obtained was 73 mm.

Results from Structural Analysis

Similar trends are observed as outlined earlier in this section. A significant difference is however observed in the residual capacities for buckling and crushing for the three different CLTs. Being exposed to a more severe fire meant that a deeper thermal penetration and additional thermomechanical degradation of a larger depth of the CLT cross-section would occur resulting in lower capacities. The EC 5 RCSM cannot be applied here due to the limits of applicability of the parametric charring rate as indicated earlier.

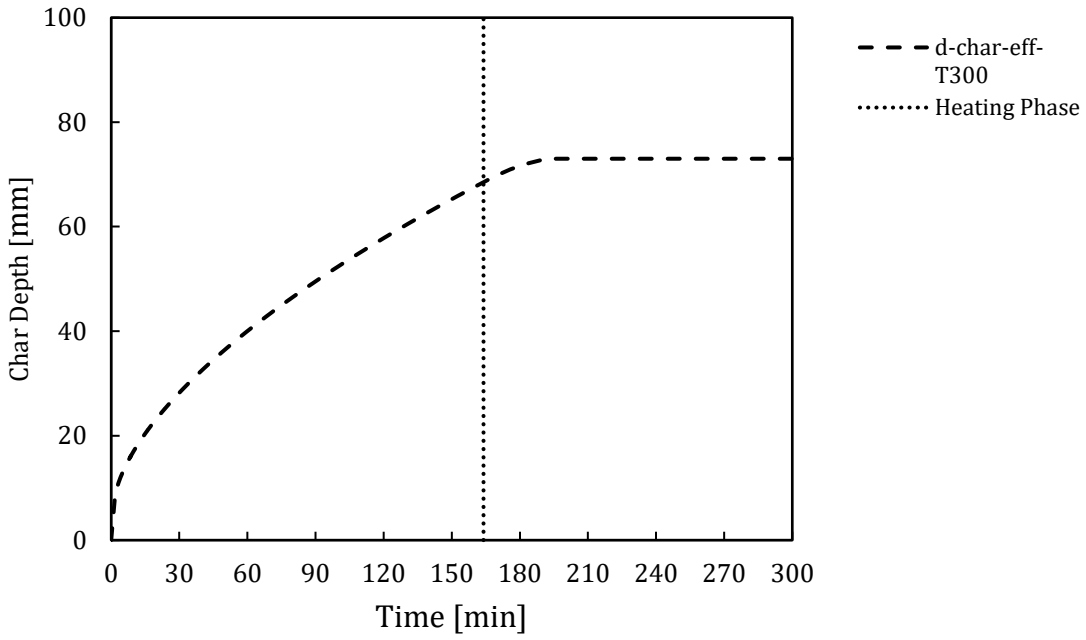

Figure B-2 Effective char depth as per 300 °C isotherm for [ISO-60]

Considering the advanced model (M1), the 3-ply CLT had 20% of its crushing capacity and only 1.7% buckling capacity as shown in Figure B-3. This would translate into certain failure of this wall under this fire curve. Worse performance was recorded for the 5-ply CLT (Figure B-4) which had only 14% of its crushing and 0.5% of its buckling capacity left. The 7-ply CLT (Figure B-5) performed slightly better with 23.9% and 4.3% for crushing and buckling capacities, respectively.

For all cases, model M3 produced very non-conservative results in terms of crushing capacity for all CLTs. Model M3 predicted similar residual buckling capacities for the 3 and 5-ply CLTs while being unconservative for the 7-ply CLT. The advanced recovery model, M2, exhibited

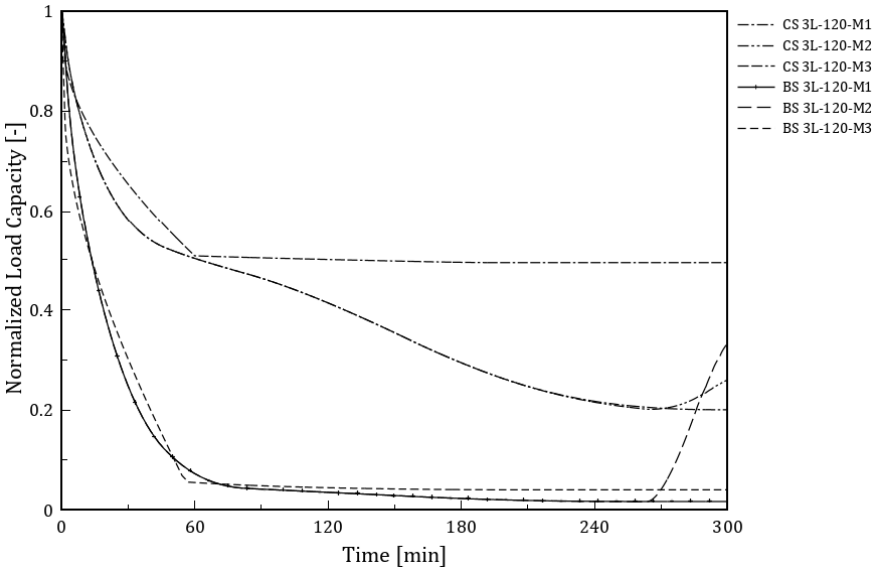

Figure B-3 Normalized load carrying capacity for 120 mm 3-ply CLT under long parametric fire

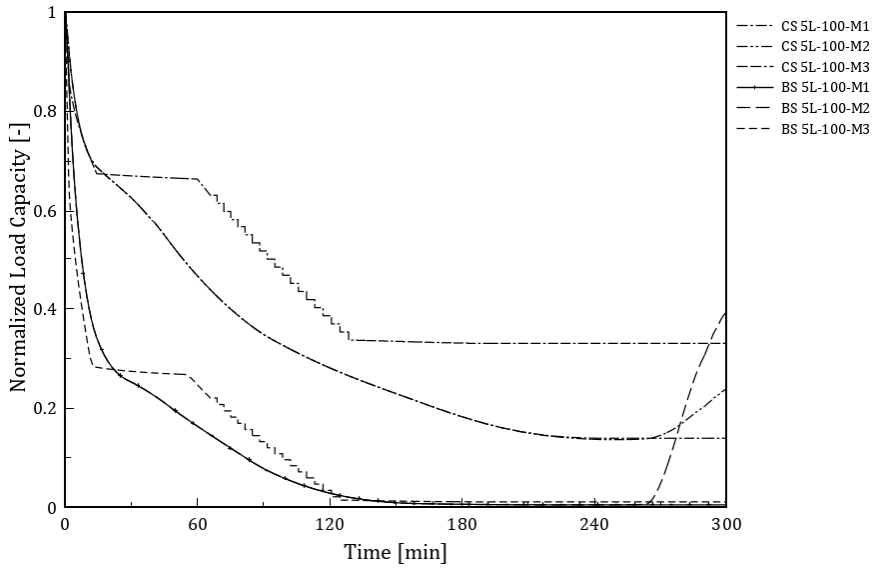

Figure B-4 Normalized load carrying capacity for 100 mm 5-ply CLT under long parametric fire

similar trends as outlined above predicting higher recovery in buckling capacity as opposed to crushing capacity for all CLTs.

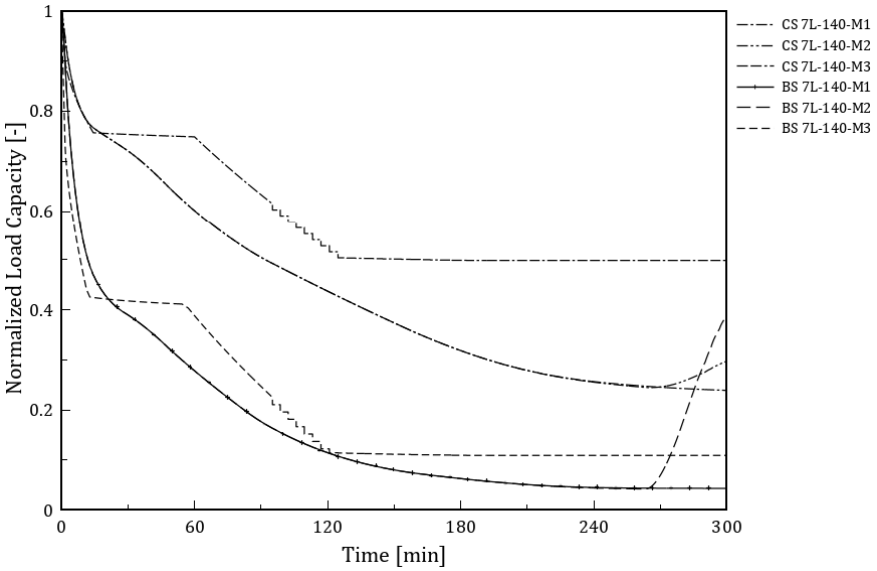

Figure B-5 Normalized load carrying capacity for 140 mm 7-ply CLT under long parametric fire

C. Appendix C: Effect of Restraint Results for 5 and 7-Ply CLT

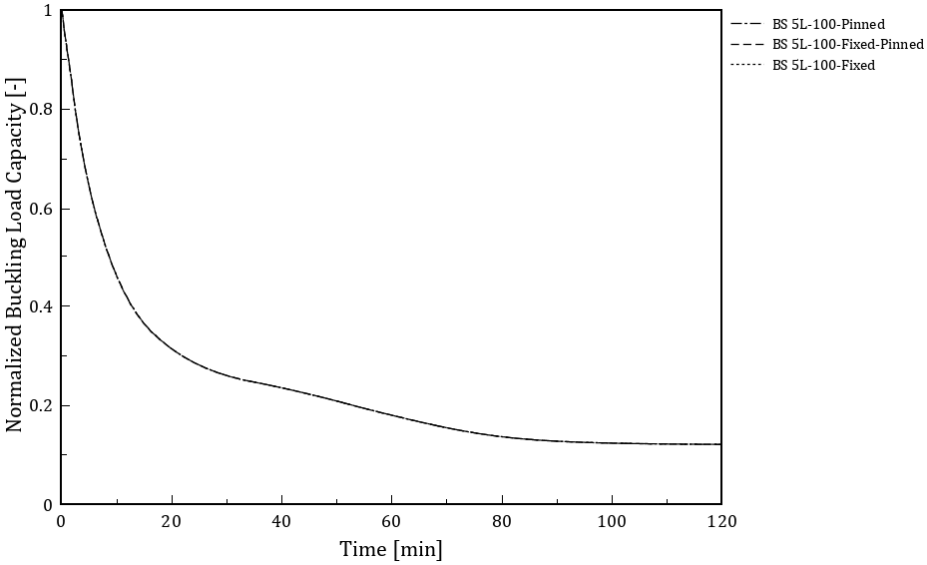

Figure C-1 Normalized buckling load capacity for 100 mm 5-ply CLT with varying end restraints [ISO – 120]

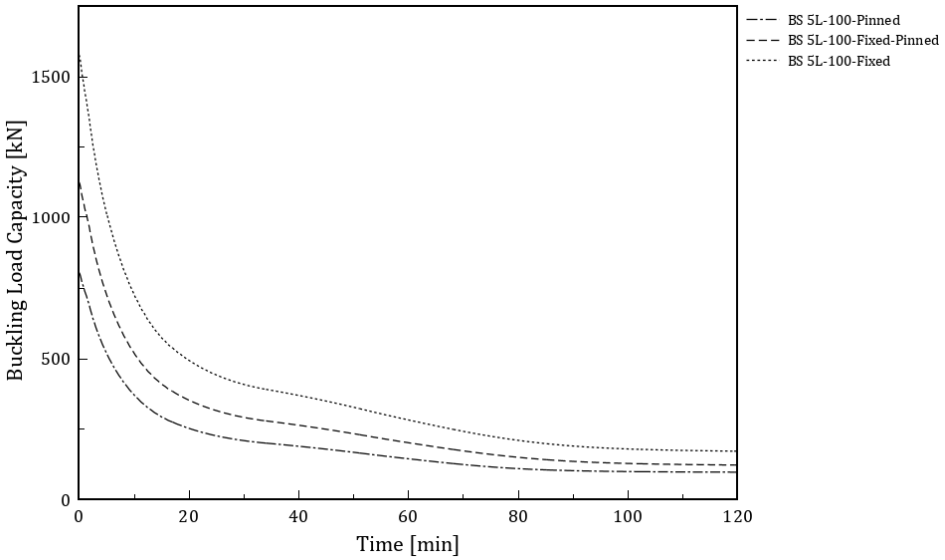

Figure C-2 Buckling load capacity for 100 mm 5-ply CLT with varying end restraints [ISO – 120]

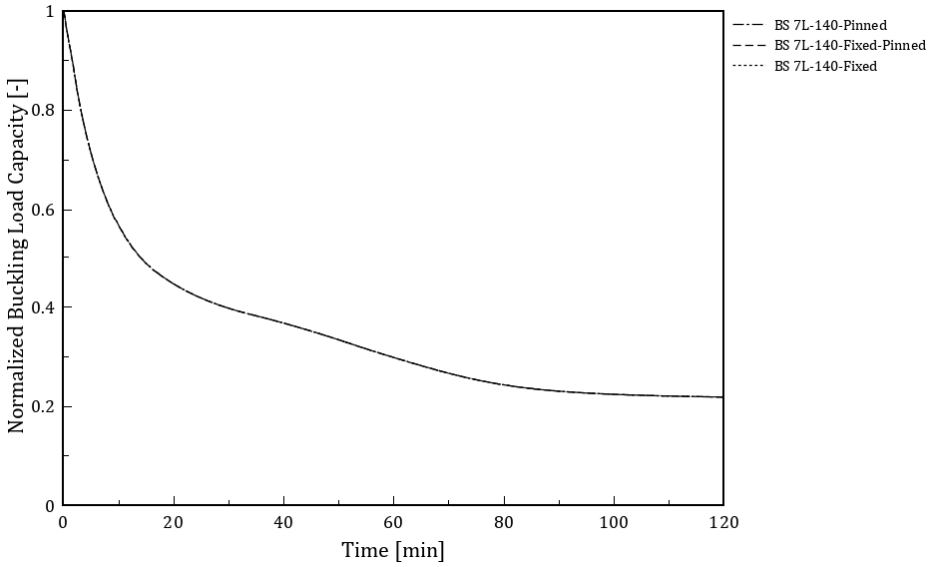

Figure C-3 Normalized buckling load capacity for 140 mm 7-ply CLT with varying end restraints [ISO – 120]

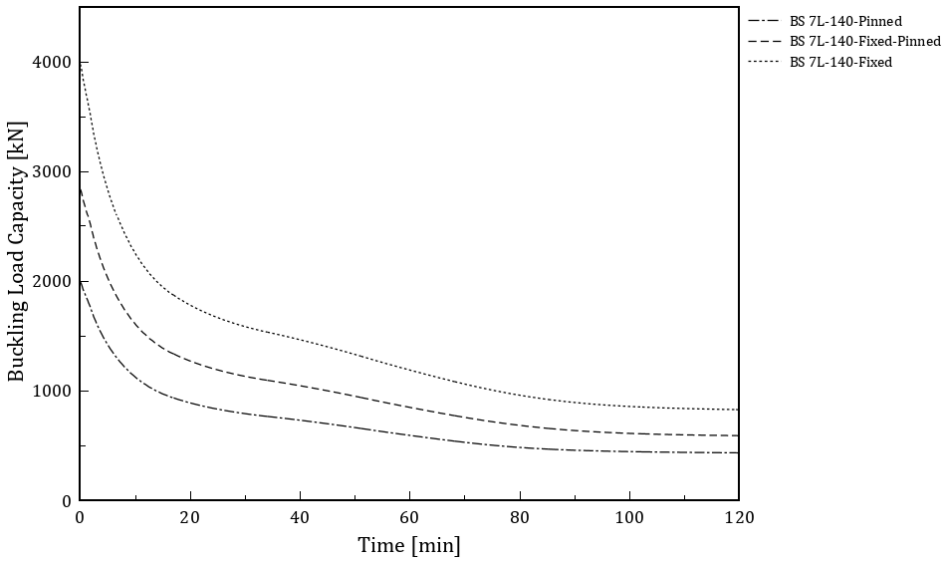

Figure C-4 Buckling load capacity for 140 mm 7-ply CLT with varying end restraints [ISO – 120]

D. Appendix D: Effect of Wall Height Results for 5 and 7-Ply CLT

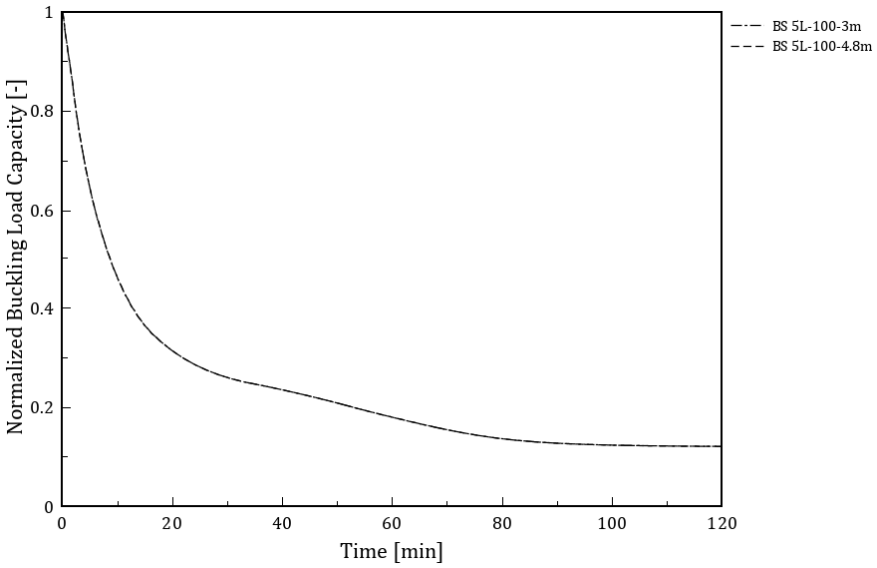

Figure D-1 Normalized buckling load capacity for 100 mm 5-ply CLT with varying heights [ISO – 120]

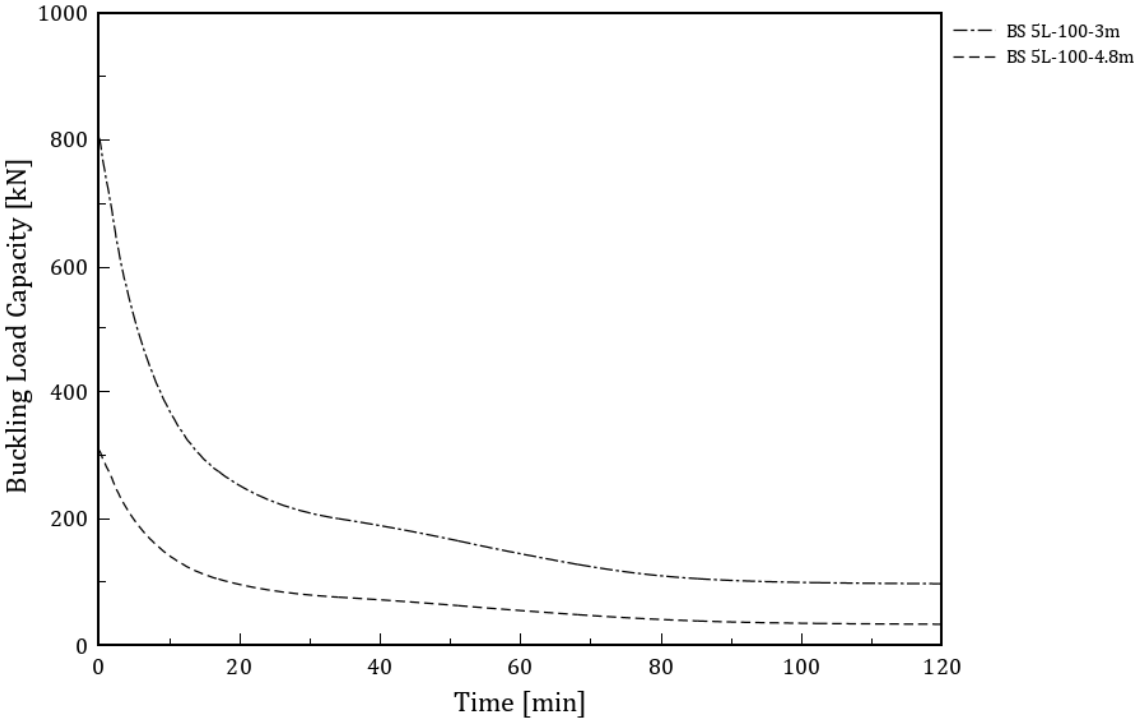

Figure D-2 Buckling load capacity for 140 mm 7-ply CLT with varying heights [ISO – 120]

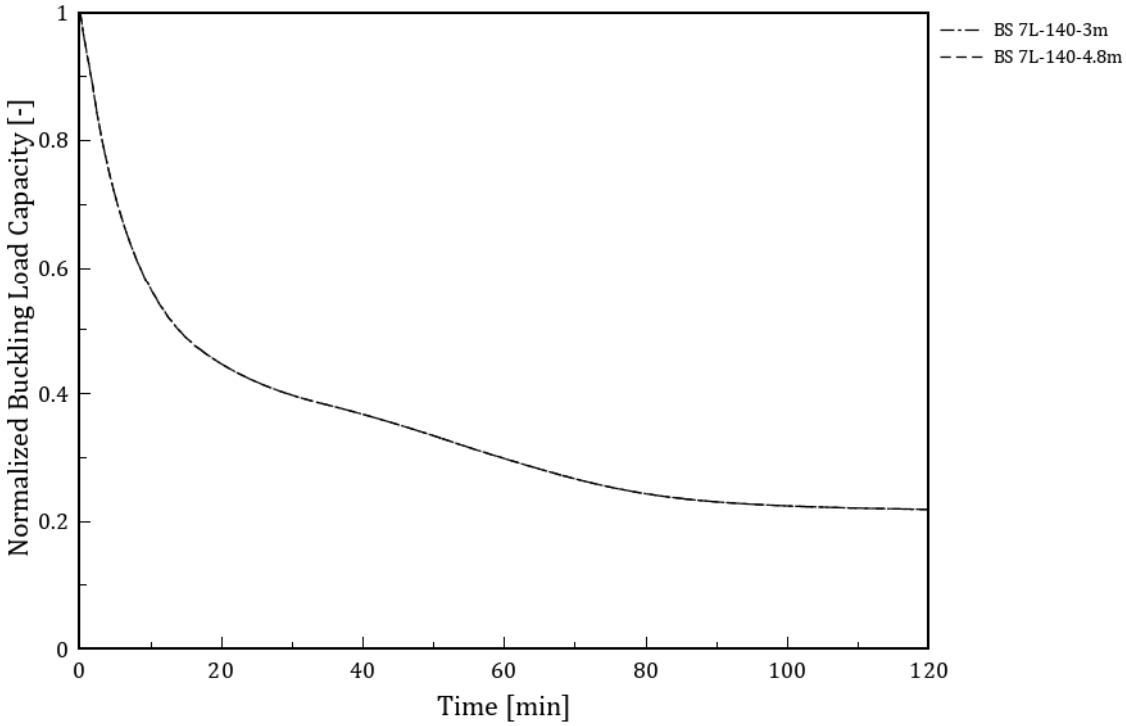

Figure D-3 Normalized buckling load capacity for 140 mm 7-ply CLT with varying heights [ISO – 120]

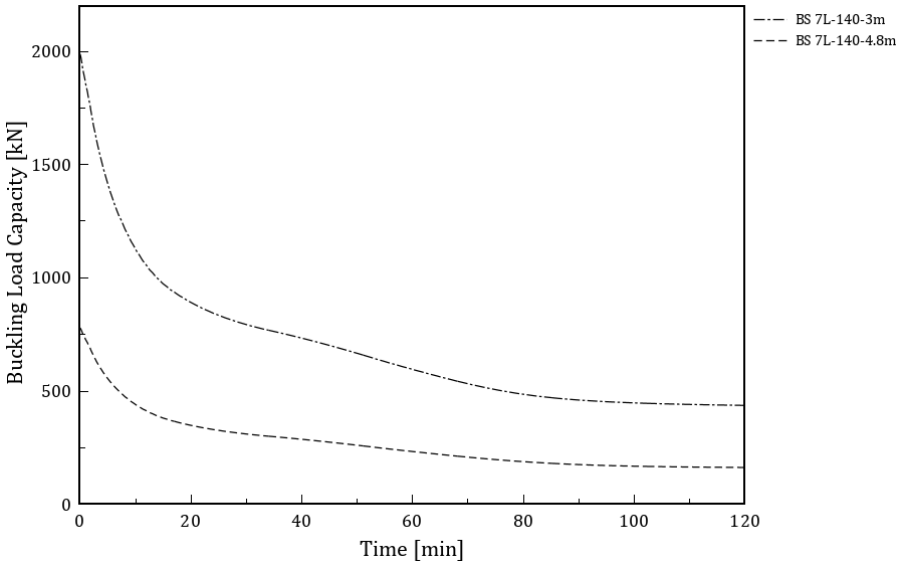

Figure D-4 Buckling load capacity for 140 mm 7-ply CLT with varying heights [ISO – 120]

E. Appendix E: Parametric Study Results Under 120-Minute ISO Fire

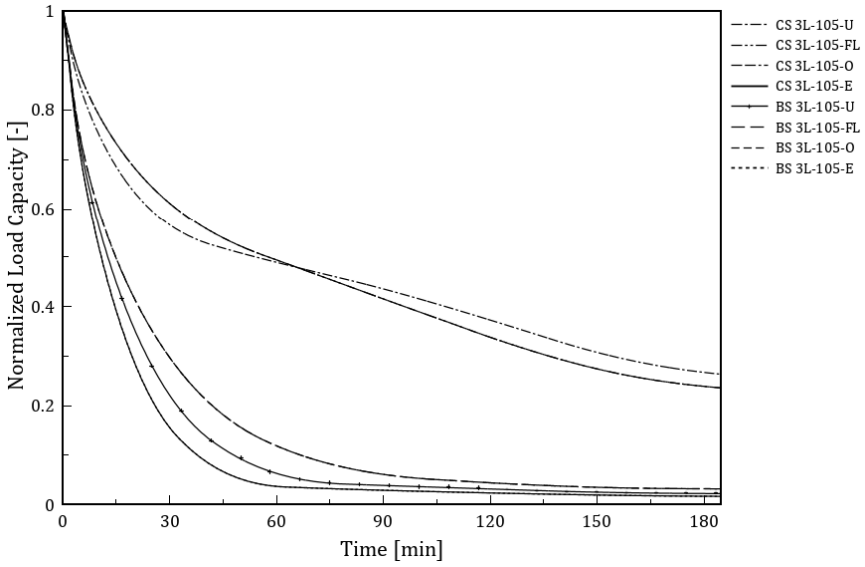

Figure E-1 Normalized load capacity for 105 mm 3-ply CLTs for varying ply arrangements [ISO-120]

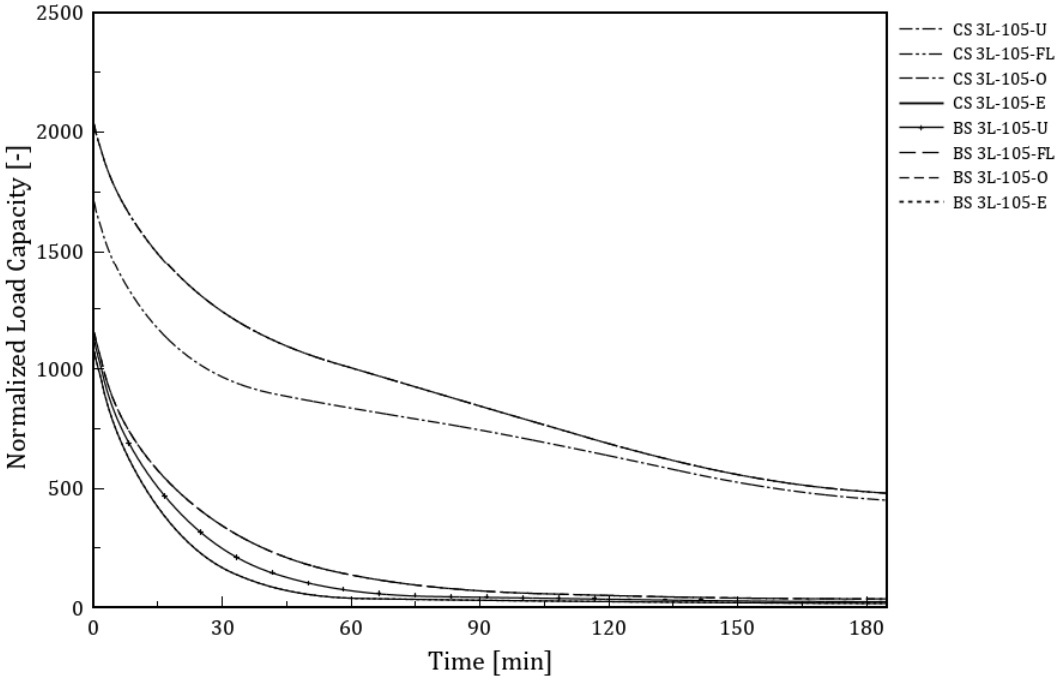

Figure E-2 Load capacity for 105 mm 3-ply CLTs for varying ply arrangements [ISO-120]

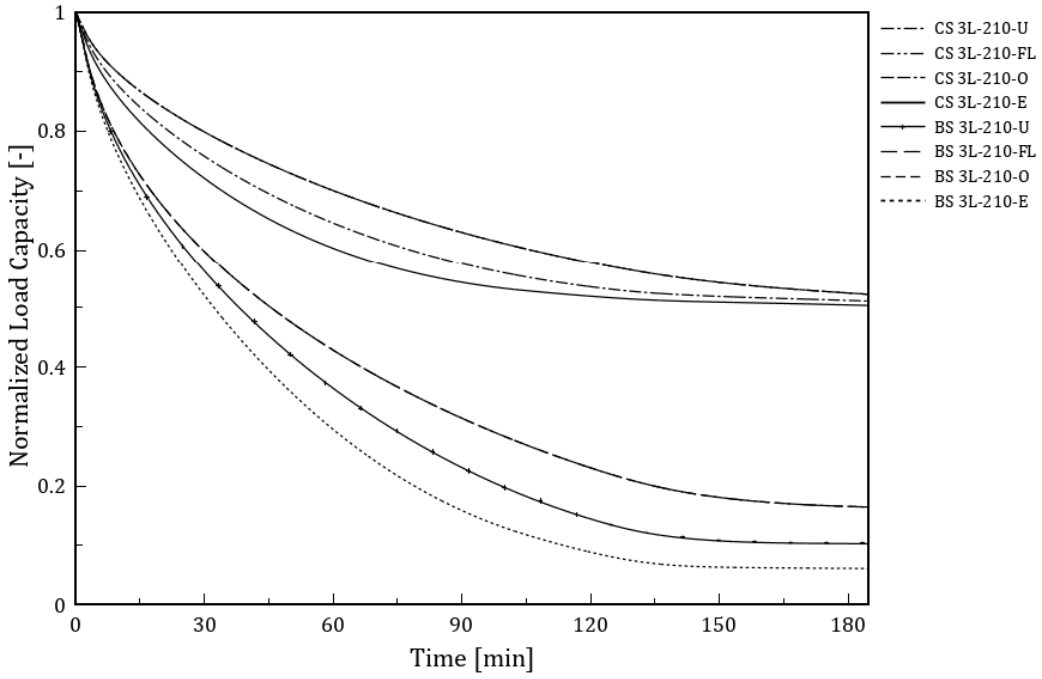

Figure E-3 Normalized load capacity for 210 mm 3-ply CLTs for varying ply arrangements [ISO-120]

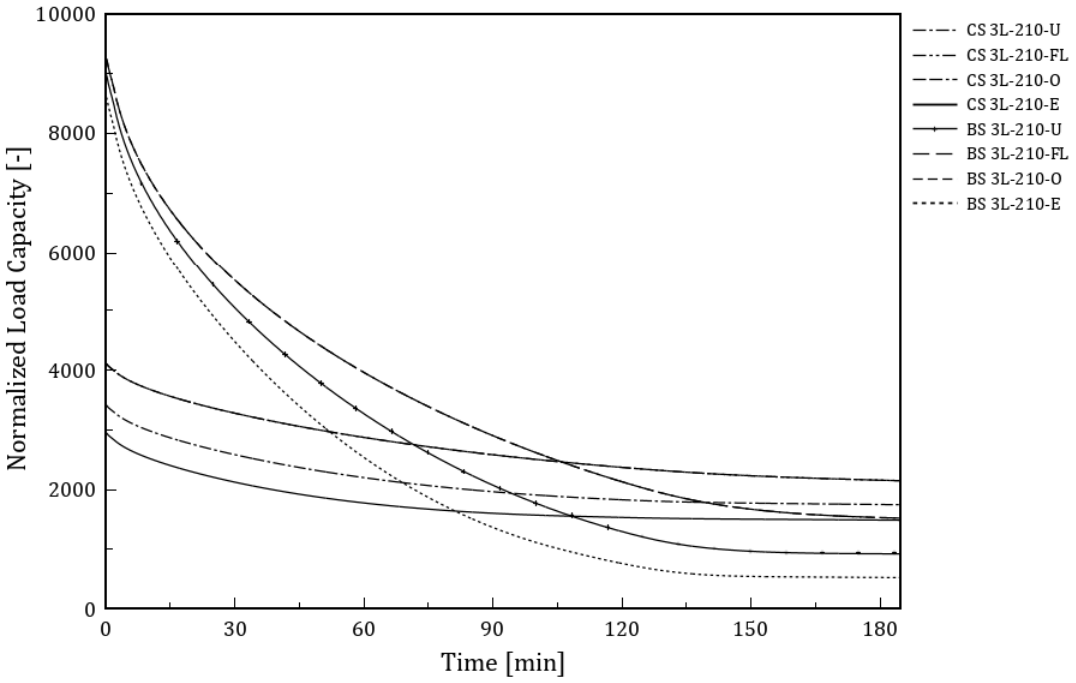

Figure E-4 Load capacity for 210 mm 3-ply CLTs for varying ply arrangements [ISO-120]

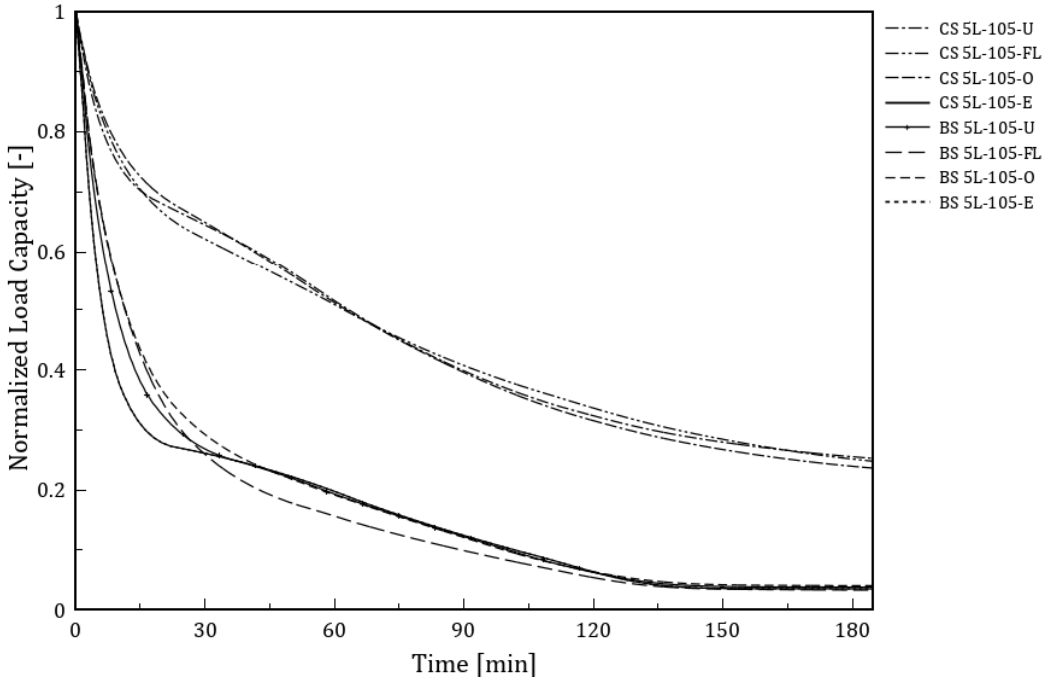

Figure E-5 Normalized load capacity for 105 mm 5-ply CLTs for varying ply arrangements [ISO-120]

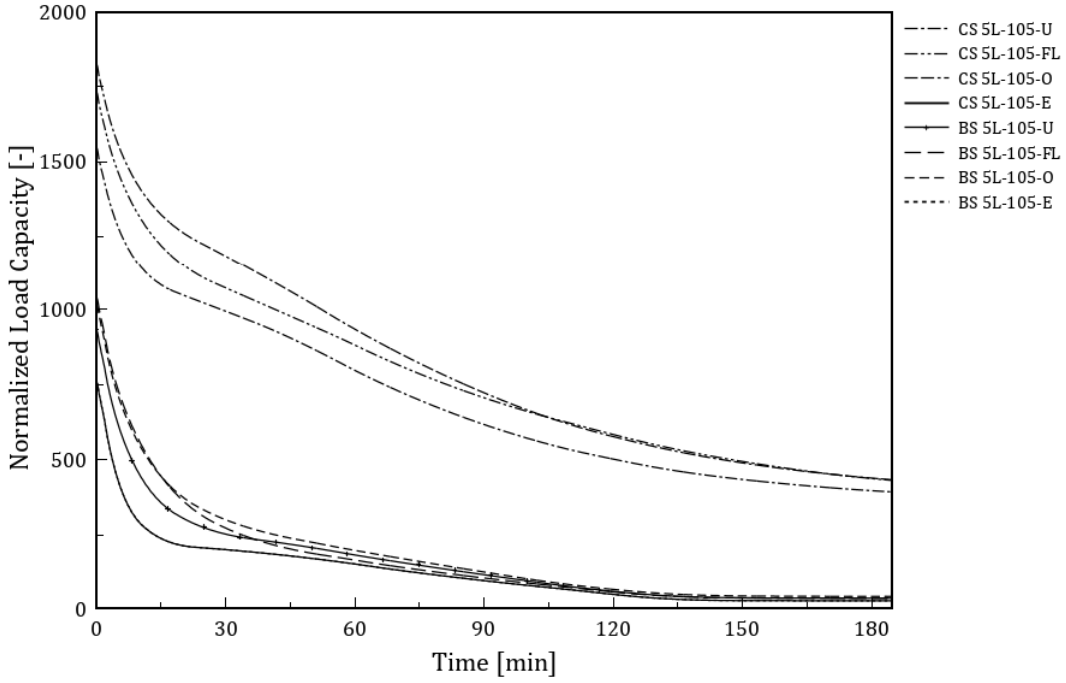

Figure E-6 Load capacity for 105 mm 5-ply CLTs for varying ply arrangements [ISO-120]

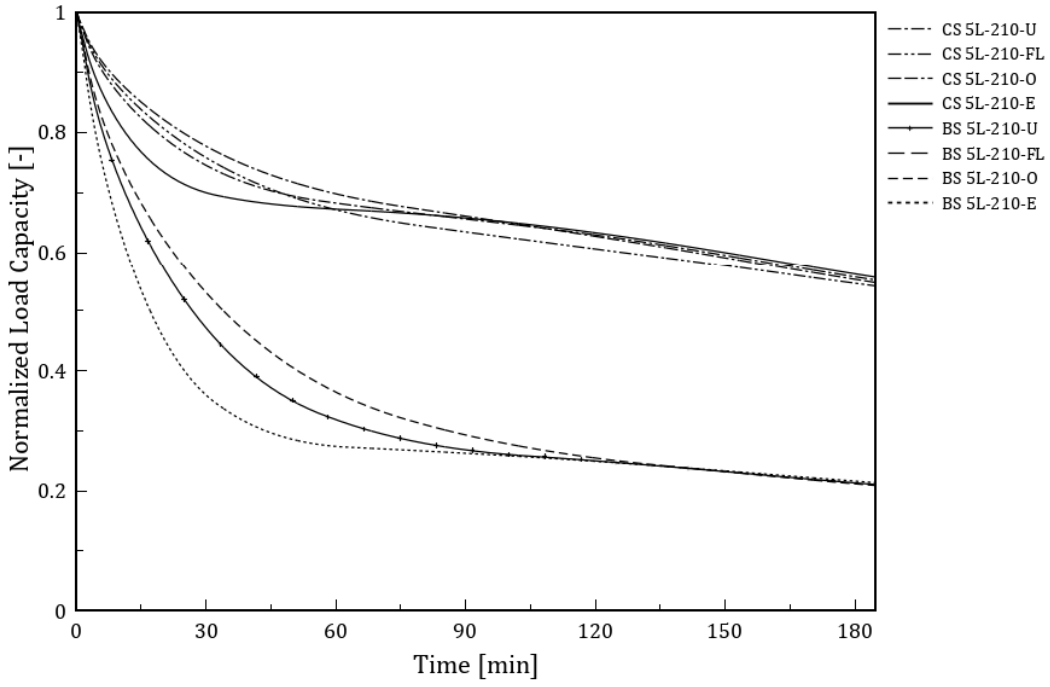

Figure E-7 Normalized load capacity for 210 mm 5-ply CLTs for varying ply arrangements [ISO-120]

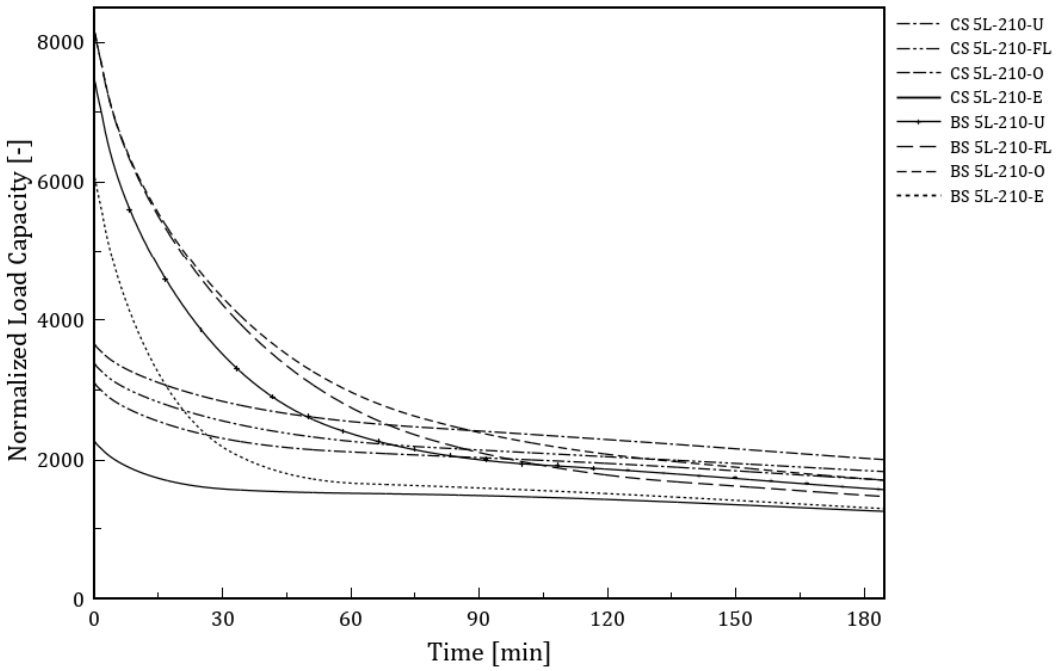

Figure E-8 Load capacity for 210 mm 5-ply CLTs for varying ply arrangements [ISO-120]

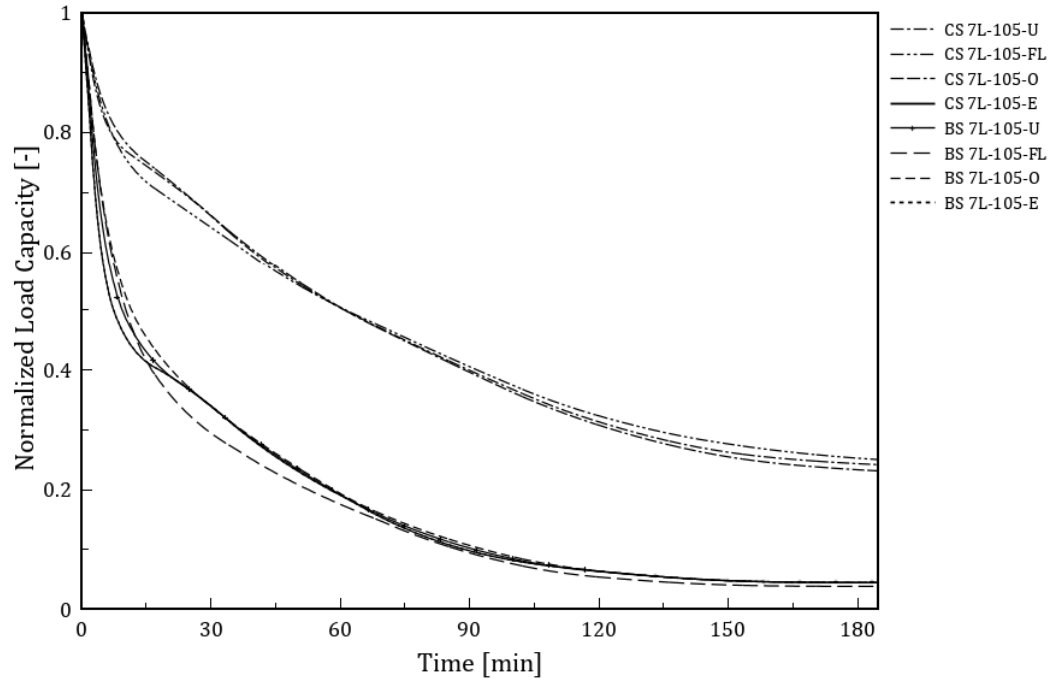

Figure E-9 Load capacity for 105 mm 7-ply CLTs for varying ply arrangements [ISO-120]

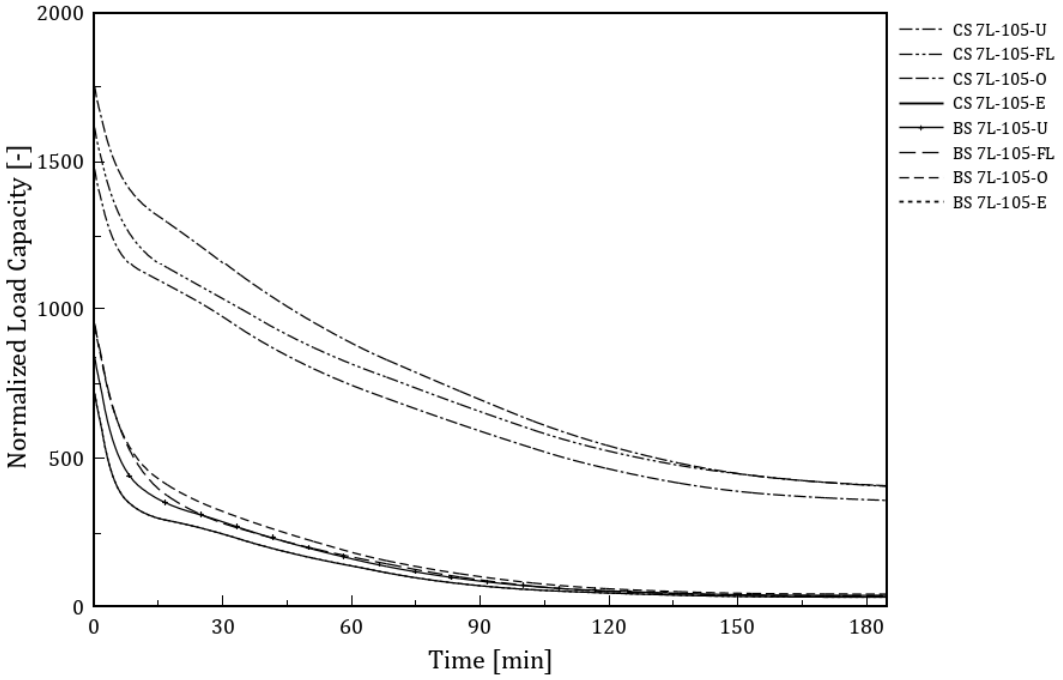

Figure E-10 Load capacity for 105 mm 7-ply CLTs for varying ply arrangements [ISO-120]

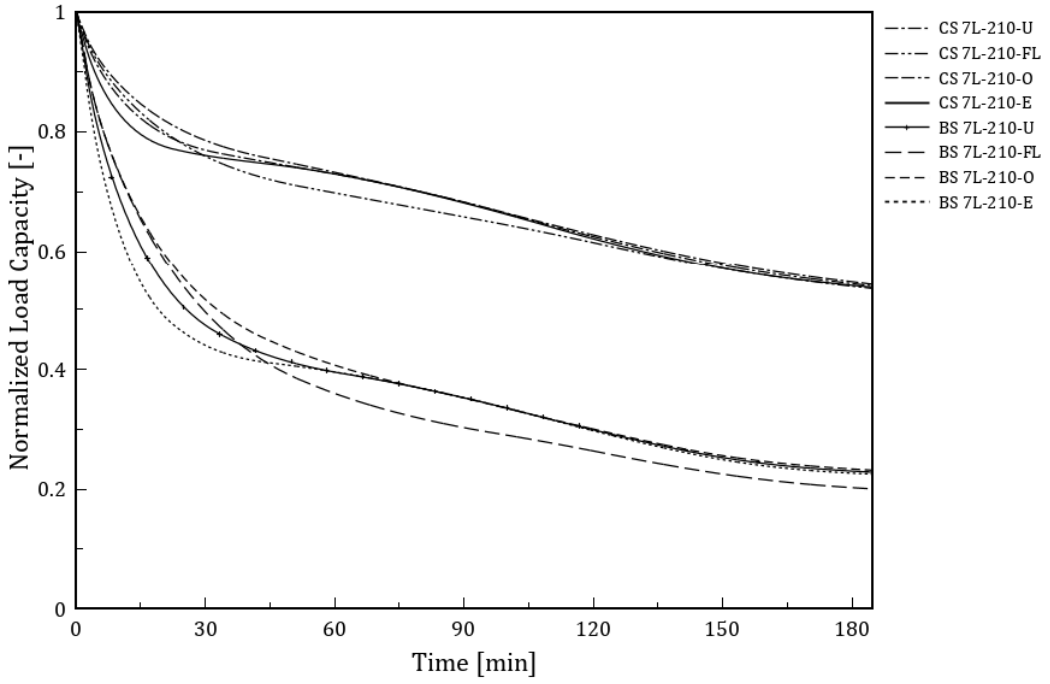

Figure E-11 Normalized load capacity for 210 mm 7-ply CLTs for varying ply arrangements [ISO-120]

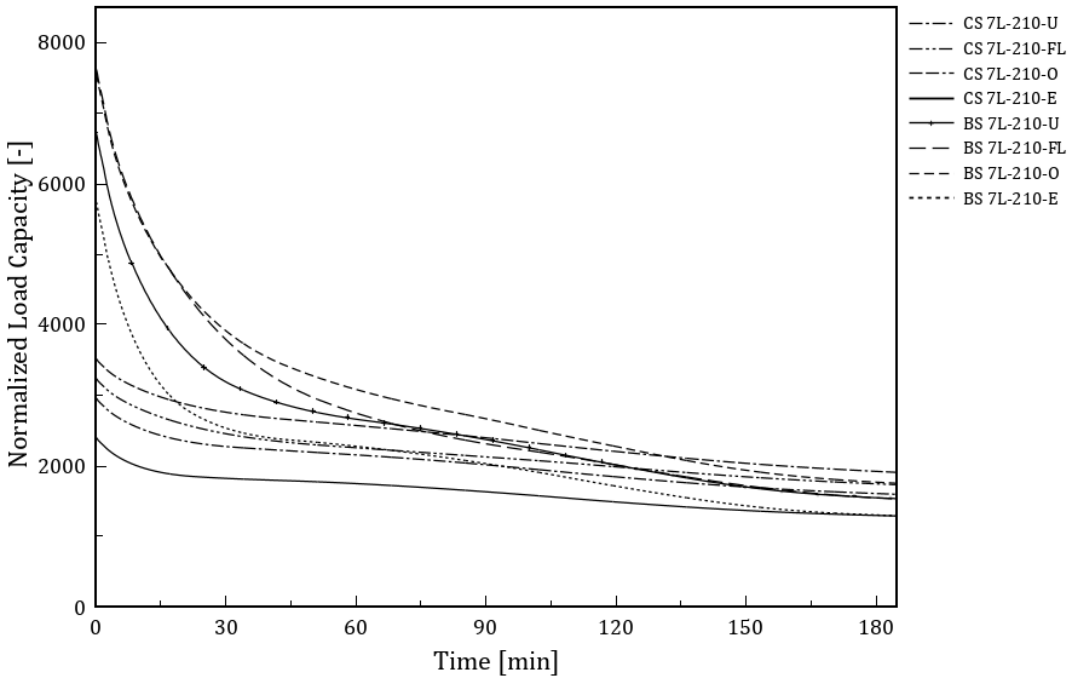

Figure E-12 Load capacity for 210 mm 7-ply CLTs for varying ply arrangements [ISO-120]

F. Appendix F: Comparison of Residual Crushing Capacity Under Different Fires

From Figure F-1 the 3-ply CLTs have a smaller percentage of their original ambient capacity when compared to the 5 and 7-ply CLTs under each ply arrangement. The 3-ply CLT with thicker crosswise plies performed the worst with about 54.8% crushing capacity left. This was closely followed by the 3-ply CLT with uniformly thick plies at approximately 57% capacity left. For all ply arrangement, the 5 and 7-ply CLTs had above 60% of their ambient crushing capacity remaining with closely similar residual capacities.

It is clear from Figure F-1 that the 3-ply CLTs lost a larger percentage of its original capacity at the end of the fire. However, the actual crushing load capacity values shown in Figure F-2 suggest otherwise. The 3-ply CLT outperformed the 5 and 7-ply CLTs except for the case with uniformly thick layers where the 5-ply CLT had slightly higher capacity. Both the 5 and 7-ply CLTs had similar capacities with the 5-ply CLT having slightly higher capacity excluding the case with larger crosswise layers.

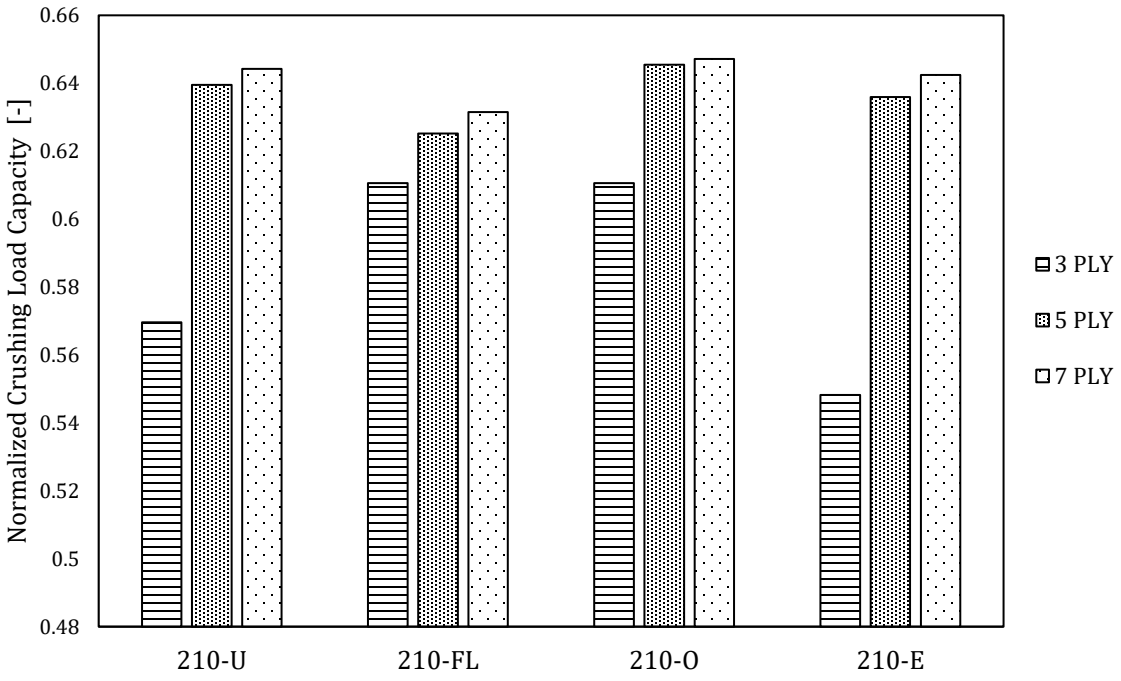

Figure F-1 Comparison of the residual normalized crushing capacity of different CLTs [ISO - 60]

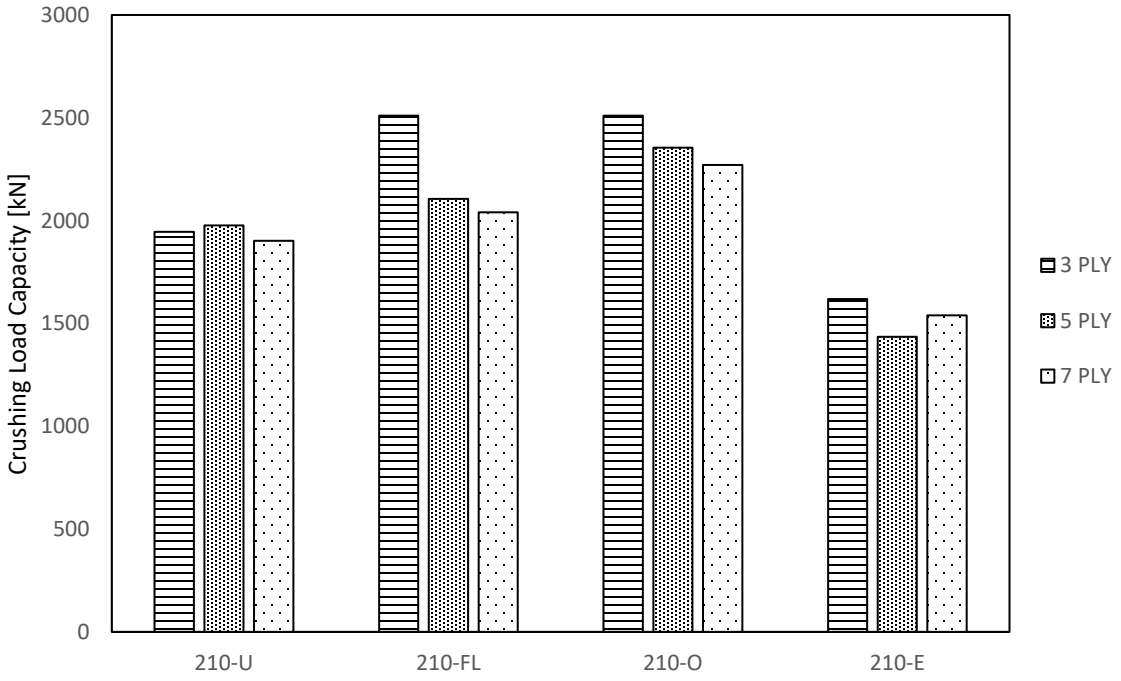

Figure F-2 Comparison of the residual crushing capacities of different CLTs [ISO - 60]

Exposing the same CLTs to a more severe fire resulted in a further reduction (although limited) in their crushing capacity as expected. It can be observed from Figure F-3 that the 5-ply CLTs retained the highest fraction of their original capacity followed closely by the 7-ply CLT and then the 3-ply CLT for all cases. However, with regards to the actual crushing capacity values (Figure F-4), the 3-ply CLTs still exhibited better performance with the 5 and 7-ply CLTs closely behind.

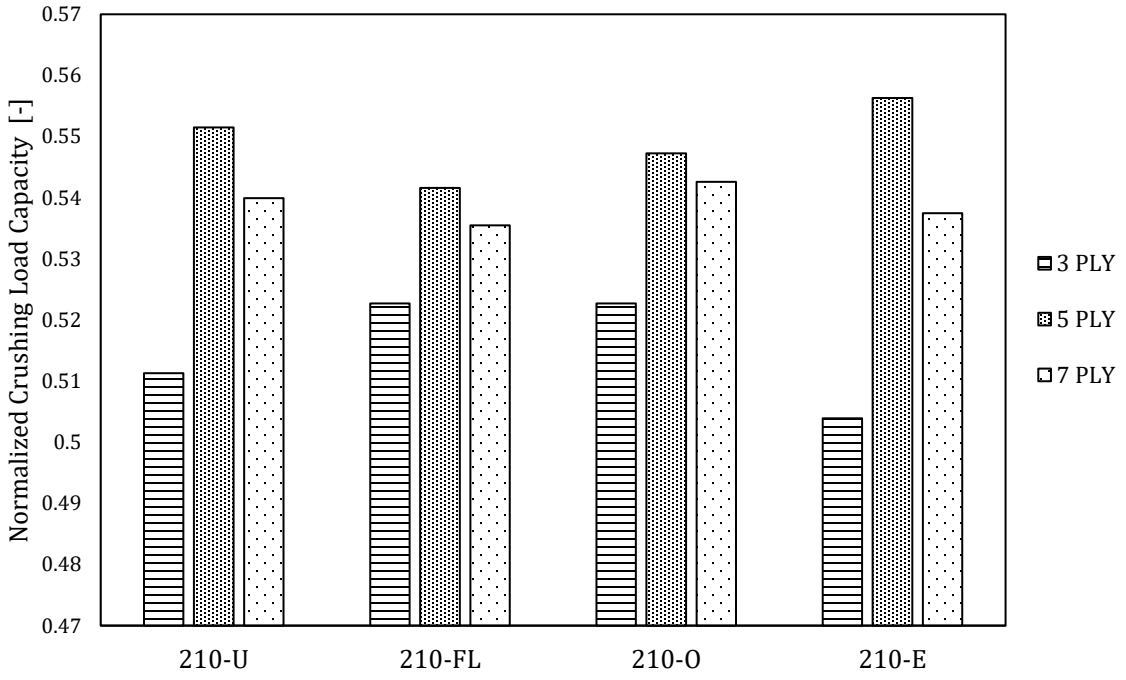

Figure F-3 Comparison of the residual normalized crushing capacity of different CLTs [ISO - 120]

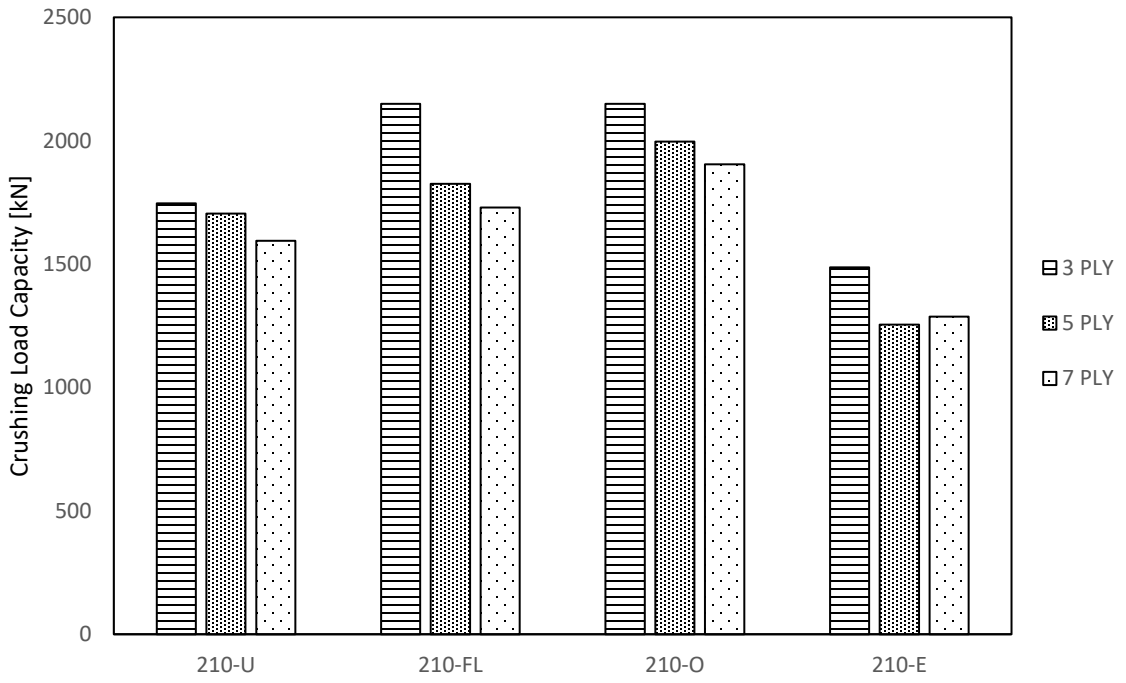

Figure F-4 Comparison of the residual crushing capacities of different CLTs [ISO - 120]